



**UNIVERSITÀ DEGLI STUDI DI ROMA
"TOR VERGATA"**

FACOLTA' DI SCIENZE M.F.N.

DOTTORATO DI RICERCA IN
SCIENZE CHIMICHE

XXI CICLO

***“Synthesis and applications of porphyrinoids:
a journey into the multifaceted chemistry
of pyrrolic macrocycles”***

Dott. Giuseppe Pomarico

A.A. 2008/2009

Docente Guida: Prof. Roberto Paolesse

Coordinatore: Prof. Bruno Crociani

Index

Glossary

VIII

Chapter 1

Porphyrins-based organic materials: synthesis, characterization and exploitation as chemical sensors

Introduction

<i>1.1 A brief history of porphyrins chemistry</i>	2
<i>1.2 General features of porphyrins</i>	4
<i>1.3 Porphyrin derivatives: organic substrates for sensors and materials chemistry</i>	9

Results and discussion

<i>1.4 Self assembled monolayer: the most straightforward way to monomolecular film</i>	16
<i>1.4.1 Synthesis and characterization of porphyrin-based SAM</i>	22
<i>1.5 Porphyrinoids supramolecular aggregates</i>	34
<i>1.5.1 Synthesis and exploitation of self-assembled porphyrinoids-bases nanotube</i>	41

Experimental section

1.6	<i>Synthesis of thiol-derivatized porphyrin</i>	52
1.6.1	<i>Synthesis of 5-(4-carboxymethylphenyl)-10,15,20-triphenylporphyrin (7a)</i>	52
1.6.2	<i>Synthesis of 5-(4-carboxyphenyl)-10,15,20-triphenylporphyrin (8a)</i>	52
1.6.3	<i>Synthesis of 5-(4-carboxy-succinimidephenyl)-10,15,20-triphenylporphyrin (9a)</i>	53
1.6.4	<i>Synthesis of 5-(4-(N-(2-tert-butyloxycarbonyl)-ethyl)-carboxamidephenyl)-10,15,20-triphenylporphyrin</i>	53
1.6.5	<i>Synthesis of 5-(4-(N-(2-aminoethyl)-carboxamidephenyl)-10,15,20-triphenylporphyrin (10a)</i>	54
1.6.6	<i>Synthesis of 12-Mercaptoacetyl-dodecanoic acid (12a)</i>	54
1.6.7	<i>Synthesis of N-(12-Mercaptoacetyl-dodecyloxyl)-succinimide (13a)</i>	55
1.6.8	<i>Synthesis of 5-(4-(N-(2-(12-mercaptoacetyl-dodecyl)-carbonyl)-ethyl)-carboxamidephenyl)-10,15,20-triphenylporphyrin</i>	56
1.6.9	<i>Synthesis of 5-(4-(N-(2-(12-mercapto-dodecyl)-carbonyl)-ethyl)-carboxamidephenyl)-10,15,20-triphenylporphyrin (14a)</i>	56
1.6.10	<i>Procedure for syntheses of Zn (II) and Co(II) complexes</i>	57
1.7	<i>Synthesis of SAM</i>	57
1.7.1	<i>Procedure for gold surfaces preparation</i>	57
1.7.2	<i>Procedure for porphyrin deposition onto gold</i>	58
1.8	<i>Synthesis of porphyrins nanotube</i>	58
1.8.1	<i>Synthesis of 5,10,15,20-[Tetra-(4-pyridyl)porphyrinato]SnCl₂ (16a)</i>	58
1.8.2	<i>General procedure for porphyrins nanotube preparation</i>	59
1.8.3	<i>Polymer membrane preparation</i>	59
1.8.4	<i>CSPT setup</i>	60

<i>1.8.5 AFM setup</i>	60
<i>1.8.6 Gas measurement setup</i>	60
<u>References</u>	62

Chapter 2

Corrole: chemistry and applications of an unusual tetrapyrrolic macrocycle

Introduction

<i>2.1 General properties of corroles</i>	67
<i>2.1.1 Spectroscopic properties of triarylcorroles</i>	67
<i>2.1.2 Corrole: acid-base equilibrium</i>	70
<i>2.2 Synthetic procedures for meso-triarylcorroles</i>	72
<i>2.3 Metalloporroles</i>	75
<i>2.3.1 Synthesis and properties of metalloporroles</i>	75
<i>2.3.2 Bonding geometries of metalloporroles</i>	76

Results and discussion

<i>2.4 Reactivity of triarylcorroles: from functionalization to new isomers</i>	79
<i>2.4.1 Isocorrole: unexpected product from oxidative synthetic step</i>	82
<i>2.5 Metalloporrole: effects of a noninnocent ligand</i>	91

2.5.1 Demetalation of corroles complexes: a starting point towards new synthetic routes	93
<u>Experimental section</u>	
2.6 Synthesis of meso-Arylcorroles	103
2.6.1 General procedure for syntheses of Triarylcorroles (10b, 11b, 12b)	103
2.6.2 Purification of 5,10,15-Triphenylcorrole (10b)	103
2.6.3 Purification of 5,10,15-Tris-(4-methylphenyl)corrole (11b)	103
2.6.4 Purification of 5,10,15-Tris-(4-methoxyphenyl)corrole (12b)	104
2.6.5 Synthesis of 5,10,15-Tris-(4-nitrophenyl)corrole (13b)	104
2.7 Syntheses of β -Alkylcorroles (26b, 27b, 28b)	104
2.8 Syntheses of Triarylisocorroles	105
2.8.1 Synthesis of 5,10,15-Triphenyl-10-ethoxyl-isocorrole (14b)	105
2.8.2 Synthesis of 5,10,15-Tris-(4-methylphenyl)-10-methoxyl-isocorrole (15b) and of 5,10,15-Tris-(4-methylphenyl)-5-methoxyl-isocorrole (16b)	106
2.8.3 Synthesis of 5,10,15-Tris-(4-methoxyphenyl)-10-methoxyl-isocorrole (17b)	107
2.9 Syntheses of Metallocorroles	108
2.9.1 Synthesis of [5,10,15-Triarylcorrolates]Cu	108
2.9.2 Synthesis of [2,3,7,8,12,13,17,18-Octaalkylcorrolates]Cu	108
2.9.3 Synthesis of [5,10,15-Triphenylcorrolato]Co(PPh ₃)	109
2.9.4 Synthesis of [2,3,7,8,12,13,17,18-Octamethylcorrolato]Co(PPh ₃)	109
2.9.5 Synthesis of [5,10,15-Triphenylcorrolato]MnCl	110
2.9.6 Synthesis of [8,12-Diethyl-2,3,7,13,17,18-hexamethylcorrolato]MnCl	110
2.9.7 Synthesis of [5,10,15-Triphenylcorrolato]FeCl	110

2.9.8 Synthesis of [2,3,17,18-Tetraethyl-7,8,12,13-tetramethylcorrolato]FeCl	111
2.9.9 Synthesis of [5,10,15-Triphenylcorrolato]GeCl	111
2.9.10 Synthesis of [2,3,17,18-Tetraethyl-7,8,12,13-tetramethylcorrolato]GeCl	112
2.10 General procedures for demetalation process	112
2.10.1 CHCl ₃ /H ₂ SO ₄ method	112
2.10.2 H ₂ SO ₄ method	113
2.10.3 HBr/HOAc method	113
<u>References</u>	114

Chapter 3

Triaryl-tetrabenzocorroles: innovative compounds for biomedical applications

Introduction

3.1 History of photodynamic therapy	119
3.2 Principles of PDT	121
3.2.1 Photochemistry of PDT	121
3.2.2 Singlet oxygen	125
3.3 Photosensitizers	127
3.3.1 Properties of photosensitizers	127

3.3.2 Photophysic of photosensitizers	128
3.4 Biological mechanism of action	131

Results and discussion

3.5 PDT: porphyrinoids in the service of medicine	133
3.5.1 Exploitation of porphyrin derivatives in PDT	133
3.5.2 Benzoporphyrins	136
3.6 Syntheses of Triaryl-tetrabenzocorroles	140
3.6.1 Synthesis of precursor: 4,5,6,7-Tetrahydroisoindole	141
3.6.2 Synthesis of Triaryl-tetrabenzocorroles: one step procedure	143
3.6.3 Synthesis of Triaryl-tetrabenzocorroles: two steps procedure	146
3.6.4 Dihydroisoindole: a closer precursor to tetrabenzocorroles	156

Experimental section

3.7 Synthesis of precursors: tetrahydroisoindole and dipyrromethane	159
3.7.1 Synthesis of 2-Carboxyethyl-4,5,6,7-tetrahydroisoindole (15c)	159
3.7.2 Synthesis of 4,5,6,7-Tetrahydroisoindole (16c)	159
3.7.3 Synthesis of 1,9-Dicarboxyethyl-2:3,7:8-dibutane -5-phenyl-dipyrromethane (17c)	160
3.7.4 Synthesis of 2:3,7:8-Dibutane-5-phenyl -dipyrromethane (18c)	160
3.8 Syntheses of Triaryl-tetrabenzocorroles	161
3.8.1 Synthesis of 5,10,15-Triphenyl-2:3,7:8,12:13,17:18- tetrabutane corrole - modified Paolesse method	161
3.8.2 Synthesis of 5,10,15-Tris-(4-methyl-carboxylatephenyl) -2:3,7:8,12:13,17:18-tetrabutane corrole - modified Paolesse method	162

3.8.3 Synthesis of 5,10,15-Triphenyl-2:3,7:8,12:13,17:18-tetrabutaneborrole - Paolesse method	162
3.8.4 Synthesis of 10-(4-Cyanophenyl)-5,15-diphenyl-2:3,7:8,12:13,17:18-tetrabutaneborrole (19c) - Gryko method	163
3.8.5 Synthesis of [10-(4-Cyanophenyl)-5,15-diphenyl-2:3,7:8,12:13,17:18-tetrabutaneborrolate]Cu	163
3.8.6 Synthesis of 5,10,15-Tris-(3-cyanophenyl)-2:3,7:8,12:13,17:18-tetrabutaneborrole (20c)	164
3.8.7 Synthesis of [5,10,15-Tris-(3-cyanophenyl)-2:3,7:8,12:13,17:18-tetrabutaneborrolate]Cu (21c)	164
3.8.8 Synthesis of [5,10,15-Tris-(3-cyanophenyl)-2:3,7:8,12:13,17:18-tetrabenzoborrolate]Cu (22c)	165
3.9 An alternative isoindole as triaryl-tetrabenzoborrole precursor	166
3.9.1 Synthesis of Ethynyl p-tolyl sulfone (24c)	166
3.9.2 Synthesis of 1-Tosyl-[(4,5-dimethyl)-cyclohexa-1,4-diene] (25c)	166
3.9.3 Synthesis of 2-Carboxyethyl-5,6-dimethyl-4,7-dihydro-2H-isoindole (26c)	167
<u>References</u>	168
<u>List of publications</u>	172

Glossary - Reagents and solvents

$\text{BF}_3 \cdot \text{OEt}_2$ = Boron trifluoride diethyl etherate

Boc = 2-(tert-butyl-carbamoyl)-ethaneamine

t-BuOK = potassium *tert*-butoxide

Chloranil = 2,3,5,6-tetrachloro-1,4-benzoquinone

DBU = 1,8-Diazabicyclo[5.4.0]-7-undecene

DDQ = 2,3-Dichloro-5,6-dicyano-1,4-benzoquinone

DMF = N,N'-Dimethylformamide

EDC = 1-[3-(dimethyl-amino)propyl]-3-ethylcarbodiimide hydrochloride

MeCN = Acetonitrile

MeOH = Methanol

PDMS = polydimethylsiloxane distearate

2-PrOH = 2-Propanol

Sc(OTf)₃ = Scandium trifluoromethanesulfonate

TEA = Triethylamine

TFA = Trifluoroacetic acid

THF = Tetrahydrofuran

Glossary of porphyrinoids - Chapter 1

p-CO₂CH₃TPPorH₂ = 5-(4-carboxymethylphenyl)-10,15,20-triphenylporphyrin

TPPorH₂ = 5,10,15,20-Tetraphenylporphyrin

[TSPPorH₂]⁴⁻ = [5,10,15,20-Tetra-(sulfonatophenyl)porphyrinate]-tetrasodium salt

TPyPorH₂ = 5,10,15,20-Tetra-(4-pyridyl)porphyrin

[TPyPor]SnCl₂ = [5,10,15,20-Tetra-(4-pyridyl)porphyrinate]Tin-dichloride

Glossary of porphyrinoids - Chapter 2

$\text{Br}_8(10\text{-OH})\text{TPIsoCH}_2 = 2,3,7,8,12,13,17,18\text{-Octabromo-5,10,15-triphenyl-10-hydroxyl-isocorrole}$

$[\text{Br}_8\text{TPCor}]_3\text{H}_3 = 2,3,7,8,12,13,17,18\text{-Octabromo-5,10,15-triphenylcorrole}$

$[\text{Br}_8\text{TPCor}]_3\text{Cu} = [2,3,7,8,12,13,17,18\text{-Octabromo-5,10,15-triphenylcorrolato}]_3\text{copper}$

$\text{Br}_8\text{TPCorH}_2 = 2,3,7,8,12,13,17,18\text{-Octabromo-5,10,15-triphenyl-10-H-isocorrole}$

$[(4\text{-ClPh})_8\text{TPCor}]_3\text{Cu} = [2,3,7,8,12,13,17,18\text{-Octabromo-5,10,15-(4-chlorophenyl)corrolato}]_3\text{copper}$

$\text{Et}_2\text{Me}_6\text{CorH}_3 = 8,12\text{-Diethyl-2,3,7,13,17,18-hexamethylcorrole}$

$\text{Et}_4\text{Me}_4\text{CorH}_3 = 2,3,17,18\text{-Tetraethyl-7,8,12,13-tetramethylcorrole}$

$(5\text{-OH})\text{TPIsoCorH}_2 = 5,10,15\text{-Triphenyl-5-hydroxyl-isocorrole}$

$(10\text{-OH})\text{TPIsoCorH}_2 = 5,10,15\text{-Triphenyl-10-hydroxyl-isocorrole}$

$\text{Me}_8\text{CorH}_3 = 2,3,7,8,12,13,17,18\text{-Octamethylcorrole}$

$[(\text{NO}_2)\text{TPCor}]_3\text{Ag} = [3\text{-Nitro-5,10,15-triphenylcorrolato}]_3\text{silver}$

$(p\text{-NO}_2)\text{TPCorH}_3 = 5,10,15\text{-Tris-(4-nitrophenyl)corrole}$

$(p\text{-OCH}_3)\text{TPCorH}_3 = 5,10,15\text{-Tris-(4-methoxyphenyl)corrole}$

$\text{TPCorH}_3 = 5,10,15\text{-Triphenylcorrole}$

$[\text{TPCor}]_3\text{Metal} = [5,10,15\text{-Triphenylcorrolo}]_3\text{metal}$

$\text{TTCorH}_3 = 5,10,15\text{-Tris-(4-methylphenyl)corrole}$

Glossary of porphyrinoids - Chapter 3

$(3\text{-CN})\text{BuTPCorH}_3 = 5,10,15\text{-Tris}$

$\text{-(3-cyanophenyl)-2:3,7:8,12:13,17:18-tetrabutane}^2\text{corrole}$

$[(3\text{-CN})\text{BuTPCor}]_3\text{Cu} = [5,10,15\text{-Tris}$

$\text{-(3-cyanophenyl)-2:3,7:8,12:13,17:18-tetrabutane}^2\text{corrolato}]_3\text{copper}$

$[(3\text{-CN})\text{TBCor}]_3\text{Cu} = [5,10,15\text{-Tris}$

-(3-cyanophenyl)-2:3,7:8,12:13,17:18-tetrabenzocorrolato]copper

Hp = 3,7-Di-(3-propyloxy)-2,8,12,17-tetramethyl-13,18-di-(2-hydroxyethyl)-
porphyrin

TBPorH₂ = 2:3,7:8,12:13:17:18-Tetrabenzoporphyrin

Chapter 1

**Porphyrins based organic materials:
synthesis, characterization and exploitation
as chemical sensors**

Introduction

1.1 A brief history of porphyrins chemistry

Thudichum^[1] developed the first preparation of porphyrin in 1867, by treatment of hemoglobin with concentrated acid. A few years later by a similar route, Hoppe-Seyler^[2] obtained a purple substance which he called hematoporphyrin (**1a**, Fig.1.1).

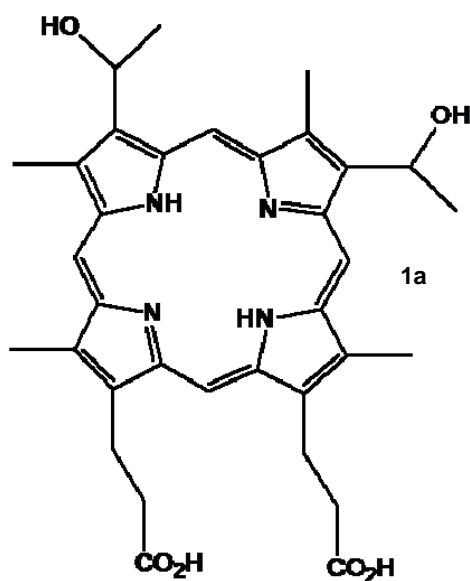


Fig. 1.1 – Structure of Hematoporphyrin

However, these procedures failed to provide a pure sample of porphyrin. Approximately 30 years later Nencki^[3] isolated the first pure sample, preparing hematoporphyrin hydrochloride from isolated hemin. These initial studies marked the beginning of porphyrin chemistry, which now includes many disciplines of science and medicine and continue to flourish.

Porphyrins possess a basic skeleton consisting of four pyrrole units linked by four methine bridges. This skeletal structure was first proposed by Küster^[4] in 1912. However, it was suggested by both Fischer and Willstätter, that such a large ring system would not be very stable; they proposed other structures containing smaller ring systems such as **2a** and **3a** (Fig. 1.2).

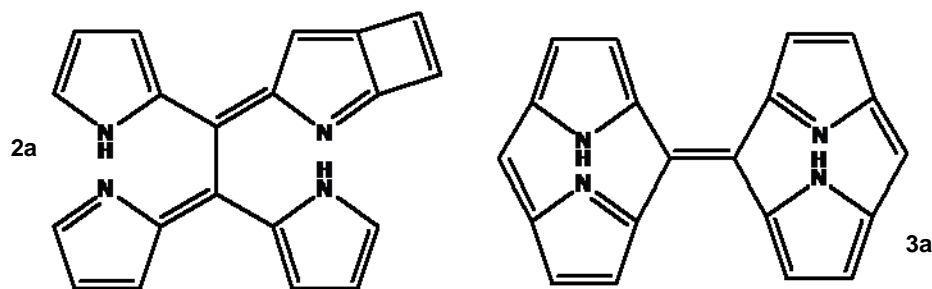


Fig. 1.2 – Earlier structures proposed for porphyrin

The debate over the actual structure of porphyrin continued until 1926, when Fischer successfully synthesized etioporphyrin-I by the first totally synthetic way^[5]. Shortly thereafter Fischer completed the synthesis of octamethylporphyrin (**4a**, Fig. 1.3) by two distinctly preparative methods^[6]. These preparations led to the acceptance of the structure initially proposed by Küster as the basic structure of porphyrins.

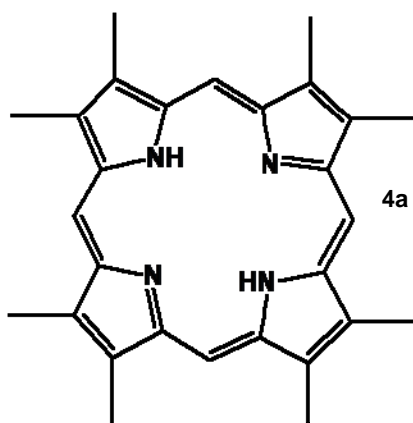


Fig. 1.3 – Me₈PorH₂, the first synthetic porphyrin

1.2 General features of porphyrins

Tetrapyrrolic macrocycle is a term used to refer to a class of compounds that have four pyrrole units connected through four sp^2 hybridized meso-carbons at the α position of the pyrrole rings. Among those, porphyrin represents the most common arrangement, with its molecular skeleton having formula $C_{20}H_{14}N_4$.

Currently there are two nomenclature systems for the numbering of porphyrins: the older is the so-called the “Fischer system”, where the meso positions are labelled by Greek lettering system, and the four pyrrolic rings are so labeled with the capital letters A, B, C, and D. However this way does not allow to the identification of all carbons of the molecular skeleton.

The more modern and more thorough scheme, is called the “IUPAC system”, which identifies every carbon in the macrocyclic ring (Fig. 1.4).

The porphyrins macrocycle is an aromatic system containing 22 π electrons 18 of which are involved in any localization pathway (Fig. 1.4).

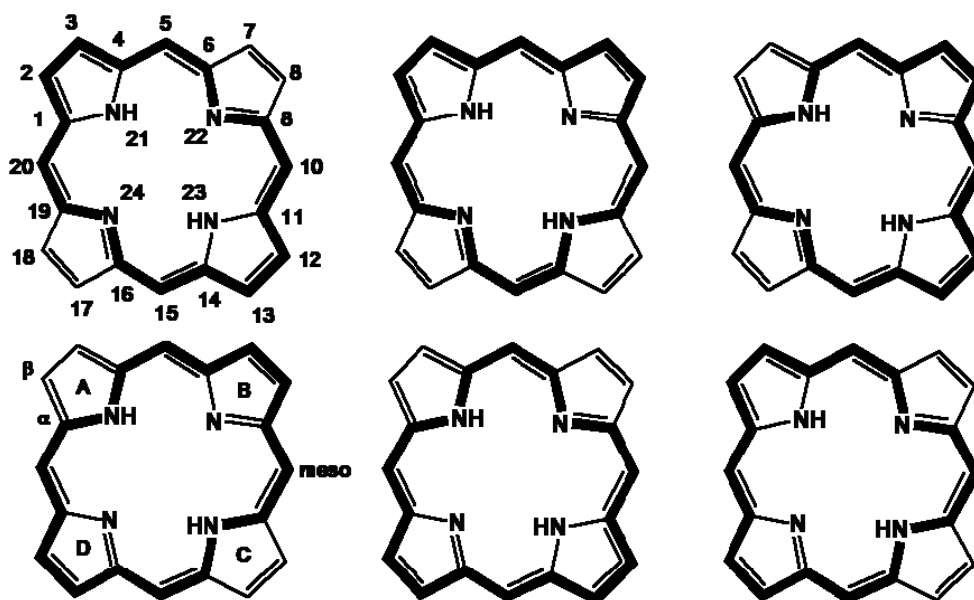


Fig. 1.4 – Porphyrin tautomers and numeration system

Porphyrins obey Hückel's rule of aromaticity ($4n+2\pi$ electrons, where $n = 4$). The aromatic character of porphyrins is also evident in their NMR spectrum. ^1H NMR spectroscopy of porphyrins shows that the N-H protons appear from $\delta = \sim -4$ to -2 ppm (upfield from TMS), indicative of NHs located in an anisotropic aromatic shielding cone^[7].

Whereas the methane protons appear at ~ 10 ppm, a δ value indicating a highly deshielding environment resulting from the aromatic ring current.

Visible absorption spectrum of porphyrins displays an intense absorption ($\epsilon > 100000$) to the second excited state ($S_0 \rightarrow S_2$) at about 400 nm, referred to as the Soret band^[8]; this is characteristic of a highly conjugated porphyrin macrocycle, and it disappears when the aromatic delocalization pathway is disrupted. There are several weaker absorptions to the first excited state ($S_0 \rightarrow S_1$) at longer wavelengths (450 to 700 nm). Both of these bands arise from π - π^* transitions, and can be explained by considering the four frontier orbitals model proposed by Gouterman^[9]. According to this theory, the absorption bands in porphyrins arise from transition between two HOMOs and two LUMOs (Fig. 1.5). The HOMOs were calculated to be an a_{1u} and an a_{2u} orbital, while the LUMOs were calculated to be a degenerate set of e_g orbitals.

Transition between these orbitals gave rise to two excited states, both of 1E_u character. Orbital mixing splits these two states in energy, creating a higher energy 1E_u state with greater oscillator strength, which give rise to the Soret band, and a lower energy 1E_u state with less oscillator strength, giving rise to the Q bands.

The lowest energy excited singlet states of porphyrins can be thought of as being formed from the molecular orbitals examined above. An excited singlet state with an $a_{1u}e_g$ configuration is formed by promoting an electron from the a_{1u} orbital to an e_g orbital.

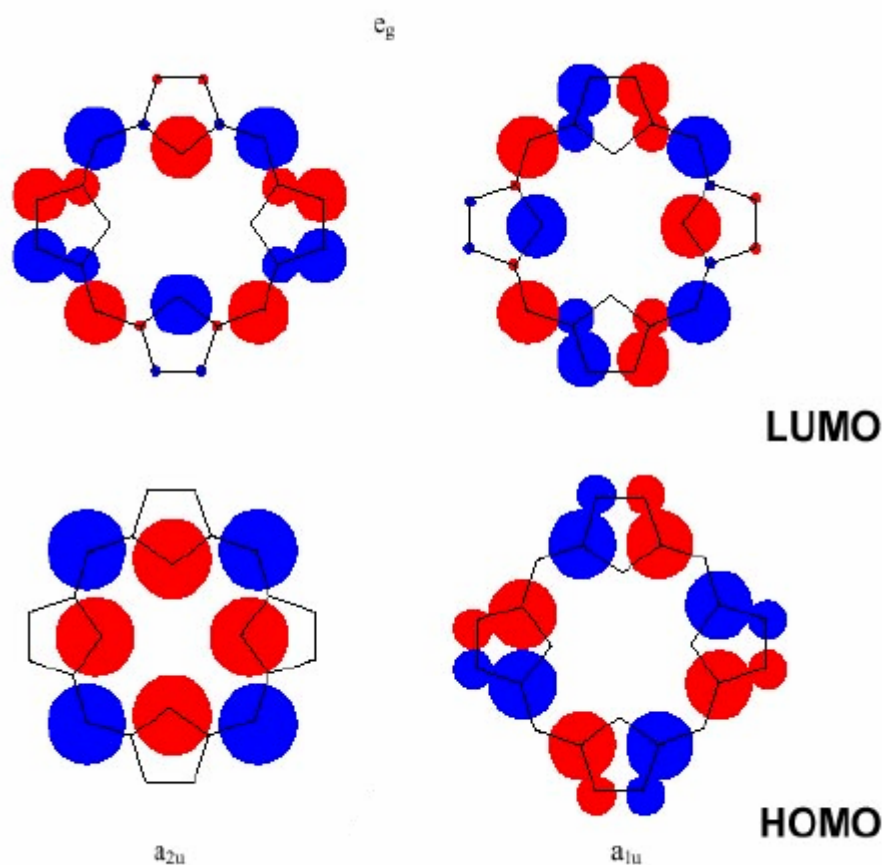


Fig. 1.5 – Porphyrin HOMO and LUMO

Likewise, an excited singlet state with an $a_{2u}e_g$ configuration is formed by promoting an electron from the a_{2u} orbital to an e_g orbital.

Variations of the peripheral substituents on the porphyrin ring often causes minor changes in the intensity and wavelength of these absorptions. Protonation of two inner imine nitrogen atoms, or insertion of a metal into the porphyrin cavity, also changes the visible absorption spectrum. These absorptions can often be very helpful in elucidating certain structural features on a porphyrin. X-ray structural determinations of both metalloporphyrins and free-base macrocycles have basically shown the core porphyrin to be planar, a fundamental requirement for perfect aromaticity^[10].

Rapid tautomerization at room temperature^[11] is a characteristic of free base porphyrins. Infrared spectroscopy has served as a key tool in investigating the existence of different N-H tautomers^[12].

Three hydrogen bonded models may be considered for porphyrins. In **5a** the hydrogens atoms are on adjacent nitrogens and hydrogens bonded to the remaining nitrogens. This is the least stable and least symmetrical according to infrared data and calculations of orbital overlap^[13].

The inner nitrogens in **6a** are placed on opposite nitrogens and hydrogens bonded to the adjacent nitrogens. Both NMR^[14] spectroscopy and X-ray crystallographic structure studies^[15], have established tautomer **6a** to be the most stable form of porphyrins (Fig. 1.6).

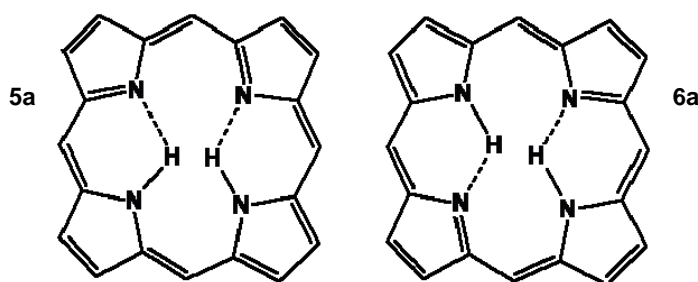


Fig. 1.6 – H-bond in porphyrin core

The porphyrin ring is very stable to both concentrated acid and base, and the macrocycle can act both as an acid and a base. Strong bases such as alkoxides remove the two central protons ($pK_a \sim 16$) on the inner nitrogens of a porphyrin to form a dianion. However, trifluoroacetic acid easily protonates the two free pyrroline nitrogens ($pK_b \sim 9$) to form a dication.

Porphyrins also undergo a number of chemical reaction typical of aromatic compounds. For example electrophilic substitution reaction such as nitration, halogenation, acetylation and formylation are often performed on porphyrins. Only the meso carbons and the β -pyrrolic carbons participate at these reactions.

The α -pyrrolic carbons rarely take part in any kind of reaction.

Porphyrins are also capable to being metallated and demetallated. Almost every metal in the periodic chart has been inserted into the porphyrin macrocycle^[16]. Demetallation can usually be achieved by treatment with acids of various strengths.

Any porphyrin derivative in which at least one of the central nitrogen atoms forms a bond to a metal atom, is called metalloporphyrin; the region containing the nitrogen atoms is called equatorial plane, and the formation or the disruption of the metal to nitrogen bonds, depend by the equatorial coordination chemistry of the metalloporphyrin. Metallo-derivatives could be classified according to either their stoichiometry or geometry.

A wide variety of geometries exist for metalloporphyrins; the geometry of the complex is affected by several parameters, such as the oxidation state and the dimension of the metal ion, and by how many ligands metal needs to reach the correct coordination number. Sometimes coordination sphere goes to completion by taking up an additional donor ligand in the axial position.

Metallation process is a five steps procedures.

The first is a protonation-deprotonation equilibrium, which produces the anionic form of the macrocycle; in the second step an active form of the metal ion, has to be produced. The dissociation of the metal carrier leads to the formation of an active and coordinatively unsaturated species, which reacts with the porphyrinate dianion in the third step. In this way an equatorial plane is formed; nevertheless this process is complicated by all the other reaction, which interfere with the consecutive addition of the four nitrogen atoms to the metal ion.

Bivalent metal ion, preferring square-planar coordination, stops reaction to this stage, because no further steps are required. If the metal ion has a positive charge larger than +2, the total charge of the complex has to be adjusted. The fulfilment of the electroneutrality is the driving force to build up the axial coordination sphere. If the formed square-pyramidal complex is coordinatively

saturated, then the reaction stops, otherwise another ligand is picked up from reaction medium to give a saturated complex with a octahedral geometry.

1.3 Porphyrin derivatives: organic substrates for sensors and materials chemistry

The versatility of porphyrin derivatives to match the requirements of scientists in several field of research, has encouraged the extensive exploitation of these compounds.

There are several factors that promoted the rapid growth of various porphyrins based applications.

First of all the richness, of their chemistry: a wide range of differently functionalized macrocycles could be easily synthesized by the procedures optimized in the second half of the twentieth century^[17,18]. Moreover, the molecular framework could be further modified, in order to finely tune the properties of the molecule to the different purposes. Another noticeable factor is the ability of the macrocycle to act as a tetradentate ligand by the four nitrogens present in the inner core, making it able to coordinate the large part of the elements of periodic table.

Since the coordination of a metal ion, or the interaction of metalloporphyrin with an axial ligand, induce changes in their physico-chemical properties, either porphyrin free base or metal complexes have shown to be very useful substrates for chemical sensors.

Finally porphyrins solid film has a semi conducting behaviour, due to the stacking association and interactions among the macrocyclic aromatic systems.

All these factors played a key role on behalf of porphyrins exploitation either for gas or liquid phase analyses, joined with several transducer systems, such as optical, mass or potentiometric transducers.

A wide number of examples^[19] have been reported in literature; for example, free base has been tested as sensing material for liquid phase sensor, to detect heavy metal ions (Hg, Cd). The coordinative interaction between porphyrins and cations is revealed by the changes in optical spectra.

Mass transducing system (quartz microbalances-QMB, surface acoustic wave-SAW, cantilever), are most common examples of no-selective devices. Every interaction among analytes and receptor molecule units (coordinated metal, aromatic system, peripheral substituents) are transduced in an output signal. The functioning mechanism of QMB is very simple: the piezoelectric quartz crystal (Fig. 1.7), is covered with an organic layer, and its fundamental vibrating frequency linearly varies, upon interaction with volatile molecules in a wide range of gravitating mass, according to Sauerbrey's law:

$$\Delta f = -K_q \Delta m$$

Where K_q is a constant of the quartz, while Δm is the mass variation; larger is the mass gravitating onto the quartz, lower is the oscillation frequency.

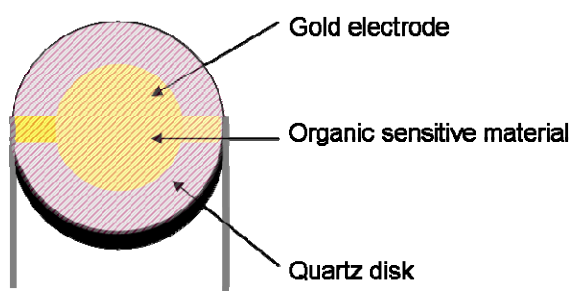


Fig. 1.7 – Quartz micro balance

The low selectivity of QMB based sensors leads to their exploitation in sensor arrays, where each QMB is coated with a different metalloporphyrin; each

metal-complex has a different sensitivity toward a class of compounds (alcohols, amines...).

Based on a similar technology, a liquid phase sensors array has been developed, exploiting potenziometry principle. Porphyrins act as ionophores, dispersed in a polymeric membrane (Fig. 1.8), and form complexes with target ions.

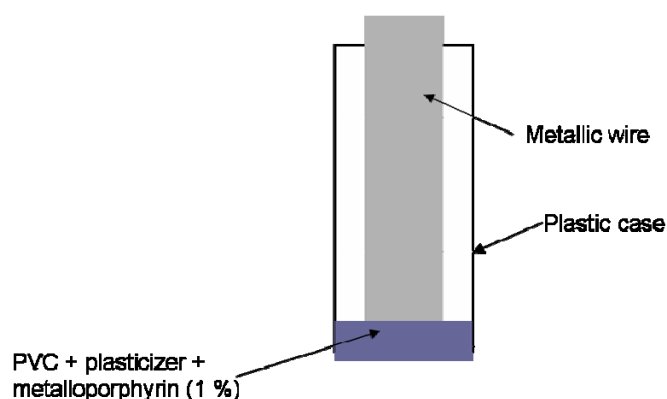


Fig. 1.8 – Ion selective electrode

The complete understanding of the working mechanism of these ion-selective membranes, is not known in detail, however it is possible to assume that porphyrin acts as ionic carrier, giving a response which depends by the activity of the target ions by an intrinsic ion-exchange mechanism, between the organic polymeric and the aqueous phase. The potential we measure is correlated to the concentration of ion in solution, according with Nernst equation:

$$E_M = E_0 + \frac{RT}{zF} \ln a_{I(aq)},$$

Where E_M is the membrane potential, E_0 is a term including all the sample independent potential contributions, R is the universal gas constant, T is the absolute temperature, F is the Faraday constant, z the charge of the ion, and a_I is its activity in solution.

Because this potentiometric sensors are able to respond at a number of different species, is essential to use an array of different sensors, and each of them should have larger selectivity towards one of the analytes present in the examined solution. By processing the experimental data with chemometric methods, likewise occurs for the gas phase sensors previously described, we obtain a chemical images of the samples.

At the beginning of the chapter, the porphyrins optical properties have been shortly described. Of course, these features can be appraised in chemical sensors, either with an extensive spectrophotometer arrangement^[20] or with a synthetic colorimetric setup^[21]. The most innovative measurement technique derives from the combination of these approaches, and it is known as CSPT (Computer Screen Photoassisted Technique, Fig. 1.9)^[22].

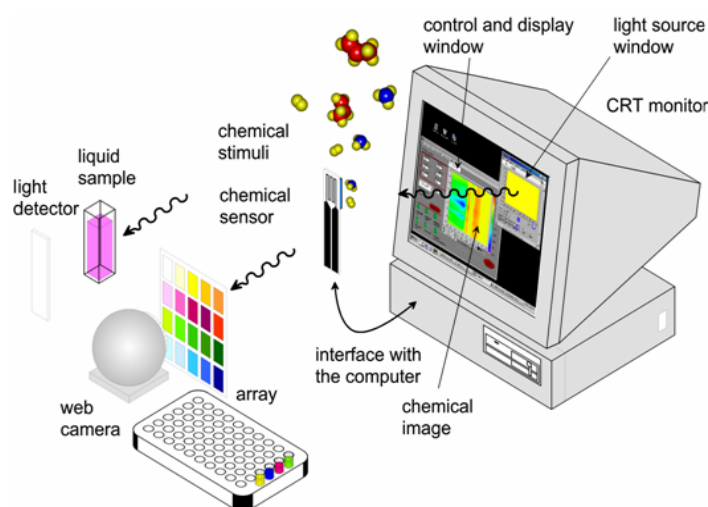


Fig. 1.9 – Schematic representation of CSPT device

In CSPT, the light source is a computer screen (LCD or CRT), while the detector is a web-camera. Computer screens are able to display more than 16 million colours, formed by different weighted combination of primary colours (red, green and blue). During a CSPT experiments the web-cam captures the images of the chromophores employed, under an illuminating sequence provided

by the screen (usually a rainbow of 50 colours). From this video stream, regions of interest (ROI) are selected (the white circles in Figure 1.10), and used to compose substance fingerprints, that are a particular combination of three points (red, green and blue channels), produces by every substance (Fig. 1.10).

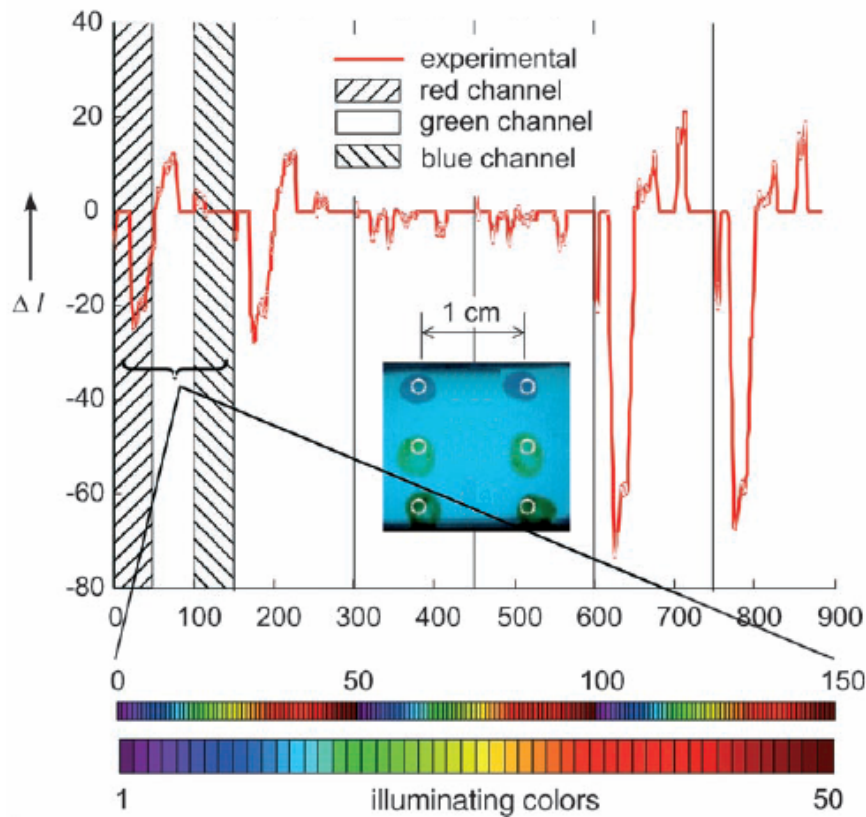


Fig. 1.10 – ROI and typical finger print

The intensity measured, for example, in the red channel of the web camera for an illuminating color i defined by the triplet (r_i, g_i, b_i) , is given by equation:

$$I_{Ri} = \int_{\lambda} [r_i R(\lambda) + g_i G(\lambda) + b_i B(\lambda)] S(\lambda, i) F_R(\lambda) D(\lambda) d\lambda$$

Where $R(\lambda)$, $G(\lambda)$, $B(\lambda)$ are the spectral radiances of the screen primary colours, $S(\lambda, i)$ accounts for the substances transmittance and emission, $F_R(\lambda)$ and $D(\lambda)$ are the filters and the spectral response of the detector. Since this analysis system is based on familiar, portable and ubiquitously diffused devices

(computer screen, web-cam or mobile phones), it can be used to realize a global network for the monitoring of food and environment quality, or for the health diagnoses.

Some transducing techniques have been depicted; however the sensors efficiency depend by many factors: which kind of chemical interactive material has been chosen, the techniques for its deposition, the morphology of the film, the transducing system...

Among those, the morphology of the sensible layer is one of the most difficult parameters to control.

An answer to this problem comes from the convenient functionalization of the macrocycle, that permits a discrete control of the film morphology and thickness. To obtain such a result, is possible to bind the molecules to a solid surface via a covalent linkage. In this way, the orientation of the molecules can be finely controlled, positively affecting the sensor performances. The modification of inorganic surfaces by chemisorption of organic compounds, is an interesting approach to the fabrication of hybrid organic/inorganic materials.

Being enthalpies of interaction for chemisorption process larger than the one of physisorption (usually $\Delta H > 10$ Kcal/mol), thin films so formed have large stability, a noticeable feature for any sensor device.

In Self Assembled Monolayers (SAM), porphyrins bearing thiol group are attached on gold or silver surfaces; porphyrin monolayers are an interesting organic material because of the peculiar photophysical and photochemical behaviour of the well ordered structures.

The advantage to control the structure on the nano-scale level, is one of the feature also in the formation of porphyrin aggregates.

The concept of aggregation is 30 years old: instead to use a covalent atom by atom approach to build large structures, is preferable to drive the formation of supramolecular aggregates by a wide range of weak interactions of different

nature (electrostatic and van der Waals forces, hydrophobic effects, π - π stacking interactions, metal coordination, hydrogen bond).

These weak interactions should allow the spontaneous and reversible formation of large aggregates, with a well-defined structures; in order to obtain these results the interaction among the monomeric units have to be strong enough to provide sufficient stability, but not so strong that first contacts are irreversibly trapped.

This new approach results a good alternative for the chemical assembly of nanostructures^[23]. Noncovalent systems have dimensions between 3 to 20 nm and fill the gap between small molecules and larger nano-objects.

Results and discussion

1.4 Self assembled monolayer: the most straightforward way to monomolecular film

One of the better definitions of self assembly was put forward by Whitesides, who stated that “self assembly is the autonomous organization of components onto patterns or structures without human intervention”^[24].

As such, a lot of processes that take place in day to day life, are guided by self assembly through the weak interactions that make different molecules arrange themselves in three dimensional structures. A popular example of this would be the DNA-helix to a large degree gets its well-known helical shape from numerous hydrogen bonds.

Even though a strict definition of self-assembly does not exist, the self assembly process must be reversible and involve already existing compounds. Reversibility is important, as “self assembly” implies self ordering, which requires the possibility to reverse an interaction in order to find the optimum configuration of the participating parts.

How the components arrange themselves depends on the structure of the components, which opens up the possibility for knowledge-based design through predictions on how a chemical group affects the overall structure.

The forces that decides how molecules assembled themselves are weak interactions, and for these interactions to be fully reversible the molecules are often required to be in a fluid or on a surface.

A special case of self-assembly is when the molecules are ordered in a monolayer on a solid surface, resulting in a so called self assembled monolayer (SAM).

This phenomenon has been known since 1946, but did not really gain any real attention from the scientific community until Nuzzo and Allara reported on the formation of a SAM from disulfide onto gold surface (Fig. 1.11)^[25].

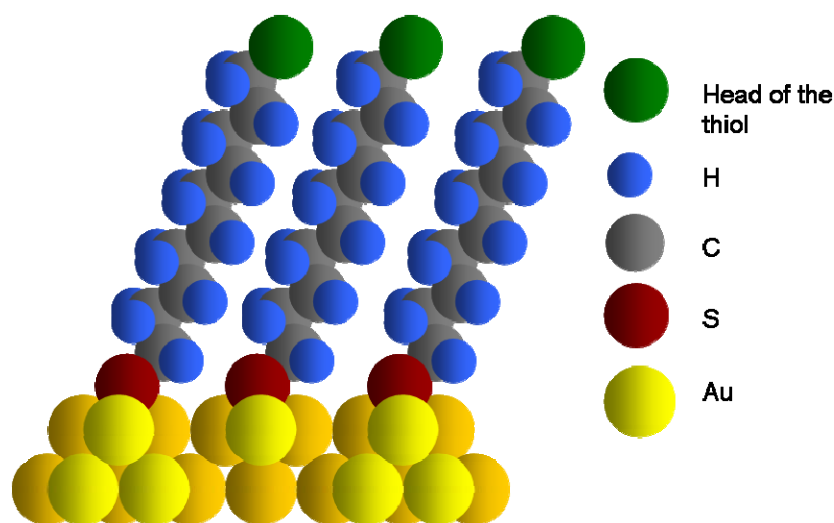


Fig. 1.11 – Pattern of thiols on Au

Ideally the molecules that constitute the SAM are attached to a two dimensional surface and organized in three dimensions using the surface as a fixed grid.

Therefore the molecules do not have the same grade of freedom as in a “true” three dimensional structure.

Often the SAM forming molecules have a specific group responsible of their attachment to the surface. This group is called an anchor group or attachment point. The anchor groups need to be suitable for the type of surface it is supposed to form a SAM on. For the gold surface the most common choice is the thiol moiety, which is justified by the strong gold-sulphur interaction and the concomitant well ordered SAMs. However, there are alternatives to sulphur. One

of the reasons why alternative anchor groups are interesting, is because of the difference in electronic coupling between the adsorbate and the gold surface.

The nature of the anchor group will thus affect the efficiency by which electrons can be transferred between the surface and the adsorbate.

In molecular electronics, the tuning of such properties can be desired. A further reason is that the attachment point is important for how the SAM organizes itself, and that is another characteristic that would be beneficial to be able to control.

How do the thiols bind to the gold surface? The surface consists of close packed atoms with regularly returning ridges every 22 to 23 atoms (Fig. 1.12).

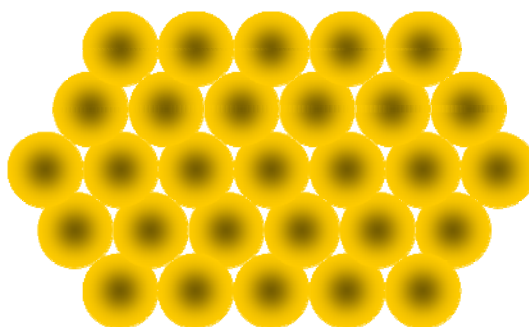


Fig. 1.12 –Structure of Au (111) surface

These are due to the reconstruction that occurs on the surface after and during annealing. A recent study of Maksymovych^[26], states that at very low thiol concentrations they react with and bind to the reconstruction ridges. Even though their experiments are carried out using thiomethane and high vacuum deposition, it is likely that the same type of process occur when a SAM is formed from a solution.

There exist many possible binding sites on the gold surfaces, and most have been proposed at one time or another as the most energetically favourable location of Au-S bond.

This uncertainty stems from the influence that the solvent might have on the close-packing of the adsorbates, because on the gold-sulphur interaction has only been elucidated for relatively short aliphatic SAMs.

When a SAM is grown from a solution, a normal concentration of the adsorbate in the solution is about 1mM or less. Forming a commensurate monolayer on the gold surface from such a solution, does not affect its concentration, which is beneficial because otherwise the SAM formation process could change depending on how many SAM adsorbates had bound to the surface.

However, it is feasible to form SAMs from solution with as low concentrations as 1 μ M, but the formation processes then takes longer time.

At normal concentration the SAMs are usually formed during 12-20 hours, where the first is a fast (milliseconds to minutes) attachment to the surface and then a slow reorganization takes place (Fig 1.13).

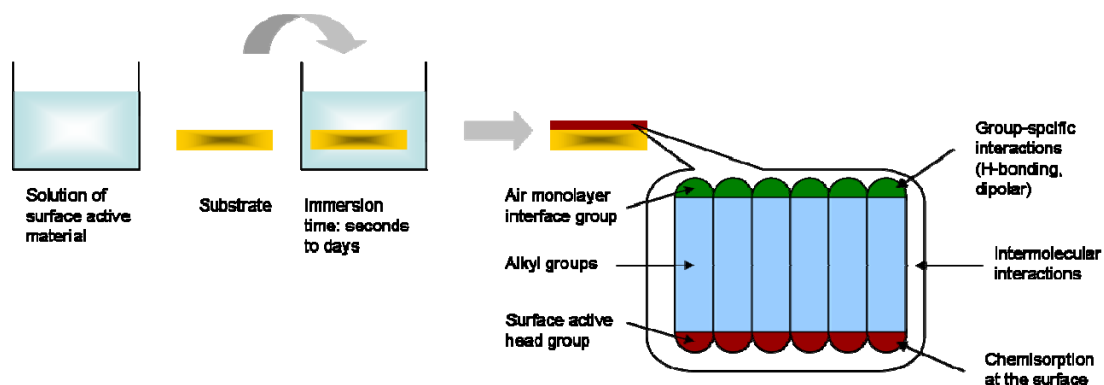


Fig. 1.13 – Mechanism for SAM deposition

During the reorganization the SAMs increase in density, as more adsorbates bind to the surface. The SAM adsorbates equilibrate with the solution and the SAM thereby attains its characteristic high degree of order.

This reorganization is the actual self-assembly and therefore the gold substrates onto which the SAMs are grown are most often immersed into the SAM solution for more than 12 h.

A very common solvent for the self-assembly is ethanol, but alternative exist such as DMF, THF, toluene. A suitable solvent should dissolve the SAM forming molecules, but not too well. SAMs grown from solvents in which the molecules have a relatively low solubility, show fewer defects than those grown from a more efficient solvent.

The optimal solvent is thus the one that fully solvates the adsorbates, but not so well that it causes an increased amount of defects.

One of the advantages with using thiols as the attachment group, is the stability of the formed SAM. The most common degradation pathway for a thiol SAM is the oxidation of the sulphur-gold bond to a sulfinic or a sulfonic acid^[27].

Oxidation during the actual SAM formation is a minor problem, because the oxidized species readily dissolve into the solvent and become replaced with a new thiol group.

Even though this is the case, it is common practice to keep the environment as inert as possible during the SAM formation.

When the SAM is finished and has been dried, this “self-healing” is no longer possible, and therefore there are some precautions that must be considered. First of all the SAM is sensitive to UV-light, especially in combination with oxygen. To counter this, the sample should be placed under inert atmosphere in the dark as soon as possible after completing the SAM formation. In an ambient environment, in the absence of light, degradation products can be detected after six hours. These products are probably the results of reactions with ambient ozone in the air^[27]. It is very likely that properly shielded from these degradation sources, the SAM stays intact for much longer periods of time than six hours. Sometimes it is desirable to make a SAM composed of more than one type molecule as adsorbate. This can be achieved in several different ways and the ensuing SAM is called a mixed SAM.

Three possible approaches to this type of SAMs exist (Scheme 1.1). One method is to have a mixture of the desired adsorbates in the SAMs solution. The

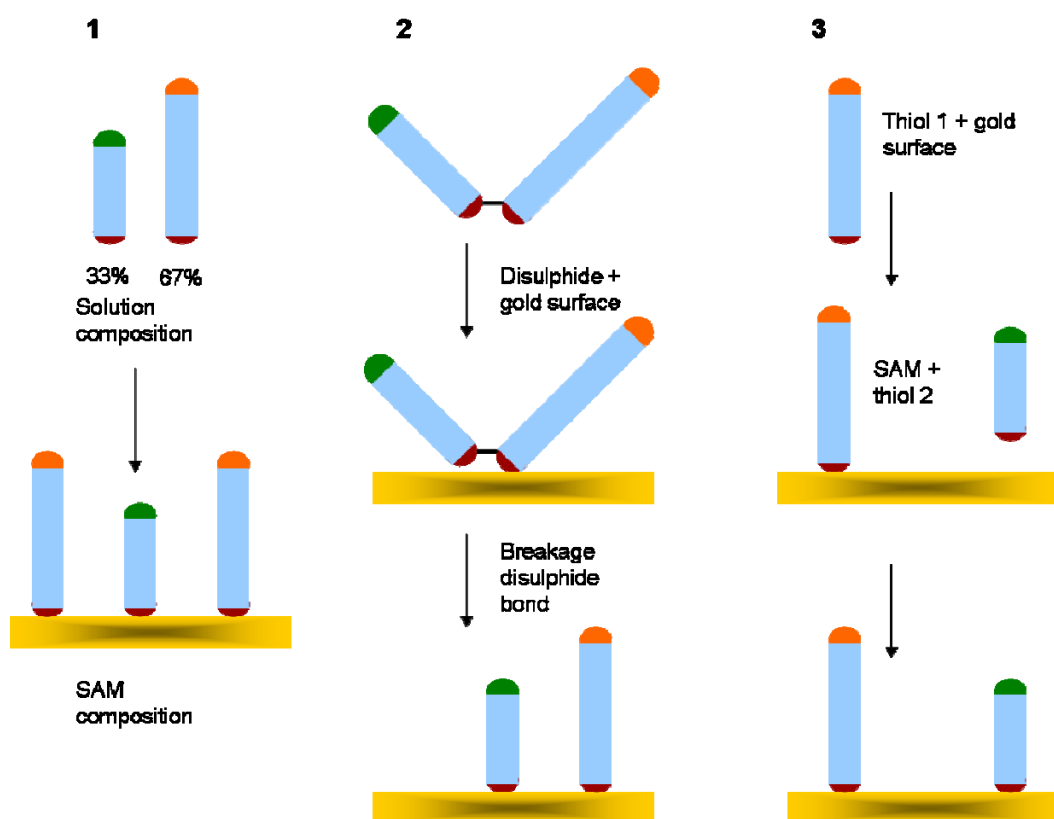
composition of the ensuing SAM will reflect, but not necessary exactly match, the relative concentrations of the SAMs adsorbate in solution.

The choice of solvent and the size of the SAM adsorbates are factors that will affect the composition.

A second approach is to use an asymmetric disulphide as the SAM forming molecules. Upon attachment to the surface, the disulphide bond will break and both moieties parte will attack as if they had been thiol. The result will be a 1:1 mixture of the two compounds, well intermixed with each other. However, exchange with the solution can affect the composition so that it moves away from the 1:1 ratio^[28].

When working with aliphatic SAMs the thiol with the longest chain is enriched in the SAM.

A third option is to make an ordinary, neat, SAM and put it in a solution containing the SAM adsorbate one wishes to mix it with.



Scheme 1.1 – Techniques for mixed SAMs formation

Exchange between the SAM and the solution will introduce the new thiol, where the ratio between the two adsorbates on the surface will depend on the solvent and the immersion time.

The molecular processes and preparation methods described *vide supra*, are characteristics shared by most thiol SAMs on gold, regardless of the type of molecule attached to the anchor group. However it is very likely that the gold-sulphur interaction and how it affects the gold surface structure, are the same for both aliphatic and aromatic systems.

The kinetics for the formation of SAMs with aromatic backbone do not differ much from the kinetics for aliphatic ones^[29].

Further, in analogy with aliphatic SAMs, the length of the adsorbate, i.e. the conjugated system, affect the close packing^[30,31]. Longer adsorbates form SAMs that are more ordered and with fewer defects. The adsorbates of the SAM are tilted with respect to the gold surface. This angle is called the tilt angle, and often defined with the Greek letter θ . The tilt angle naturally correlates to the thickness of the SAM, which is often measured and given as an indication of the quality of the packing. The plane of the molecules can also be twisted relative to a surface made up by surface normal and the molecular long axis. This angle, the twist angle, is often defined with the Greek letter ψ .

1.4.1 Synthesis and characterization of porphyrin-based SAM

So far there have been several attempts to organize molecules in a well ordered monolayer; one common way is to coat a surface using Langmuir-Blodgett technique (LB). However this procedure works with amphiphilic molecules, having a polar and hydrophilic head and a non-polar, hydrophobic tail. The instability of so formed film is a drawback of LB procedure.

Self Assembled Monolayer (SAM) guarantees the formation of ordered structures, such as LB technique, but provided of increased robustness.

The synthesis of a suitable molecule, the deposition onto gold and the characterization of the so formed monolayer, were the purpose of the research I carried out during the seven months spent at Linköping University, under the supervision of professor Peter Konradsson of Organic Chemistry division, and of professor Ingemar Lundström of Applied Physics division.

Of course the molecule we want to attach on the solid surfaces, has to be functionalized with an anchor group. The best choice is represented by gold for the surface and sulphur atom as anchor group.

Having in mind to control as better as possible the morphology of the monolayer, we decided to use a long spacer to bind the thiol group to the porphyrin (Fig. 1.14).

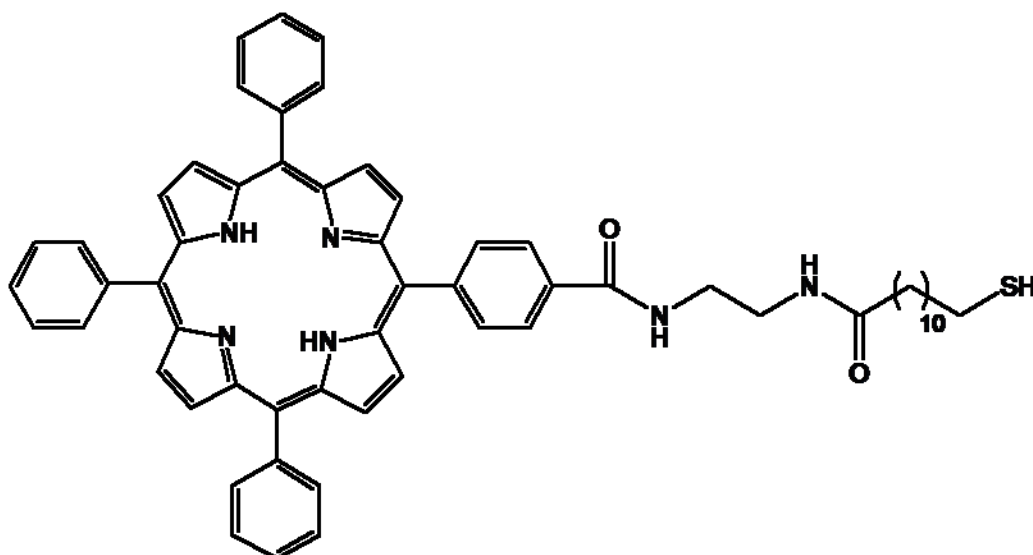


Fig. 1.14 - Structure of the porphyrin for SAM

The spacer affects the order of the SAM in different way: the amides increase the stability by H-bond they can establish each other, resulting in a closest packaging of the porphyrins on the top of the chain.

The structure of the porphyrin monolayer also depends by the length of the alkyl chain: the structure of the adsorbed alkylthiol monolayer is dictated by interactions between neighbouring alkyl chains. With the polar S atom bonded to

the Au surface, the nonpolar alkyl chains pack in a dense arrangement to maximize van der Waals forces, which strongly contribute to the formation of the monolayer. This arrangement generates densely packed layers which are believed to be crystalline-like, enhanced by the increasing in length of the alkyl chain. The magnitude of weak interactions, liable for high order of film morphology, is greater if more than 10 carbons are present in the lateral chain.

Moreover, exists a dependence^[32] of the even and odd number of methylene groups on the peripheral position.

The first bond (S-Au) is perpendicular to the surface; assuming that the spacer with even number of the methylenes is oriented at an angle of 30° from the surface normal, the porphyrin plane is tilted heavily to the gold surface.

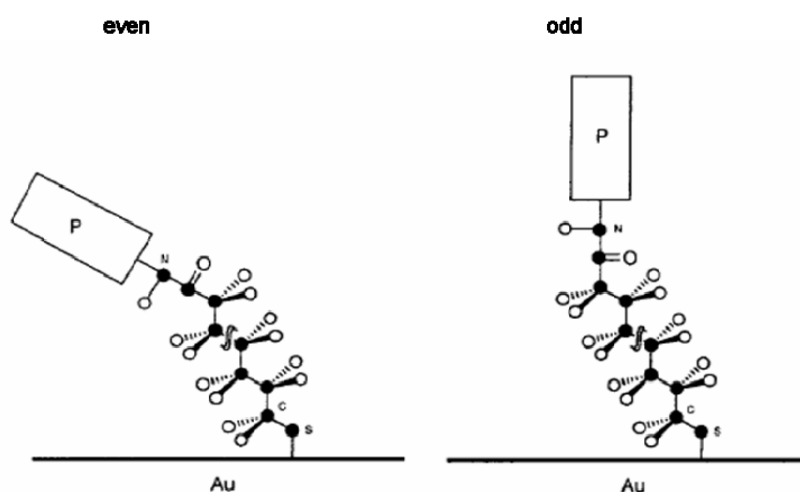


Fig. 1.15 – Effect of methylenes number on molecule orientation

On the other hand, the porphyrin is almost perpendicular to the gold surface when the spacer has the odd number of the methylenes (Fig 1.15).

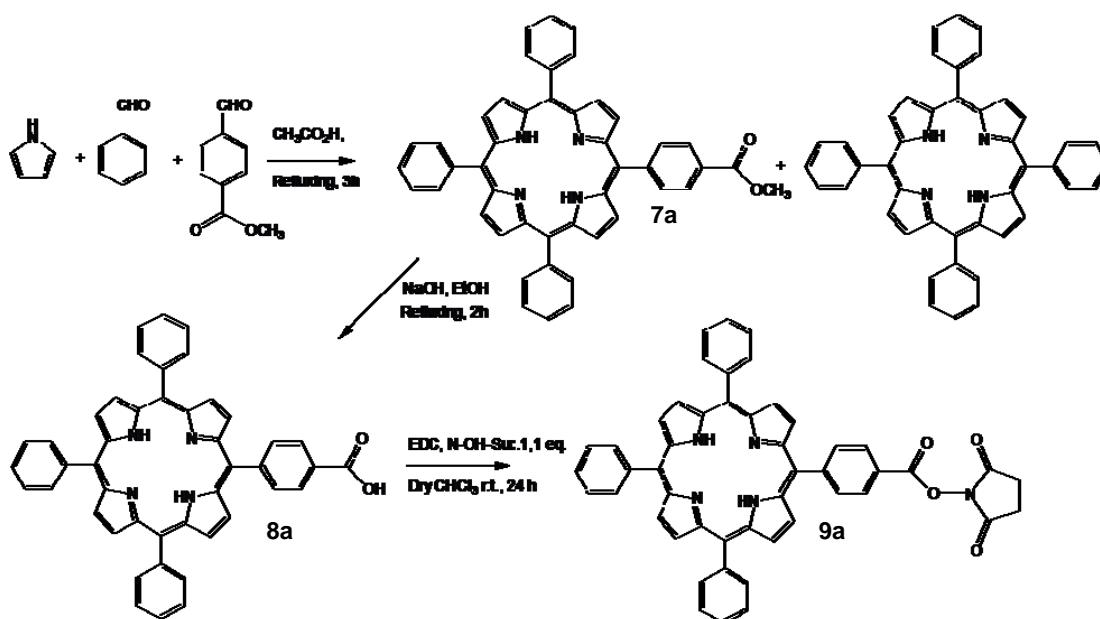
All these hypotheses are correct assuming for alkyl chain an all trans conformation that should be the most favourable condition; being every amide bond planar, they have no effects on the final orientation of the macrocycles.

Since we totally have an odd number of methylenes (13: 11 in the long chain linked to gold, and other 2 methylenes as spacer between the amides), we

assumed that porphyrins likely arrange themselves in a disposition almost orthogonal with respect to the surface. Moreover, we choose a long chain because previous experiments^[32] conducted to study the effect of the chain length on the structures on porphyrins-based SAM, suggested, by analysis of the Soret band intensity, that the amounts of the adsorbed molecules become saturated when 7 carbons stay in the peripheral chain. When the chain has less than 7 carbons, the absorbance at the Soret band increases gradually with an increase in the number of methylenes.

The instrumental characterization has been done to confirm our hypothesis.

The synthetic pathway for the synthesis of the target molecule **14a** is shown in scheme 1.2: reacting a ten fold excess of benzaldehyde and methyl-4-formylbenzoate with pyrrole (total amount of the aldehydes is equimolar with pyrrole), leads to the formation of TPPorH₂ and *p*-CO₂CH₃TPPorH₂ (**7a**) (Scheme 1.2).

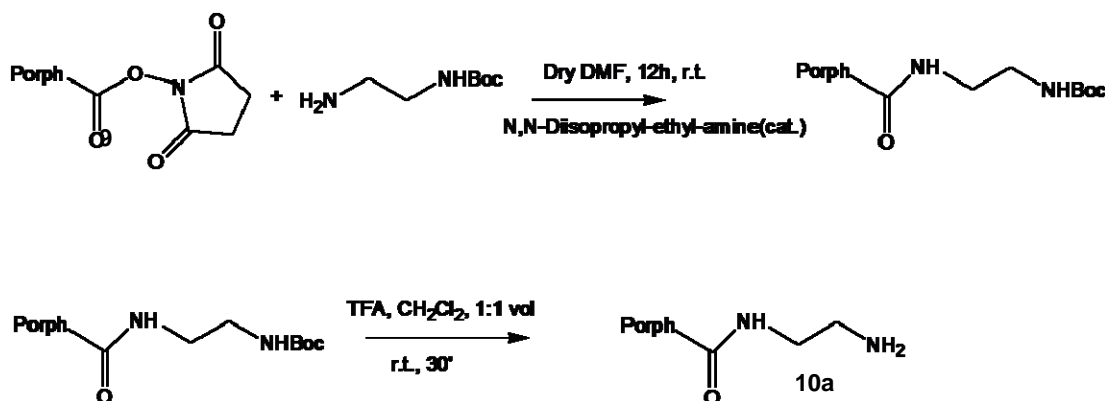


Scheme 1.2 – Synthesis of the activated porphyrin

Even if we needed of the acidic derivative of the porphyrin, we preferred to start from the ester group, due to the easier separation of the *p*-CO₂CH₃TPPorH₂ from TPPorH₂ with respect to **8a**; porphyrin bearing carboxylic group was

obtained by alkaline hydrolysis in refluxing ethanol^[33]. **8a** was then converted in **9a**^[34] by activating the $-\text{CO}_2\text{H}$ moiety with EDC and N-hydroxy-succinimide in dry chloroform under inert atmosphere; the activated species **9a** was used for the coupling with an amine.

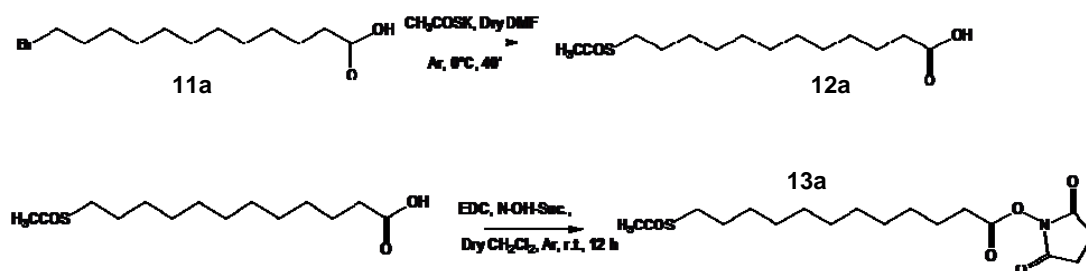
The chain on porphyrin derivative was initially extended coupling **9a** with 1,2-diaminethane; one of the $-\text{NH}_2$ of this reactant is protected with a *tert*-butylcarboxylic ester, to avoid the concomitant reaction with two porphyrinoid molecules. Protecting group was easy removed in CH_2Cl_2 -TFA mixture. The so formed pendant-functionalized porphyrin (**10a**) was reacted with a suitable carboxylic acid previously synthesized^[35] (Scheme 1.3).



Scheme 1.3 – First coupling and deprotection of porphyrin derivative

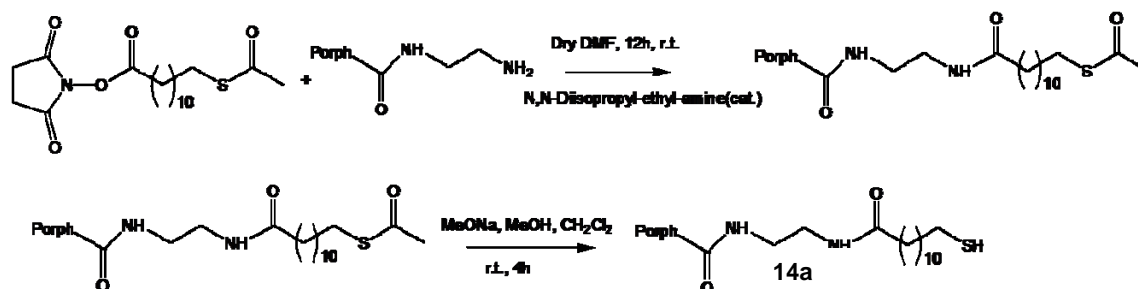
12-Bromo-dodecanoic (**11a**) acid was reacted^[34] with potassium thioacetate to insert a sulphur atom replacing halogen atom; we did not directly insert a thiol group because of its prominent sensitivity. Indeed it is quickly oxidized, making impossible the subsequent reaction with gold.

12-Mercaptoacetyl-dodecanoic acid (**12a**) was then activated (**13a**), with the same procedure used on porphyrin^[34] (Scheme 1.4), and **13a** used for the second amide bond formation in dry DMF, with a bulky base as catalyst (Scheme 1.5).



Scheme 1.4 – Synthesis of suitable peripheral substituent

Hydrolysis of thioacetate to obtain **14a**, may be carried out either in alkaline or acid conditions, but we preferred to use an alkaline mixture because of the instability of amides toward acidic agents.



Scheme 1.5 – Pathway for the target molecule

Compound **14a** was finally characterized by ^1H NMR and mass spectrometry (Fig. 1.16), where traces of a dimer product ($M/Z^+ = 1832$) were detected.

Dimer formation does not impede the binding process on gold because the cleavage of S-S bond is followed by the formation of the more stable Au-S bond.

After the synthesis of the target molecule, the second step was the optimization of the condition for SAMs growth.

Several parameters can be tuned, in order to obtain an organic film with the desired features.

Ethanol is commonly used as solvent to make SAM, but the poor solubility of our molecule in ethanol prompted us to choose THF; we didn't use halogenated

solvents (CH_2Cl_2 , CHCl_3) because they have a larger solubilising power, and because of their low vapour pressure.

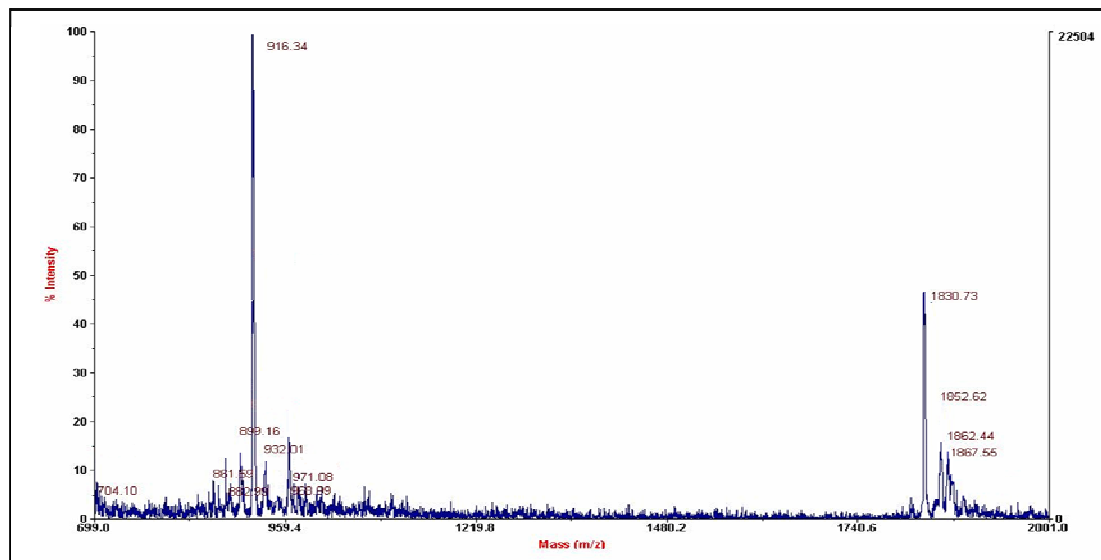


Fig. 1.16 – MALDI spectra of porphyrin bearing thiol group

Ethanol is commonly used as solvent to make SAM, but the poor solubility of our molecule in ethanol prompted us to choose THF; we didn't use halogenated solvents (CH_2Cl_2 , CHCl_3) because they have a larger solubilising power, and because of their low vapour pressure. A rapid evaporation of the solvents does not allow to maintain a constant concentration of the solution with binding molecule, negatively affecting SAMs formation. To avoid external contamination, the gold surfaces were accurately cleaned up with an alkaline solution, to remove any traces of organic material; surfaces were then rinsed with water, ethanol (to remove water) and THF (to remove ethanol) before the incubation. Also the strength of the alkaline solution is a parameters that has to be controlled, because affects the final result. It has been demonstrated that it could modify the dimension of the grains^[36].

Incubation solution was prepared dissolving porphyrins in THF till a concentration of 50 μM , then the surfaces dipped inside for two days, and stored

in the dark; at the end of the incubation time, the excess of organic material was removed cleaning the surfaces by sonicating the samples in fresh THF two times for some minutes.

Many techniques exist to characterize SAMs, the most immediate of those is ellipsometry, which measures the change in polarization state of light reflected from the surface of the sample; because this value is different between neat gold and metal covered with an organic substance, is possible to determine how thick the layer is.

The results of the experiments showed that the thickness of the film is in the range 30-35 Å. A very small effect can be adduced to the initial concentration: when solutions 5 times higher or lower in concentration were employed, the thickness was in the same range value. No any effect was detected changing the incubation time (24-48-72 hours), while little variations can be attributed to the solvent chosen: although the thickness of the film is in the same range, toluene leads to a thinner layer (less than 30 Å), while CH₂Cl₂ leads to the formation of a larger film (> 35 Å).

Surprisingly, film Zn-porphyrin based, showed a value a few Ås shorter than those of free base (from 30 to 23 Å); it happens either using already formed metal complex for the SAM synthesis, or if Zn is inserted after macrocycle deposition on the gold surface. Otherwise cobalt ion did not show the same effect (thickness = 29 Å). Molecular mechanic calculation asserts that porphyrin derivative is 36.5 Å long, if we consider S atom and C-4 of the phenyl group on the other side of the macrocycle as extremities of the molecule. The data obtained for our samples, showed that the free base is slightly tilted with respect to the surface; in this way a π - π interaction among the aromatic ring of the porphyrins is possible, so enhancing the stability of the SAM. The lower value for Zn-porphyrin based film, can be explained in term of an interaction between Zn (soft Lewis acid) and nitrogens of peripheral amides (soft Lewis base), but

unfortunately we don't have any other experimental data to confirm this hypothesis.

Solution UV-vis spectroscopy displays that Soret band of free base and of some metal complexes, lies in the range 410-420 nm; edge to edge or face to face aggregates cause, respectively, a red or a blue 10-15 nm shifting of Soret band with respect to what happens for monomeric unit.

UV-vis spectra of the SAMs, recorded in reflection mode, showed distinctly the presence of free base or metal complexes (Fig. 1.17), such as confirmed by the different number of the Q bands; there was no relevant shift of Soret band in the samples we examined, which was usually located around 450 nm.

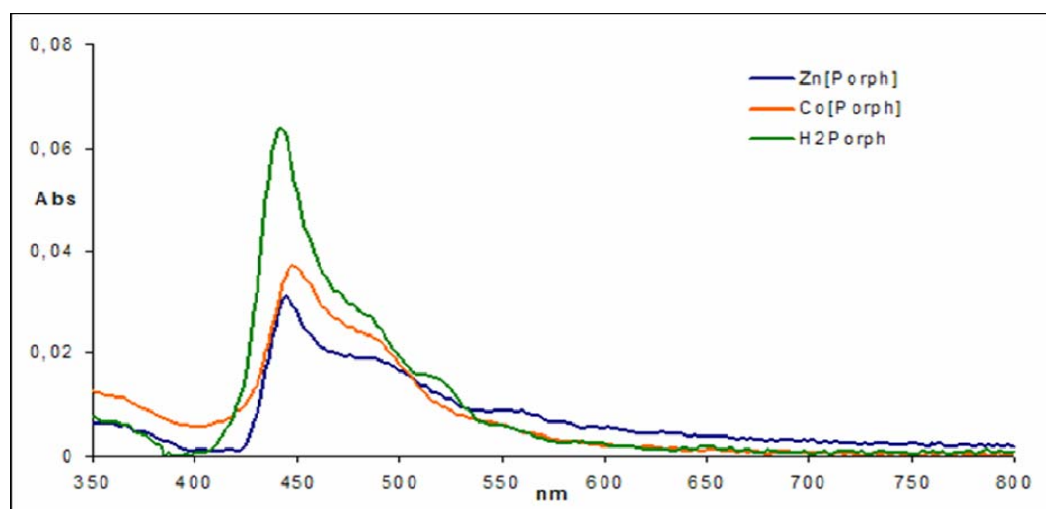


Fig. 1.17 – UV-vis spectra of free base, Zn and Co complexes

Such a red shift is probably due to two factors: the formation of J type aggregates, and the interaction among the molecules in the solid state. These effects reinforce each others, giving as final result the peaks around 450 nm. However the Soret band is quite shaped, showing the absence of disordered aggregates, which would have caused a serious broadening of the absorption bands. Despite the data obtained by UV-vis spectrometry are in favour of a well defined, J-type aggregate, by the analysis of the others experimental data, we did

not obtain confirmations about this first hypothesis, but we rather thought to the formation of a low ordered stacked structures.

More difficult was the interpretation of IRAS (Infrared Reflection-Absorption Spectra) (Fig 1.18, 1.19).

All the signal referred to the macrocycle were extremely weak, if compared with a classical IR spectra recorded with a porphyrin dispersion in a KBr pallet, where a most favourable concentration of the samples is present; the strongest signals appearing at 2919 and 2852 cm^{-1} , suggest a slightly amount of gauche defects along the alkyl chain.

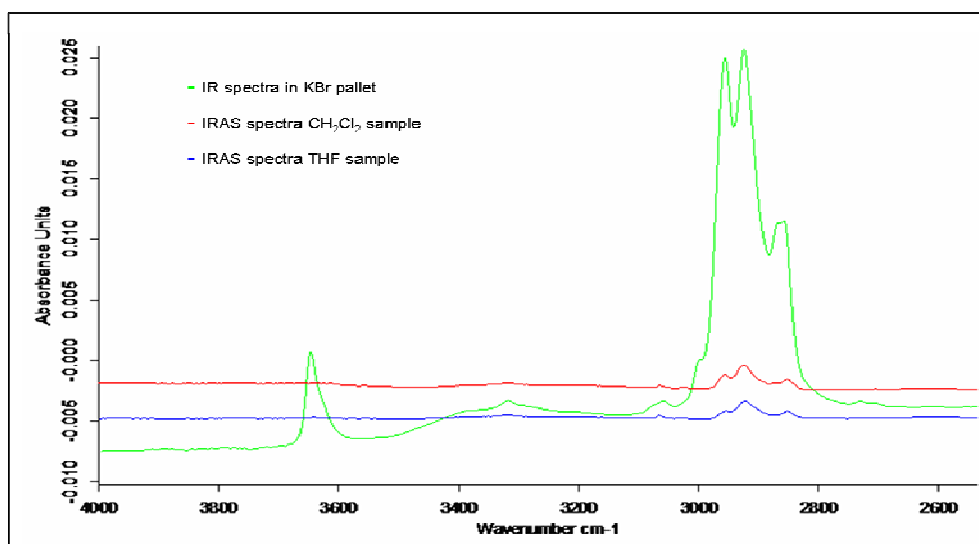


Fig 1.18 – IRAS spectra in the higher frequency region

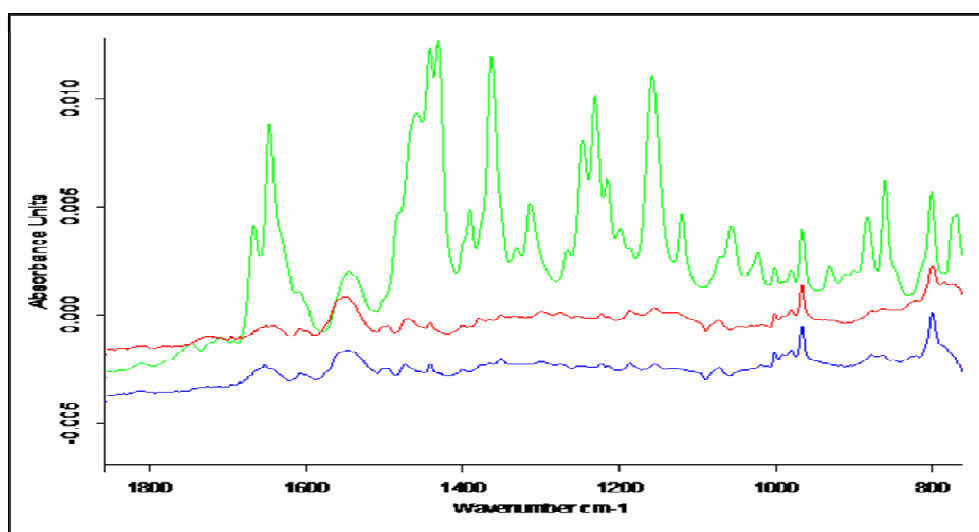


Fig. 1.19 – IRAS spectra in the lower frequency region

All the signal referred to the macrocycle were extremely weak, if compared with a classical IR spectra recorded with a porphyrin dispersion in a KBr pellet, where a most favourable concentration of the samples is present.

The strongest signals appearing at 2919 and 2852 cm^{-1} , are indicative of crystalline like packing of the alkyl chains. This reasoning in turn strongly implies all trans conformation sequences, because just a slightly amount or none gauche defects along the alkyl chain is consistent with high packing densities.

Since in IRAS analysis only vibrations having transition dipole moments oriented orthogonal to the surface were excited, and the absence of vibrations at about 1650 cm^{-1} characteristic for amide linkages implied alignment of the carbonyl group parallel to the surface, as it should be for a spacer with an odd number of methylenes (Fig. 1.15). However, because of the weakness of all other peaks, and because of the overlapped signals referred to the porphyrin and to the chain, we could not do any more accurate assumption about the disposition of the molecule.

Density and degree of order of the SAMs were analyzed also by contact angle goniometry (Table 1.1): it measures the angle between a droplet of a desired liquid, often water, and the SAM on the substrate surface; the tilted red line shown in figure 1.20 individuate the measured angles. The data gives information on how hydrophilic or hydrophobic the SAM is.

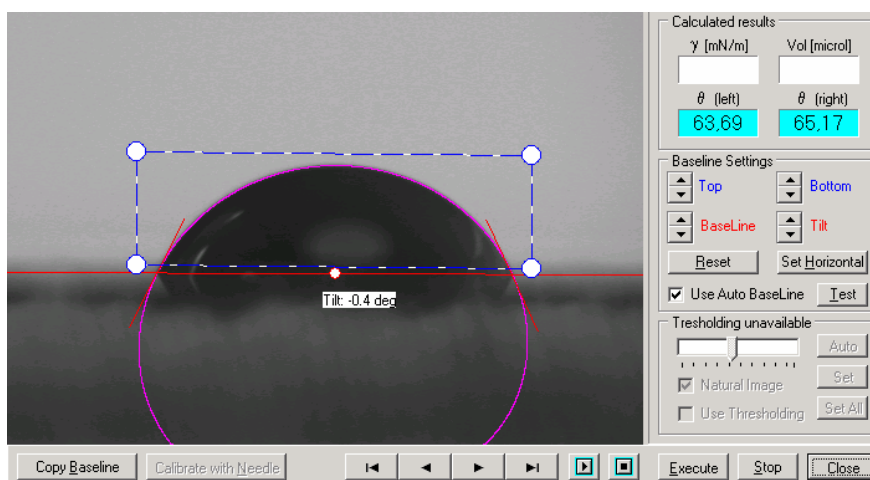


Fig 1.20 - Example of contact angle goniometry measurement

It is the physical properties of the topmost 3-10 Å of the SAM that determine the contact angle^[37], but this is, in turn, dependent on the surface smoothness and the SAM density. The angle was determined analyzing the pictures collected in three phases: when the drop is forming (advancing angle), when the drop is stationary on the surface (static angle), and when it is removed (receding).

The advancing and receding water contact angles (85°/65°) show the surface of the film is at the limit of, actually it is more likely hydrophilic.

This phenomena could indicates a low level of compactness of the layer, such as the porphyrins have formed local aggregates by interacting each other, allowing gold uncovered in some points. However it was possible to detect the hydrophilic character of the film, only carrying out the measurements as soon the samples were drawn by the solution.

Gold quickly reacts with environmental organic impurities, restoring its hydrophobicity.

The low order has been confirmed by contact angle hysteresis, which points out a significant degree of disorder existing in the SAM.

	Time	C.A.-Left side	C.A.-Right side
Advacing-1	0,000	82,062	81,608
Advacing-2	0,891	82,542	82,054
Advacing-3	1,893	81,945	81,996
Advacing-4	2,884	82,148	82,239
Advacing-5	3,885	81,997	81,678
Static-1	24,615	57,458	59,532
Static-2	25,567	57,199	58,801
Static-3	26,568	57,033	58,425
Static-4	27,610	56,850	57,931
Static-5	28,611	57,004	57,865
Receding-1	42,371	69,574	68,647
Receding-2	43,372	69,514	68,650
Receding-3	44,374	69,613	68,764
Receding-4	45,375	69,421	68,688
Receding-5	46,377	69,346	68,787

Table 1.1 - Contact angle goniometry values

A possible explanation comes from the following consideration: the area of an alkyl chain is estimated to be about 20 \AA^2 , whereas that of the porphyrin is around 100 \AA^2 . This means that if the alkyl chains were all-trans, even tilted at an angle of 30° from the surface normal, there should be a significant free volume in the alkyl spacer region of the SAM.

Considering the results so far obtained, suggest, with a good level of confidence, that the structures of the monolayer are controlled by the interactions among the porphyrins as well as the length of the spacers containing the methylene chains.

The samples were also checked by atomic force microscopy (AFM), where the surfaces seem to be homogeneously coated. More accurate results can be obtained by SAM microscopy: this technique has a larger resolution, allowing to see how the single molecules arrange themselves, and confirming the orientation of the organic layer by the trend of the V/I curve.

1.5 Porphyrinoids supramolecular aggregates

Self assembled arrays made by highly-ordered units, have potential application in several field of research^[38], because the supramolecular architecture so generated, exhibits different and usually enhanced properties with respect those of the single molecules.

Porphyrins and metalloporphyrins aggregation has been studied for several decades^[39].

The results about the first investigation of protoporphyrin behaviour on water surface, displayed that molecules are packed in a face to face way and vertically oriented. In this manner, the polar carboxylic acid groups are in the water, while the vinyl groups remain far from water. Afterwards, similar results were found

by other groups, leading to the formulation of a basic assumption in virtually all the aggregation studies for both porphyrins and metalloporphyrins, that is the “face-to-face” model. Further investigation allowed to clarify the different geometries presented in porphyrin aggregates.

Porphyrins, may be arranged in different ways in an aggregate structure, because of the strong electrostatic interactions between the electronic clouds of the different macrocycles. The aggregates are usually classified into three types^[40,41]:

- J-aggregates that are “edge-to-edge” structures;
- H-aggregates that are “face-to-face” structures;
- non-specific aggregates, having middle features between J and H types.

Recently, theoretical studies have shown that, the simple picture of a π -system as a sandwich of the positively charged σ -framework between two negatively charged π -electron clouds, accounts well for the observed interactions between π -systems. It is a π - σ attraction rather than a π - π electronic interaction which leads to favourable interactions, that determine, together with van der Waals forces, the preferential cofacial arrangement of porphyrins both in solution and crystals. The presence of a metal atom coordinated into the inner core of the macrocycle, does not alter the geometry of the aggregate, and enhances the magnitude of the π - π interaction: the greater the intramolecular polarization between the porphyrin and the metal, the stronger is the π - π interaction between two porphyrins, while coordination of the metal by a ligand reduces the magnitude of the π - π interaction in metalloporphyrins and generally leads to disaggregation.

The aggregation phenomena are often accompanied by UV-vis spectral shifts, such as hypsochromicity, bathochromicity and broadening of the starting band, or

the appearance of new spectral bands due to the excitonic interactions between the chromophores (Fig. 1.21).

These changes can be explained using a vectorial picture and considering the interactions between the electrostatic dipole moments of the molecules. Two extreme cases exist, where the interaction is between two monomeric units having dipole moments lying along the molecular plane.

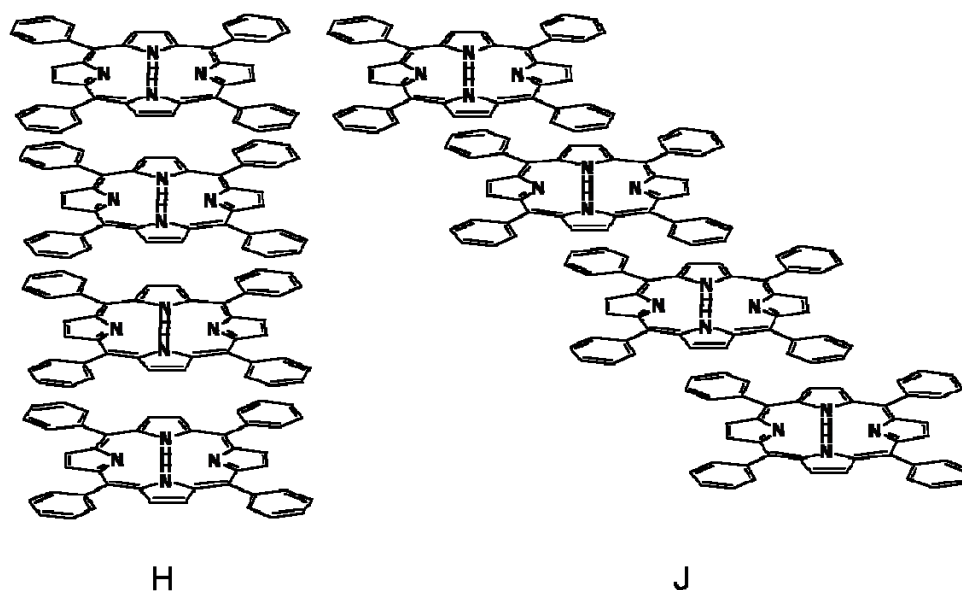


Fig. 1.21 – Geometries of porphyrin aggregates

For H-aggregates two types of alignments are possible (Fig. 1.22). The “orientation mode” **A** corresponds to the transition at higher energy because the dipoles coupling provides for this event an alignment “in-phase”, determining repulsion between partial charges of the same sign: the resulting vectorial sum is not equal to zero.

The “orientation mode” **B** provides a more favourable coupling (that is at lower energy), but dipole moments cancel each other, resulting in a virtually “zero” dipole moment vector.

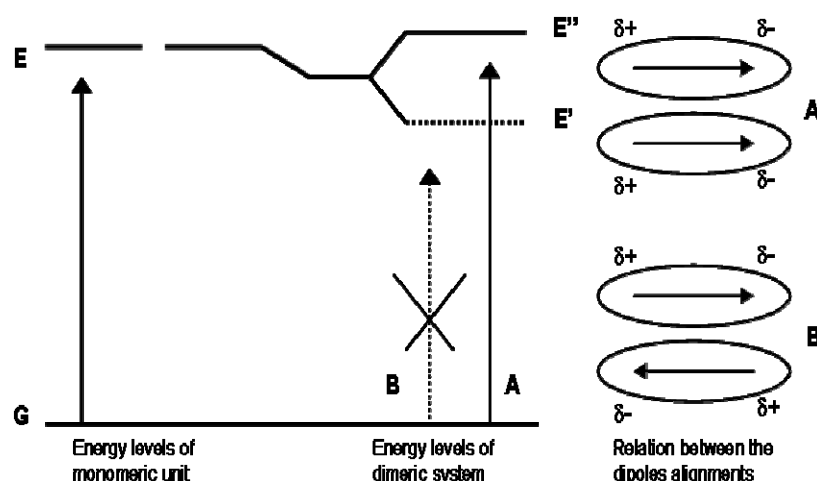


Fig. 1.22 – Orientation of dipole moments of two porphyrins forming H-aggregate.

The ΔE_{tran} is larger for the dimer resulting form compared to the monomer, because the arrangement of the dipole moments of monomers within the dimeric system is energetically unfavourable.

This leads to the blue-shift of the Soret band of the aggregate compared to the one of the monomeric unit.

An opposite situation concerns J-aggregates, because the dipole moments of the monomers are parallel and lie along the line joining the molecular centres (Fig. 1.23). Again, two types of alignments are possible for the transition dipoles.

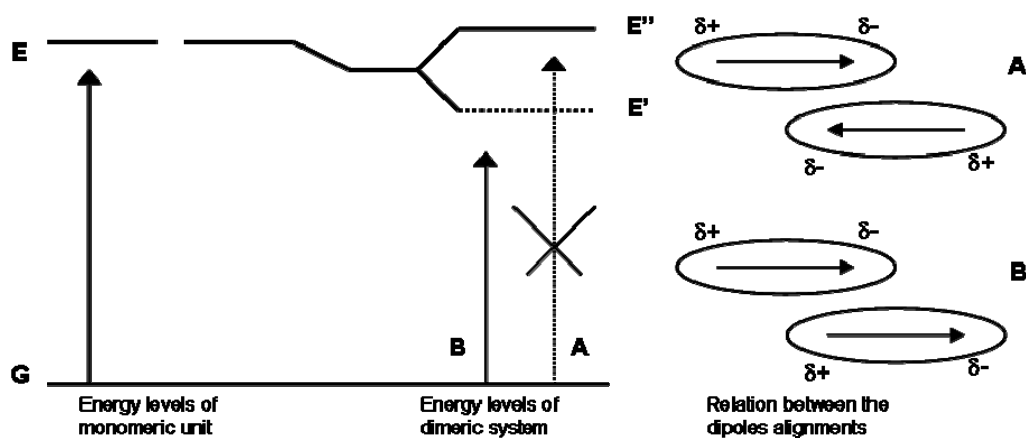


Fig. 1.23 - Orientation of dipole moments of two porphyrins forming J-aggregate.

The “aggregation mode” **A** corresponds to the transition at higher energy because the dipoles coupling provides for this event an alignment determining repulsion between partial charges of the same sign: the resulting vectorial sum is zero. In the orientation **B** this vectorial sum is not zero and coupling results energetically more favourable (that is at lower energy).

The ΔE_{tran} is smaller for the dimer resulting form compared to the monomer, and leads to a red-shift of the Soret band of the aggregate compared to the single unit of porphyrin.

With respect to intermediate geometries featuring by non-specific aggregates, both transitions can be partially allowed, so that the electronic spectrum is characterized by the presence of two bands simultaneously: the former at a blue-shifted wavelength and the latter at a red-shifted wavelength in the aggregate relative to the monomer, or a general, less specific, broadening of the starting band resulting from the aggregation.

Because the possible implication in biological systems, aggregation process is particularly relevant when occurs in aqueous environment. However most native or synthetic porphyrins are poorly water soluble, so it is necessary to increase their affinity to water by functionalization of the macrocycle with a charged or polar group. Tetrapyrrole bearing sulfonate, phosphonate or pyridyl units, are employed to study the behaviour of porphyrin derivatives in aqueous solvent. The total charge of these molecules is pH depending, because protonation-deprotonation equilibrium process involves the inner nitrogens and the peripheral substituents. In this way their solubility may be increased or decreased, triggering the aggregation process.

One of the most important element able to promote the aggregation, is the interaction among groups with different charge. Purrello^[42] showed that a positively charged matrix (polylysine) interacts with porphyrins bearing negative charged groups; once a critical porphyrin concentration has been reached, van der Waals and solvophobic forces induce their aggregation.

The normal fluorescence of the porphyrin monomers, is quenched by the aggregation process. The changing of fluorescence emission is a measure of the occurring aggregation, and it could be modulated by controlling pH.

The interaction with a matrix, is a relevant features when the matrix is a biopolymer such as DNA or RNA; in this case the own fluorescence of the chromophore becomes a useful tool for the investigation of intracellular environment.

We have recently observed that the spontaneous deposition of ordered self-assembled porphyrin films can be obtained by functionalization of porphyrin with a peripheral cationic substituent. This group infers to the macrocycle an amphiphilic character, leading to the formation of mesoscopic ordered structures upon aggregation process^[43].

Macrocycles with charged substituents are able to interact with a opposite charged surface, but they can also interact each other. The electrostatic interaction occurring between oppositely charged macrocycles, has attracted our interest because this process is involved in the formation of a structure with a well defined geometry, such that nanotube shaped^[44], where the concomitant presence of electrostatic, van der Waals, hydrogen-bonding and axial coordination forces, drives the shape and the stability of the final aggregate.

Among the different tri-dimensional arrangements of molecules, leading to the formation of supramolecular system, we focused our attention on structures nanotube-like; in particular we were interested to the effect of the surface to volume ratio, because changing it, the probability of interaction with the analyte molecules increases, and consequently the sensitivity of the device.

However, ionic self-assembly is only one of the procedure developed for the construction of porphyrins nanotubes; a different method has been developed by Kojima et al.^[45] (Fig. 1.24).

He choose, as building block, a saddle distorted metallo-porphyrin; the aggregation process is driven by the π - π interactions of the macrocycle and the

molecular structure is reinforced by an internal frame based on metallic oxo-cluster.

In details, dodecaphenylporphyrinato-Mo(V), having a curved surface due to both the steric hindrance of the peripheral substituents, and the presence of a high valent metal ion, has been crystallized in presence of methanol, giving an assembly with a nanotube shape.

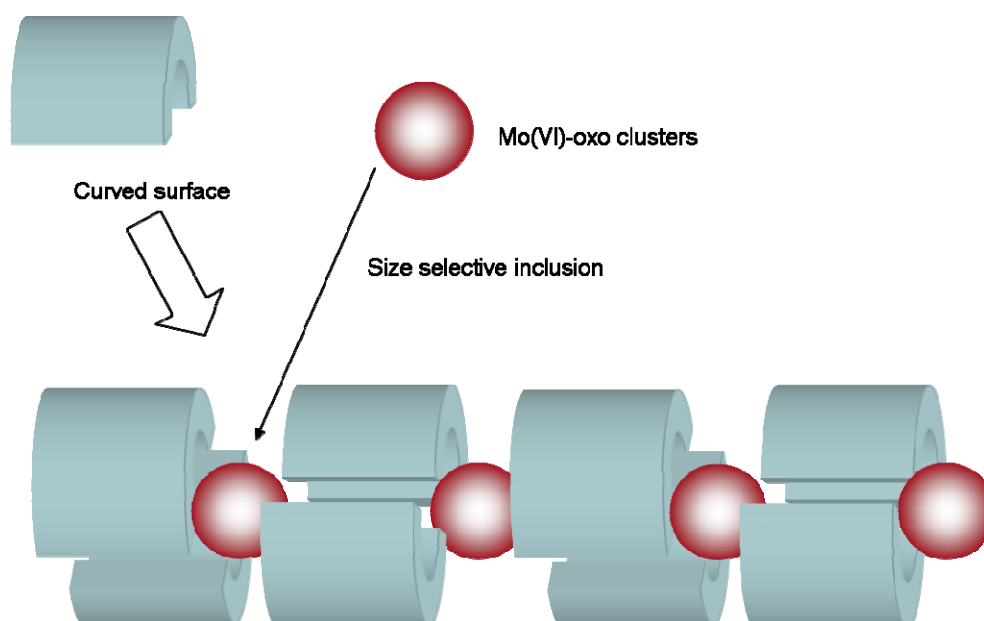


Fig. 1.24 – [Ph₁₂Porphyrin]Mo-based nanotube

The peculiarity, is the presence of hydrophilic environment in its inside, which facilitates inclusion of hydrophilic entities such as Mo-oxo clusters inside of hydrophobic porphyrin aggregates.

The tubular assembly is derived from intermolecular π - π interactions of alternatively inserted peripheral phenyl groups and intermolecular hydrogen bonding with tetranuclear Mo(VI)-oxo clusters: probably they could be formed and protected in accordance with the porphyrin aggregation in the hydrophilic cavity, and they could also act as templates for the tube stabilization.

A remarkable feature of this tubular structure is the formation of the hydrophilic isolated inner sphere in the hydrophobic porphyrin supramolecule.

1.5.1 Synthesis and exploitation of self-assembled porphyrinoids-based nanotube

Current methodologies in organic synthesis and supramolecular chemistry offer a wide range of opportunity to synthesize molecules endowed with suitable features for the recognition process^[46]. There can be no doubt that the ability to coordinate metal ions is of primary importance to determine the sensitivity and selectivity properties of porphyrin derivatives; the role of the coordinated metal, is very important because the axially bind with volatile molecules, mimics the biological functions of these compounds. However, many factors are contemporaneously present to cooperate to bind the guest molecule: hydrogen bond, polarization, and polar interactions^[47]. Because of this extensive richness of interactions, metalloporphyrins do not usually behave as receptors for molecular recognition of specific target molecules, but rather as globally selective sensors.

As recently reported by Shelnutt and co-workers^[45], the ionic self-assembly of two porphyrins bearing opposite ionic charge, leads to the formation of J-aggregates, whose non-planar shape induces the formation of nanotubular structures, reaching free floating aggregates having lengths of tens of nanometers.

Porphyrins are able to arrange themselves in different ways, but aggregates nanotube-like are distinguished by the so called “cavity effect”, that means the inclusion of a guest inside the aggregate. This phenomenon causes some kind of modification in the molecular skeleton arrangement, which is the origin of variation in the optical spectra of the aggregate. These changes can be used for sensing mechanism.

The interest for that architecture is due to the enhanced sensing properties which is not possible to find in the single subunits or in other kind of arrangements. For example the presence of the inner cavity can give rise to selective endohedral inclusion of different guests, or the interaction with analytes can alter the supramolecular arrangement of the molecular nanostructure; both interaction pathways lead to dramatic changes of the porphyrin J-aggregate optical properties, which can consequently be used for sensing mechanism. We investigated the sensing properties of the porphyrin nanotubes in solution and as solid-state layers, having in mind to develop a sensor platform based on the detection of optical changes.

Indeed, the UV-vis spectroscopy provides a typical signature of porphyrin nanotube formation^[43]. At the pH (2) needed for aggregation process, [TSPPorH₂]⁴⁺ is protonated in the inner core (two positive charges), while the peripheral group remain in the anionic form (four negative charges), so on the whole it exists as [TSPPorH₄]²⁻ (**15a**).

[TPyPor]SnCl₂^[48] is protonated at the pyridyl units (four positive charges), while a further positive charge is given by the metal (oxidation number: +4) if one chloride ion is replaced by a water molecule. It exists as [(TPyPor)SnCl₂]⁺⁴ (**16a**) or [(TPyPor)SnCl(H₂O)]⁵⁺ (Fig. 1.25).

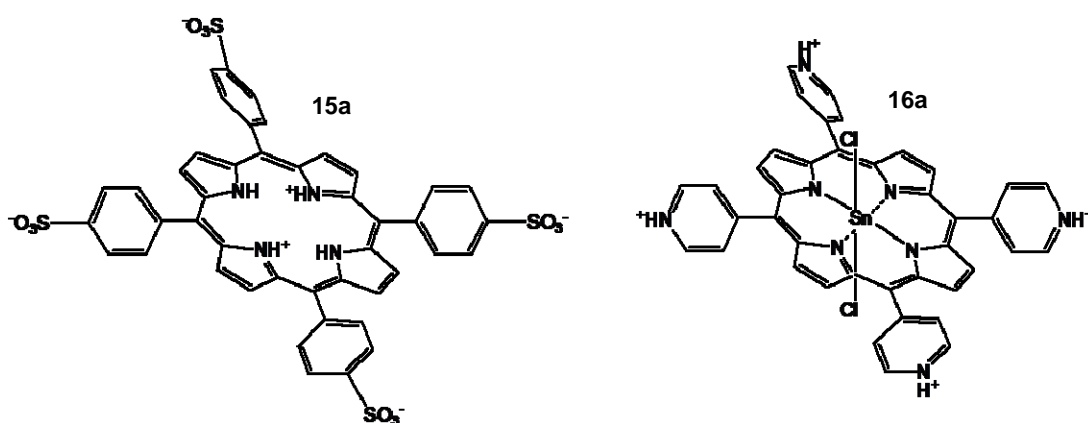


Fig. 1.25 - Structure of porphyrins used for aggregation

In figure 1.26, the corresponding UV-Vis spectra are shown for aqueous solutions of the two constituents and for the self-assembled nanotubes.

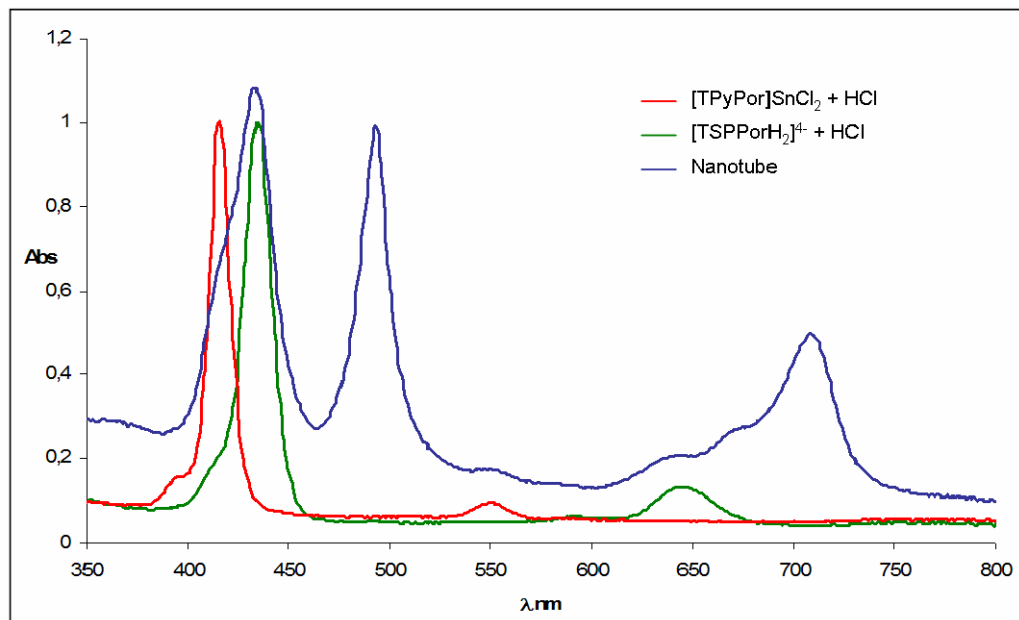


Fig. 1.26 –Nanotube and precursors UV-vis spectra

Looking at the potential exploitation of such a nanostructures as sensing materials, we have first investigated the active role of porphyrin molecular arrangement in their sensing properties, to understand if the porphyrin nanotubes can offer additional features with respect to those of the single isolated components.

To verify this initial conjecture, we compared the effects of the modification of absorption spectra induced by the addition of different salts to solutions of precursor porphyrins and formed nanotubes.

In these conditions, in fact, we can safely exclude the influence of analyte coordination interactions with the porphyrin subunits. In acidic solution, the porphyrin free base is protonated (formation of $(\text{TSPPorH}_4)^{2-}$), and in this form is not possible to coordinate any metal cations, while the anion chosen were chloride or nitrate salts, in order to reduce the influence of axial ligation

equilibria for [TPyPor]SnCl₂. On the other hand, even small variation in porphyrin J-aggregation, induced by the interaction with analytes, can be amplified by the modification of optical signatures.

Moreover, the salts we choose [Pb(NO₃)₂, NaCl, CdCl₂, SnCl₂, MnCl₂, and Cu(NO₃)₂], after their dissolution, do not change the pH of the solution; we need to control [H⁺] concentration because nanotube formation is a results of the precursors protonation, in the inner core, or at the peripheral positions, occurring at low pHs. In all cases absorbance spectra in the visible region of the two precursors did not show relevant changes, while noteworthy modification occurs in case of nanotube solutions. Figure 1.27 shows the spectra obtained in 10⁻² and 10⁻⁴ mol/L Pb(NO₃)₂ solutions containing two single porphyrins and the assembled structure.

Also with CdCl₂, Cu(NO₃)₂, MnCl₂, SnCl₂, nanotubes spectra change, showing a kind of interaction among the aggregate and the ions salt.

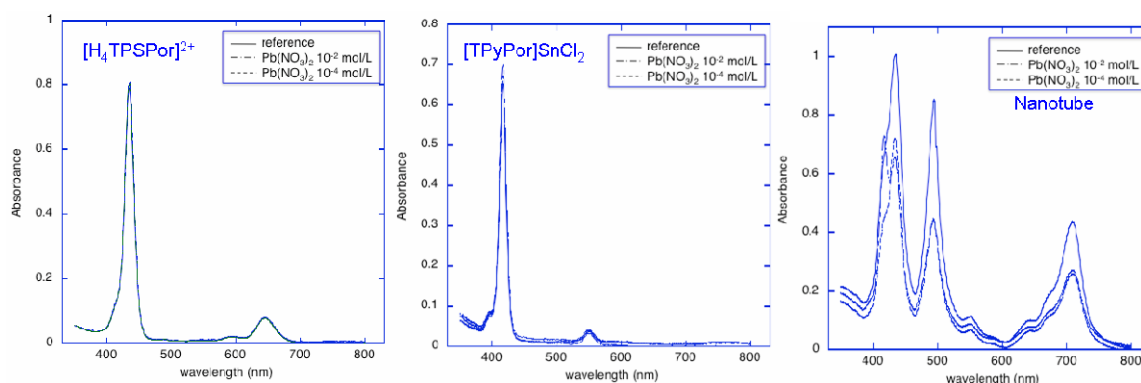


Fig. 1.27 – UV-vis spectra before and after interaction with Pb(NO₃)₂

The effect may largely be attributed to the sensitivity of the forces holding together the nanotube toward the ionic strength of the solution, by shielding effect of the ionic charges, which induces a partial disassembling of the tubular aggregates. The decrease of interaction between porphyrins is indicated by the fact that the typical signals of the nanotube tend to disappear concomitantly it evolves into the spectrum of the individual precursors. Nonetheless, beside a non

specific reaction to different metal ions, spectra also show a peculiar signature for each ion, evidencing that the nanotube interacts differently with respect to the individual porphyrins. This feature results in an enhanced discrimination capability of the particular metal ion.

After these experiments conducted with inorganic analytes, we have studied the variations induced by the addition of organic compounds dissolved in solution, such as triethylamine (Fig. 1.28); in this case, other interaction mechanisms should be involved, such as acid-base or even coordination for the [TPyPor]SnCl₂ moiety.

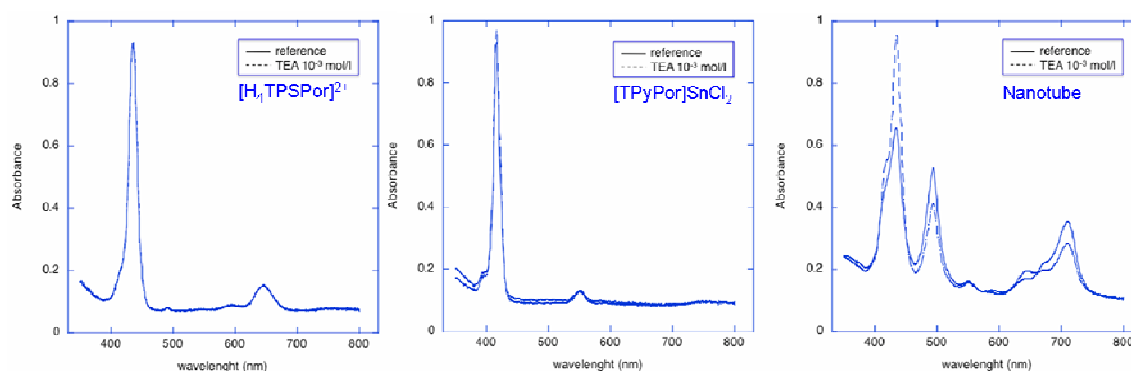


Fig. 1.28 – UV-vis spectra before and after interaction with TEA

Even in this case the porphyrin nanotube showed a larger sensitive than the subunits to the analyte addition. While no appreciable modifications were observed in the optical spectra of both (TSPPorH₄)²⁻ and [TPyPor]SnCl₂, TEA addition led to a partial disassembling of the nanotube structure, as evidenced by the appearance of [TPyPor]SnCl₂ bands in the UV-vis spectrum.

This behaviour prompted us to explore the possibility to utilize the chemical sensitivity of porphyrin nanotubes to detect compounds in gaseous phase; we thought to use CSPT as optical sensing platform to investigate the potential exploitation of this nanostructure in chemical sensors. For this kind of investigation, nanotubes should be deposited as solid layers; so, our first target, was the optimization of the deposition method, because is necessary to preserve

the porphyrin aggregate properties when they are moved from the solution to the solid state. A few μL s of the solution containing the porphyrins nanotubes, were dropped on a glass surface carefully cleaned, then the morphology of the film was evaluated via atomic force microscopy (Fig.1.29).

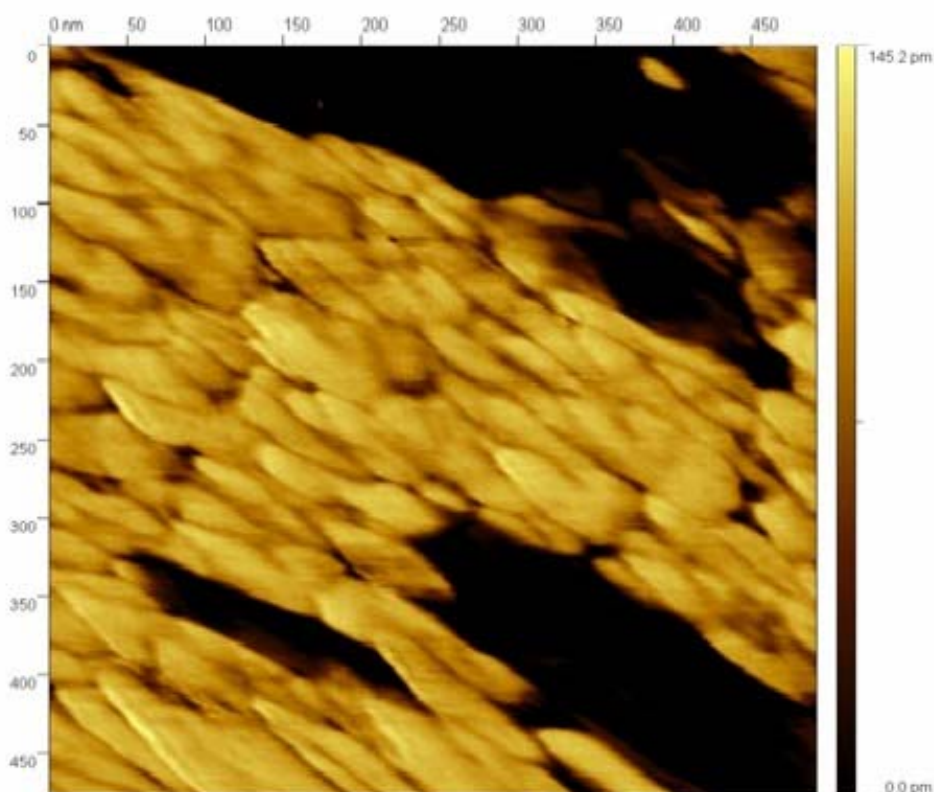


Fig. 1.29 – AFM picture of porphyrins nanotube

The image shows that a tubular structure is retained in the solid state, although the not rigid nature of the porphyrin aggregates can plausibly lead to their deformation, with the consequent flattening of the nanotubes.

Even if the precursors solution had a low concentrations, in the range 5×10^{-6} - 5×10^{-5} M, the solid state containing the porphyrins aggregate showed a large excess of sensitive molecules after the solvent evaporation. Indeed the direct deposition of nanotubes, resulted in a film characterized by an excessive optical density, that was not adequate to be measured with the CSPT.

In order to overcome this problem, we thought to disperse the aggregates in a polymeric matrix compatible with the formation process of the nanostructures. PDMS was found compatible and the embedding of nanostructures inside the polymer took place was evidenced by optical spectra. Also in this case we cannot exclude a flattening of the porphyrin nanotubes into the polymeric matrix, but the retention of the aggregate features in the resulting optical spectra allowed anyway their exploitation for sensing purpose. In order to study the sensing properties of nanotubes-polymer mixture, PDMS was also requested to not interfere with the sensing process and to this purpose the chosen polymeric matrix shown a good permeability to the investigated compounds^[49].

CSPT may produce a fingerprint of the optical spectra disassembling the light generated by a computer screen and transmitted by an absorbing layer in the three channels corresponding to the primary colours. Herewith, for sake of simplicity, instead of the extended fingerprints, we consider a CSPT absorbance that follows the usual definition; the light intensity is simply measured summing the intensity recorded in the red, green, and blue channel^[50]. The absorbance is then defined as:

$$A_{sample}(color) = -\log \frac{R_{sample}(color) + G_{sample}(color) + B_{sample}(color)}{R_{back}(color) + G_{back}(color) + B_{back}(color)}$$

Where sample and back identifies two regions of interest corresponding to the sensitive layer and to the background. Differently from usual spectroscopy, the quantity A is a function of colours where each colour is a computer controlled blend of the emission spectra of red, green, and blue screen pixels.

The response of sensing layer to the exposure of volatiles was measured by the differential absorbance obtained as the difference between the absorbance measured in pure nitrogen atmosphere and sample diluted in nitrogen.

Fig. 1.30 shows the differential absorbance collected during the experiments, while in the inset of the figure, are shown the sensing layer as imaged by the digital camera and four spots of nanotubes dissolved in PDMS.

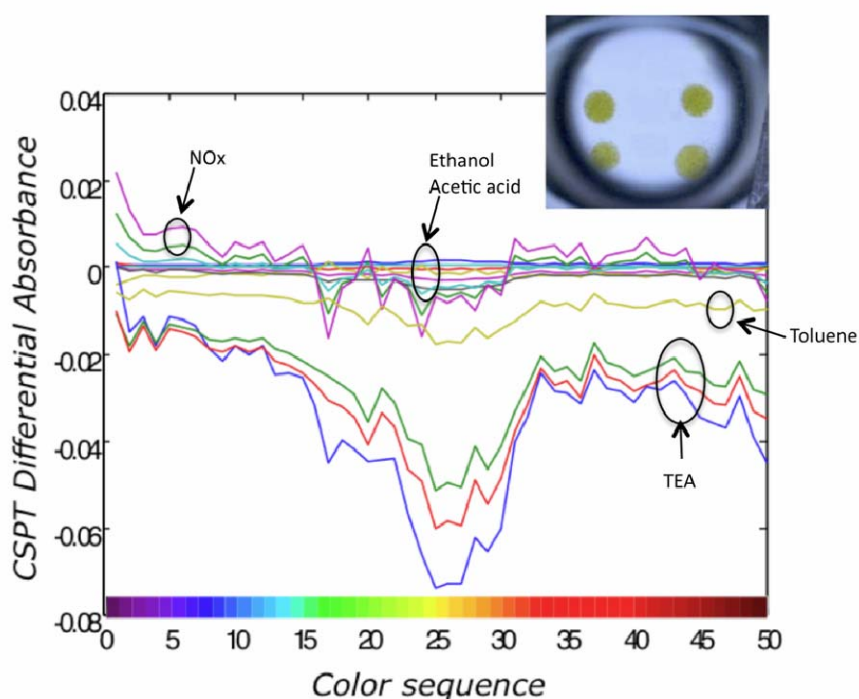


Fig. 1.30 – Response to analytes and spots of sensitive layer

Each spot defines a sample region of interest for which absorbance can be calculated according to above reported equation. Each spectrum is related to a different gas or vapour. When we measured the interaction with TEA, NO_x and ethanol, we noticed the largest absorbance changes, which were found in correspondence of green – yellow illuminating colours.

As shown from optical spectra, the optical sensitivity is, in large part, likely due to the modulation of the interaction between porphyrins constituting the nanotube; nonetheless the differences between the changes of CSPT absorbance in presence of ethanol and triethylamine suggest that a manifold of interactions are likely to take place. A simple method to visualize these behaviours may be obtained calculating the principal components (PCA) of the absorbance fingerprints^[51]. PCA is a standard method in multivariate analysis to represent, for instance in a bidimensional plot, multivariate data such as spectra. These plots are usually interpreted assuming that the distance between data in the principal components plane is a measure of the dissimilarity among samples, and

clusters of data identify similar samples. Fig. 1.31 shows the plot of the first two principal components of the fingerprints plotted in figure 1.30.

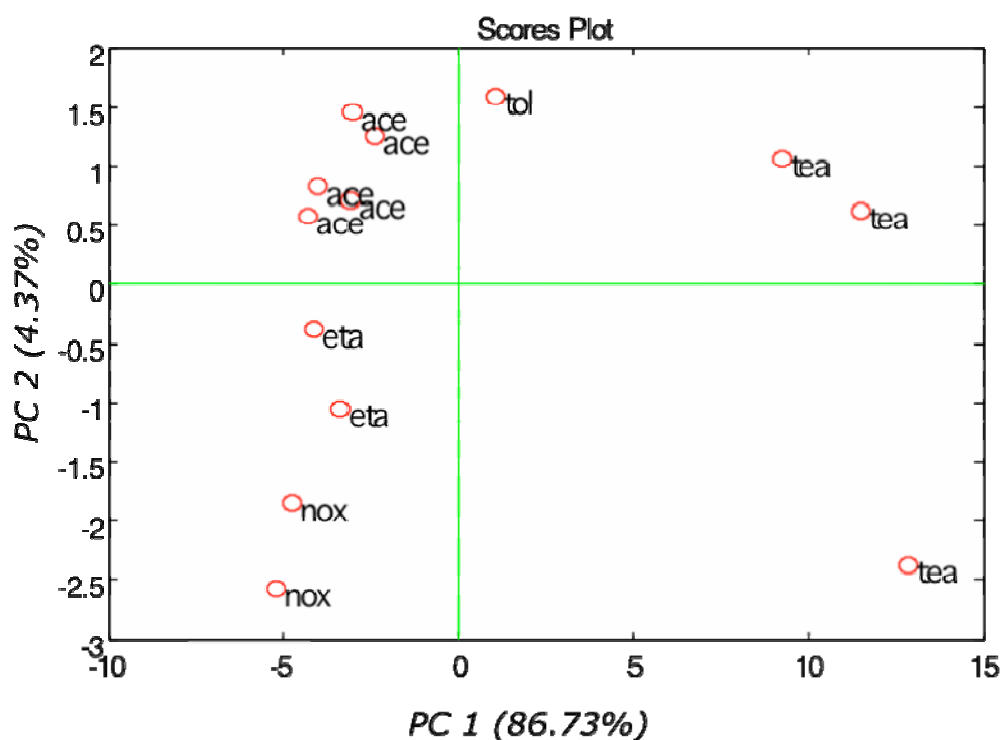


Fig. 1.31 – Result of PCA analysis

A clear separation between TEA and other compounds is observed along the first principal component where more than 86% of the total data variance is explained. TEA detection provides the largest CSPT signal, as can be expected for the basic character of this volatile compound; the pH variation induces the partial disassembling of the nanotube, as evidenced by the appearance of $(\text{TSPPorH}_4)^{2-}$ subunit bands in the UV-vis spectrum. However it should be noted that the residual variance displayed along the second principal component (carrying less than 5% of total variance) can discriminate among the other test compounds. Eventually, even if with different magnitudes, all tested compounds can be satisfactorily distinguished by the CSPT fingerprint of a solid-state porphyrin nanotubes layer.

Experimental section

Reagents

Reagents and solvents (Sigma-Aldrich, Fluka and Carlo Erba Reagenti) were of the highest grade available and were used without further purification.

5,10,15,20-Tetrakis-(4-sulfonatophenyl)porphyrin was purchased from Johnson Matthey GMBH alfa products, and used without further purification.

5,10,15,20-Tetrakis-(4-pyridyl)-porphyrin was purchased from Sigma Aldrich.

Materials

Silica gel 60 (70 -230 mesh) and neutral alumina (Brockmann Grade III) were used for column chromatography

Silica gel 60 (Merck) and neutral alumina 60 F₂₅₄, both on aluminium support, were used for TLC.

Instruments

¹H NMR spectra were recorded either with a Bruker AV 300 (300 MHz) or on a Varian 300 (300 MHz) spectrometers, using CDCl₃ as solvent. Chemical shifts are given in ppm relative to tetramethylsilane (TMS).

Routine UV-vis spectra were recorded in CH₂Cl₂ on a Varian Cary 50 and on a Varian Cary 100 spectrophotometers.

Reflection mode UV-vis spectra were recorded on a Perkin Elmer Lambda 950 spectrophotometer.

Mass spectra (MALDI-TOF) were recorded on a Voyager-DE STR Biospectrometry workstation, in positive mode, using an α -cyano-4-hydroxycinnamic acid matrix.

Gold surfaces for SAMs preparation were prepared with Balzers UMS 500 P system.

Single-wavelength ellipsometry was performed on an automatic Rudolph Research AutoEl ellipsometer with a He-Ne laser light source, $\lambda = 632.8$ nm, at an angle of incidence of 70° .

Infrared reflection-absorption spectra were recorded on a Bruker IFS 66 system, equipped with a grazing angle (85°) infrared reflection accessory and a liquid nitrogen-cooled MCT detector. The acquisition time was about 10 min at 2 cm^{-1} resolution and a three-term Blackmann-Harris apodization function was applied to the interferograms before Fourier transformation. The measurement chamber was continuously purged with nitrogen gas during the measurements.

Contact angles were measured with a Ramé-Hart NRL 100 goniometer in air, without control of the humidity in the ambient atmosphere using freshly deionized water from a MilliQ unit. Advancing and receding angles were recorded using a captive drop.

AFM measurements were performed in air (at room temperature), with the microscope working in the weak repulsive regime of non-contact mode.

1.6 Synthesis of thiol-derivatized porphyrin

1.6.1 Synthesis of 5-(4-carboxymethylphenyl)-10,15,20-triphenylporphyrin (7a)

A solution of pyrrole (5.32 g, 79 mmol) in acetic acid (50 mL) was added dropwise to a solution of methyl-4-formylbenzoate (1.30 g, 7.9 mmol) and benzaldehyde (8.42 g, 79 mmol) in refluxing acetic acid (400 mL), over a period of 30 minutes. The reaction mixture was stirred at reflux temperature for an additional 3 h, then solvent was removed under vacuum. Residue was dissolved and purified by chromatography on silica gel eluting with toluene. The first fraction corresponds to TPPorH₂, while the second fraction corresponds to the desired product. Both the fractions were further purified by crystallization with CH₂Cl₂/CH₃OH, to give 1.71 g of TPPorH₂ (yield 14%) and 0.57 g of **7** (yield 11%) as a purple solid.

1.6.2 Synthesis of 5-(4-carboxyphenyl)-10,15,20-triphenylporphyrin (8a)

Porphyrin **7a** (0.35 g, 0.52 mmol) was dissolved in 200 mL of 95% EtOH and NaOH (1.4 g, 35 mmol) was added. The mixture was stirred at reflux temperature for 3 h, then cooled to room temperature and filtered, washing the precipitate several times with distilled H₂O. The residue was dissolved with a mixture of CHCl₃ and CH₃OH, and washed with a saturated solution of aqueous NH₄Cl. The organic phase was dried on Na₂SO₄, and the residue purified by CHCl₃/hexane (0.29 g, 85%) as a purple solid.

¹H NMR (CDCl₃, 300 MHz): δ ppm 8.86 (s, 6 H, β-pyrrole), 8.80 (d, ¹J = 3.0 Hz, 2 H, β-pyrrole), 8.48 (d, ¹J = 7.0 Hz, 2 H, phenyl), 8.32 (d, ¹J = 7.0 Hz, 2 H, phenyl), 8.22 (m, 6 H, phenyl), 7.77 (m, 9H, phenyl). UV-vis (CH₂Cl₂): λ max,

nm: 419, 516, 551, 590, 647. MS (MALDI, M+1), calculated for C₄₅H₃₀N₄O₂ 658.75; found 659.83.

1.6.3 Synthesis of 5-(4-carboxy-succinimidephenyl)-10,15,20-triphenylporphyrin (9a)

Porphyrin **8a** (300 mg, 0.45 mmol), was dissolved in 20 mL of dry CHCl₃, followed by the addition of N-Hydroxysuccinimide (209 mg, 1.81 mmol) and EDC (349 mg, 1.81 mmol). Mixture was stirred under Ar at room temperature for 24 hours and checked by TLC (silica, CH₂Cl₂). Residue was diluted with CHCl₃, washed twice with water, dried over Na₂SO₄ and following crystallization by CH₂Cl₂/CH₃OH afforded the titled compound in 97% yield (331 mg, 0.43 mmol).

¹H NMR (CDCl₃, 300 MHz): δ ppm 8.88 (s, 6 H, β-pyrrole), 8.78 (d, ¹J = 3.0 Hz, 2 H, β-pyrrole), 8.57 (d, ¹J = 7.2 Hz, 2 H, phenyl), 8.24 (m, 6 H, phenyl), 7.74 (m, 9H, phenyl), 2.97 (s br, 4H, -COCH₂CH₂CO-). MS (MALDI, M+1), calculated for C₄₉H₃₃N₅O₄ 755.83; found 756.45.

1.6.4 Synthesis of 5-(4-(N-(2-*tert*-butyloxycarbamoyl)-ethyl)-carboxyamidophenyl)-10,15,20-triphenylporphyrin

Porphyrin **9a** (160 mg, 0.23 mmol) was dissolved in a few mLs of dry DMF, and 38 μL (0.23 mmol) of N-Boc-ethylendiamine were added. Mixture was stirred at room temperature under inert atmosphere for one hour. Since the starting material did not react completely (TLC silica gel, toluene/ethyl acetate 1:2), a catalytic amount of N,N-Diisopropyl-ethylamine was added, and mixture left to react for others two hours. After the disappearance of starting material, mixture was diluted with CH₂Cl₂, washed with NaHCO_{3(aq)}, water and dried over Na₂SO₄.

Residue was purified with a short silica gel column eluted with toluene/ethyl acetate 1:2. Residue was crystallized by CH₂Cl₂/CH₃OH. Yield 86% (157 mg, 0.20 mmol).

¹H NMR (CDCl₃, 300 MHz): δ ppm 8.89 (s, 6 H, β-pyrrole), 8.80 (d, ¹J = 3.1 Hz, 2 H, β-pyrrole), 8.32 (d, ¹J = 7.1 Hz, 2 H, phenyl), 8.24 (m, 8 H, phenyl), 7.74 (m, 9H, phenyl), 7.52 (s br, 1H, amide), 5.09 (s br, 1H, carbamate), 3.72 (m, 2H, -NHCH₂CH₂-), 3.58 (m, 2H, -NHCH₂CH₂-), 1.24 (s, 9H, -C(CH₃)₃). MS (MALDI, M+1), calculated for C₅₂H₄₄N₆O₃ 800.96; found 801.70.

1.6.5 Synthesis of 5-(4-(N-(2-aminoethyl)-carboxamidephenyl))-10,15,20-triphenylporphyrin (10a)

Protected porphyrin (180 mg, 0.23 mmol) were dissolved in 40 mL of a mixture of CH₂Cl₂/TFA 1:1 in volume, and reaction stirred for 40 minutes. Water was added to quench the reaction, and residue extracted with CHCl₃, washed with NaHCO_{3(aq)}, water, then solvent removed under reduced pressure and residue crystallized with CH₂Cl₂/hexane, to afford the deprotected porphyrin with 60% yield (96 mg, 0.14 mmol).

¹H NMR (CDCl₃, 300 MHz): δ ppm 8.89 (s, 6 H, β-pyrrole), 8.81 (d, ¹J = 2.9 Hz, 2 H, β-pyrrole), 8.57 (d, ¹J = 7.1 Hz, 2 H, phenyl), 8.35 (d, ¹J = 7.1 Hz, 2 H, phenyl), 8.18 (m, 8 H, phenyl), 7.78 (m, 9H, phenyl), 6.18 (s br, 1H, amide), 3.38 (m, 2H, -NH₂), 3.16 (m, 2H, -NHCH₂CH₂-), 2.86 (m, 2H, -NHCH₂CH₂-). MS (MALDI, M+1), calculated for C₄₇H₃₅N₆O 699.84; found 701.25.

1.6.6 Synthesis of 12-Mercaptoacetyl-dodecanoic acid (12a)

12-Bromo-dodecanoic acid (**11a**, 400 mg, 1.43 mmol), was dissolved in 8 mL of dry DMF; potassium thioacetate (245 mg, 2.15 mmol) was added and

mixture stirred at 0 °C for 40 minutes under argon atmosphere. Reaction mixture was then diluted with CH₂Cl₂, washed twice with water, dried over Na₂SO₄, and solvents removed under vacuum. Residue was purified by column chromatography (silica gel, toluene/ethyl acetate 4:1). Yield 90% (353 mg, 1.29 mmol).

¹H NMR (CDCl₃, 300 MHz): δ ppm 2.86 (t, 2 H, AcSCH₂-), 2.35 (t, 2 H, -CH₂CO₂H), 2.30 (s, 3 H, CH₃COS-), 1.70-1.50 (m, 4 H, AcSCH₂CH₂- and -CH₂CH₂CO₂H), 1.28 (s br, 14 H, inner -CH₂-). MS (MALDI, M+1), calculated for C₁₄H₂₆SO₃ 274.42; found 275.63.

1.6.7 Synthesis of N-(12-Mercaptoacetyl-dodecyloxy)-succinimide (13a)

Acid **12a** (322 mg, 1.17 mmol), N-Hydroxysuccinimide (540 mg, 4.7 mmol) and EDC (902 mg, 4.7 mmol) were dissolved in 20 mL of dry CHCl₃. Mixture was stirred under Ar at room temperature for 24 hours and checked by TLC (silica, CH₂Cl₂; after exposure of the TLC plate to an acid solution and heating, mercaptoacetyl group is oxidized, appearing as a yellow-brown spot). Residue was diluted with CHCl₃, washed twice with water, dried over Na₂SO₄ and following crystallization by CH₂Cl₂/CH₃OH afforded the titled compound in 92% yield (400 mg, 1.08 mmol).

¹H NMR (CDCl₃, 300 MHz): δ ppm 2.86 (t, 2 H, AcSCH₂-), 2.81 (s br, 4 H, -COCH₂CH₂CO-), 2.59 (t, 2 H, RCH₂CO-), 2.32 (s, 3 H, AcS-), 1.80-1.70, 1.60-1.50 and 1.44-1.22 (m, 18 H, inner -CH₂-). MS (MALDI, M+1), calculated for C₁₈H₂₉NSO₅ 371.49; found 373.16.

1.6.8 Synthesis of 5-(4-(N-(2-(12-mercaptoacetyl-dodecyl)-carbamoyl)-ethyl)-carboxamidephenyl)-10,15,20-triphenylporphyrin

Porphyrin derivative **10a** (120 mg, 0.17 mmol) and activated acid **13a** (95 mg, 0.26 mmol), were dissolved in 15 mL of dry DMF, then a catalytic amount of N,N-diisopropyl-ethylamine was added, and mixture stirred under Ar at room temperature for 2 hours, checking the course of the reaction via TLC (silica, toluene : ethyl acetate 1/2). After the completion of the reaction, mixture was diluted with CH₂Cl₂, washed with water, dried over Na₂SO₄ and solvent removed under reduced pressure. Purification by silica gel column eluted with CHCl₃, afforded the desired compound in 58% yield (94 mg, 0.01 mmol).

¹H NMR (CDCl₃, 300 MHz): δ ppm 8.85 (m, 6 H, β-pyrrole), 8.78 (d, ¹J = 3.0 Hz, 2 H, β-pyrrole), 8.29 (d, ¹J = 7.0 Hz, 2 H, phenyl), 8.20 (m, 8 H, phenyl), 7.75 (m, 9H, phenyl), 6.21 (s br, 2H, amides), 3.77 (m, 2H, -NHCH₂CH₂NH-), 3.62 (m, 2H, -NHCH₂CH₂NH-), 2.63 (t, 2H, -NHCOCH₂-), 2.22 (t+s, 5H, -CH₂SAc), 1.77-1.60, 1.60-1.43 and 1.42-1.05 (m, 18H, alkyl chain). MS (MALDI, M+1), calculated for C₆₁H₆₀N₆SO₃ 957.24; found 958.09.

1.6.9 Synthesis of 5-(4-(N-(2-(12-mercapto-dodecyl)-carbamoyl)-ethyl)-carboxamidephenyl)-10,15,20-triphenylporphyrin (14a)

Long chain porphyrin (25 mg, 0.026 mmol) was dissolved in a mixture of CH₂Cl₂ and CH₃OH (2+4 mL), then CH₃ONa (7 mg, 0.13 mmol) was added. Mixture was stirred for three hours at room temperature, then solvent removed under reduced pressure. Residue was dissolved with CHCl₃, washed with NH₄Cl, water, dried over Na₂SO₄ and solvent removed under vacuum. Alumina (5%

water) column eluted with CHCl_3 , and crystallization by $\text{CH}_2\text{Cl}_2/\text{CH}_3\text{OH}$ afforded the titled compound in 42 % yield. (10 mg, 0.011 mmol).

^1H NMR (CDCl_3 , 300 MHz): δ ppm 8.85 (m, 6 H, β -pyrrole), 8.78 (d, $^1\text{J} = 3.0$ Hz, 2 H, β -pyrrole), 8.26 (d, $^1\text{J} = 7.0$ Hz, 2 H, phenyl), 8.19 (m, 8 H, phenyl), 7.73 (m, 9H, phenyl), 6.41 (s br, 2H, amides), 3.77 (m, 2H, $-\text{NHCH}_2\text{CH}_2\text{NH}-$), 3.62 (m, 2H, $-\text{NHCH}_2\text{CH}_2\text{NH}-$), 2.53 (t, 2H, $-\text{NHCOCH}_2-$), 2.22 (t, 2H, $-\text{CH}_2\text{SH}$), 1.34 (s br, 1H, $-\text{SH}$). MS (MALDI, M+1), calculated for $\text{C}_{59}\text{H}_{58}\text{N}_6\text{SO}_2$ 915.24; found 916.28.

1.6.10 Procedure for syntheses of Zn (II) and Co(II) complex

Porphyrin **14a** was dissolved in CH_2Cl_2 and few mLs of a saturated solution of $\text{Zn}(\text{AcO})_2$ or $\text{Co}(\text{AcO})_2$ in methanol were added. Mixture was stirred at room temperature, monitoring the formation of complex by UV-vis spectroscopy and TLC (alumina, CHCl_3). After the disappearance of the starting material, solvent was removed under reduced pressure and residue purified by crystallization ($\text{CH}_2\text{Cl}_2/\text{CH}_3\text{OH}$). Zn-complex: yield 90% UV-vis (CH_2Cl_2): λ max, nm: 419, 548. Co-complex: yield 80% UV-vis (CH_2Cl_2): λ max, nm: 410, 528.

1.7 Synthesis of SAM

1.7.1 Procedure for gold surfaces preparation

A standard silicon (100) wafer 100 mm in diameter, was precutted (40×20 mm or 20×10 mm areas) and cleaned with TL1 solution (water/ammonium hydroxide (25 %)/hydrogen peroxide (30 %) 5:1:1 at 80 °C for ten minutes, washed several times with deionized MilliQ water dried under a nitrogen flow. Silicon surface was coated with 25 Å (3 Å/s) of titanium followed by 2000 Å of

gold (10 Å/s), using electron beam evaporation. Surfaces were cleaned again before the incubation, checking the cleanliness level of the surface by ellipsometry ($\Delta > 110$).

1.7.2 Procedure for porphyrin deposition onto gold

Dark glass (avoid light exposure and plastic materials!) containers were chosen to store solution for SAM synthesis. They were cleaned by the following procedure: container was filled with hexane, sonicated for 10 minutes, filled with ethanol (99%), sonicated for further 10 minutes then rinsed three times with ethanol and dried under nitrogen flow.

Porphyrin solutions were prepared by dissolving the porphyrin powder with spectroscopic grade THF till the desired concentration.

Gold surfaces, previously cleaned with TL1 solution, were washed with water, ethanol, THF (or in the solvent chosen for the incubation), where they were stored to avoid any external contamination, before to transfer them into the container with the porphyrin solution.

At the end of the incubation time, surfaces were sonicated in THF (or in the chosen solvent if different) for several minutes, then rinsed with THF, ethanol and dried with nitrogen before their exploitation.

1.8 *Synthesis of porphyrins nanotube*

1.8.1 Synthesis of 5,10,15,20-[Tetra-(4-pyridyl)porphyrinato]SnCl₂ (16a)

TPyPorH₂ was dissolved in acetic acid with a three fold excess of SnCl₂, and refluxed for four hours. After the disappearance of typical free-base absorption

bands, solvent was removed under vacuum and complex purified by crystallization with methanol/THF. Yield 60%. UV-vis (CH_2Cl_2): λ max, nm: 424, 560, 598.

1.8.2 General procedure for porphyrins nanotube preparation

$[\text{TSPPorH}_2]^{4+}$ was dissolved in aqueous HCl (0.02 M); the concentration of the solution was 10.5×10^{-5} M, while $[\text{TPyPor}]\text{SnCl}_2$ was dissolved in water to a concentration of 3.5×10^{-5} M; equal volumes of the solutions were mixed. More diluted solution ($[\text{TSPPorH}_4]^{2+} = 5.25 \times 10^{-5}$ M; $[\text{TPyPor}]\text{SnCl}_2 = 1.75 \times 10^{-5}$ M; and $[\text{TSPPorH}_4]^{2+} = 10.5 \times 10^{-6}$ M; $[\text{TPyPor}]\text{SnCl}_2 = 3.5 \times 10^{-6}$ M) were prepared diluting the initial solution of the unmixed porphyrins and adjusting the final acidity in order to have the same value of pH (2). Solutions were stored in the dark at room temperature for three days. Afterwards a green precipitate is formed. Precipitate and solution showed the same UV-vis spectra, which indicates aggregate formation. Few drops of the solution containing the precipitate were used for the following experiments.

1.8.3 Polymer membrane preparation

Polymeric membranes were prepared by dissolving 33 mg of polydimethylsiloxane distearate (PDMS) in 1 mL of THF; 10 μL of the nanotube suspension was then added to the polymer solution and, after vigorous mixing, the solution was deposited onto a 25 mm diameter Thermanox[®] plastic coverslip (from Nunc[™]). The solvent was evaporated under a gentle stream of N_2 to allow the formation of the polymeric membrane.

1.8.4 CSPT setup

A transparent measurement cell was placed in the optical path between a computer screen and a digital camera.

During a measurement the camera captures the image of the sensing layers under an illuminating sequence provided by the screen (a rainbow of 50 colours in this work). From this video stream two regions of interests (ROI) for each sensing layer are selected. One ROI is centered on the layer spot and the other on a close background. RGB values of the pixel enclosed by a ROI are averaged, and a fingerprint for each sensitive layer of each substance is then calculated subtracting the RGB sequence of the two ROI's. The background subtraction is necessary to take into account non-uniformity of the digital images.

1.8.5 AFM setup

For AFM measurements the solution containing the porphyrin nanotubes (2 μL) was deposited onto a glass surface previously cleaned up with alkaline solution and deionized water.

1.8.6 Gas measurement setup

Sensor responses were measured in presence of the following test compounds: NO_x , TEA, ethanol, toluene, and acetic acid. Except nitrogen oxides, the other compounds are in liquid phase at standard pressure and temperature. All compounds were properly mixed with a nitrogen flow to reach desired concentrations. For liquid compounds, saturated vapours were diluted in pure nitrogen and injected in the measurement cell. Saturated vapour concentrations were calculated by Antoine's law; Antoine parameters available at the database

of National Institute of Standards and Technology (NIST)^[52] were used. Dilution ratios were controlled by a set of mass flow controllers (MKS).

For each measurement the sensors were exposed to the test gas for 15 minutes, where after the test chamber was flushed with a pure nitrogen flow for 30 minutes.

References

1. Thudicum, J.L.W. *Report Med. Off. Privy Council*, **1867**, Appendix 7-10, 152.
2. Hoppe-Seyler, F. *Med. Chem. Unters.*, **1871**, 4, 531.
3. Nencki, M.; Sieber, N. *Arch. Exptl. Path. Pharmacol.*, **1884**, 18, 401.
4. Küster, W. *Z. Physiol. Chem.*, **1912**, 82, 463.
5. Fischer, H.; Klarer, J. *J. Liebigs Ann. Chem.*, **1926**, 450, 181.
6. Fischer, H.; Wallach, B. *J. Liebigs Ann. Chem.*, **1926**, 468, 98.
7. Becker, D.C.; Bradley, B.R.; Watson, C.J. *J. Am. Chem. Soc.*, **1961**, 83, 3743.
8. Soret, J.L. *Compt. Rend.*, **1883**, 97, 1267.
9. Gouterman, M. *J. Chem. Phys.*, **1959**, 30, 1139.
10. Hoard, J.L. In “*Porphyryns and Metalloporphyryns*”; Smith, K.M., Ed.; Elsevier: Amsterdam, **1975**; p. 317.
11. Abraham, R.J.; Hawkes, G.E.; Smith, K.M. *Tetrahedron Lett.*, **1974**, 1483.
12. Falk, J.E.; Willis, J.E. *Aust. J. Sci. Res., Ser. A*, **1951**, 4, 579.
13. Badger, G.M.; Harris, R.N.L.; Jones, R.A.; Sasse, M.J. *J. Chem. Soc.*, **1962**, 4329.
14. Limbach, H.H.; Kendrick, R.; Yannoni, C.S.; *J. Am. Chem. Soc.*, **1984**, 106, 4059.
15. Tulinsky, A. *Ann. N.Y. Acad. Sci.*, **1973**, 206, 47.
16. Buchler, J.W. In “*Porphyryns and Metalloporphyryns*”; Smith, K.M., Ed.; Elsevier: Amsterdam, **1975**; pp. 157-231.
17. Smith, K.M. In “*The Porphyrin Handbook*”, Vol. 1, Kadish K.M., Smith K.M., Guillard R. (Eds.) Academic Press: San Diego, **2000**; pp 1-44.

18. Lindsey, J.S. In “*The Porphyrin Handbook*”, Vol. 1, Kadish K.M., Smith K.M., Guillard R. (Eds.) Academic Press: San Diego, **2000**, pp 45-118.
19. Paolesse, R.; Mandoj, F.; Marini, A.; Di Natale, C. *Encycl. Nanosci. Nanotech.*, **2004**, *9*, 21-42.
20. Di Natale, C.; Magnani, A.G.; Paolesse, R.; Macagnano, A.; *IEEE Sens. J.*, **2005**, *5*, 1165-1174.
21. Rakow, N.; Sea, A.; Jantzen, M.; Ponder, J.; Suslick, K. *Angew. Chem. Int. Ed. Engl.*, **2006**, *44*, 4528-4532.
22. Filippini, D., Lundström, I. *Appl. Phys. Lett.*, **2002**, *81*, 3891-2893.
23. Reinhoudt, D.N.; Crego-Calama, M. *Science*, **2002**, *295*, 2403.
24. Whitesides, G.M.; Grzybowski R.C. *Science*, **2002**, *295*, 2418-2421.
25. Nuzzo R.G.; Allara D.L. *J. Am. Chem. Soc.*, **1983**, *105*, 4481-4483.
26. Maksymovych P; Sorescu D.C.; Yates J.T. *Phys. Rev. Lett.*, **2006**, *97*, 146103.
27. Schoenfish M.H.; Pemberton J.E. *J. Am. Chem. Soc.*, **1998**, *120*, 4502-4513.
28. Heister, K.; Allara, D.L.; Bahnck, K.; Frey, S.; Zharnikov, M.; Grunze, M. *Langmuir*, **1999**, *15*, 5440-5443.
29. Jakubowicz, A.; Jia, H.; Wallace, R.M.; Gnade, B.E. *Langmuir*, **2005**, *21*, 950-955.
30. Dhirani, H.; Zehner, R.W.; Hsung, R.P.; Sionnest, P.G.; Sita, L.R. *J. Am. Chem. Soc.*, **1996**, *118*, 3319-3320.
31. Fery, S.; Stadler, V.; Heister, K.; Eck, W.; Zharnikov, M.; Grunze, M.; Zeysing, B.; Terfort, A. *Langmuir*, **2001**, *17*, 2408-2415.
32. Imahori, H.; Norieda, H.; Nishimura, Y.; Yamazaki, I.; Higuchi, K.; Kato, N.; Motohiro, T.; Yamda, H.; Tamaki, K.; Arimura, M.; Sakata, Y. *J. Phys. Chem. B*, **2000**, *104*, 1253-1260.
33. Stefanelli, M.; Monti, D.; Van Axel Castelli, V.; Ercolani, G.; Venanzi, M.; G. Pomarico; Paolesse, R. *J. Porphyrins Phthalocyanines*, **2008**, *12*, 1279.

34. Ohlsson, J.; Magnusson, G. *Tetrahedron*, **2000**, *56*, 9975-9984.
35. Shendage, D.M.; Fröjlich, R.; Haufe, G. *Org. Lett.*, **2004**, *6*, 3675-3678.
36. Bertilsson, L.; Liedberg, B. *Langmuir*, **1993**, *9*, 141-149.
37. Johnston E.E.; Ratner B.D. *J. Electron. Spectrosc. Related. Phenom.*, **1996**, *81*, 303-317.
38. Elemans, J.A.A.W.; Van Hameren, R.; Nolte, R.J.M.; Rowan, A.E. *Adv. Mater.*, **2006**, *18*, 1251.
39. White, W.I. In “*The Porphyrins*”; Dolphin, D., Ed.; Academy Press: New York, **1978**, Vol. V.
40. Kasha, M.; Rawls, H.R.; El Bayoumi, M.A. *Pure Appl. Chem.*, **1965**, *11*, 371.
41. Hunter, C.A.; Sanders, J.K.M. *J. Am. Chem. Soc.*, **1990**, *112*, 5525.
42. Purrello, R.; Bellacchio E.; Gurrieri, S.; Laceri, R.; Raudino, A.; Monsù Scolaro, L.; Santoro, A.M. *J. Phys. Chem. B*, **1998**, *102*, 8852-8857.
43. Monti, D.; Venanzi, M.; Russo, M.; Bussetti, G.; Goletti, C.; Montalti, M.; Zaccheroni, N.; Prodi, L.; Rella, R.; Naera, M.; Mancini, G.; Di Natale, C.; Paollesse, R. *New J. Chem.*, **2004**, *28*, 1123-1128.
44. Wang, Z.; Medforth, C.J.; Shelnutt, J.A. *J. Am. Chem. Soc.*, **2004**, *126*, 15954-15955.
45. Kojima, T.; Harada, R.; Nakanishi, T.; Kaneko, K.; Fukuzumi, S.; *Chem. Mater.*, **2007**, *19*, 51-58.
46. Anslyn, E. *J. Org. Chem.*, **2007**, *72*, 687-699.
47. Ohshiro, T.; Ito, T.; Bühlmann, P.; Umezawa, Y. *Anal. Chem.*, **2001**, *73*, 878-883.
48. Fuhrhop, J.H.; Smith, K.M. In “*Porphyrins and Metalloporphyrins*”; Smith, K.M., Ed.; Elsevier: Amsterdam, **1975**.
49. Merkel, T.; Bondar, V.; Nagai, K.; Freeman, B.; Pinnau, I. *J. Polym. Sci. B*, **2000**, *38*, 415-434.
50. Filippini, D.; Lundström, I. *Anal. Chim. Acta*, **2004**, *521*, 237-244.

51. Johnson, R.; Wichern, D. In "*Applied multivariate statistical analysis*", Pearson Education, Prentice Hall, New Jersey, **2002**.
52. <http://webbook.nist.gov/chemistry>

Chapter 2

Corrole: chemistry and applications of an unusual tetrapyrrolic macrocycle

Introduction

History of corroles began in 1960^[1], when Johnson obtained the first example of corrole as a by-product in the attempts to develop a synthetic method for the preparation of vitamin B₁₂.

For a long time corroles chemistry has not been investigated as well as porphyrins one; situation has changed in the last decade, after the development of new synthetic methodologies that have improved yield of synthetic processes, making possible an extensively study about the reactivity of this macrocycle.

In this chapter the behaviour of free bases or metal complexes of triarylcorroles bearing the same substituents on the *meso* positions (A₃ corroles) has been studied, and the results obtained will be later on discussed.

2.1 General properties of corroles

2.1.1 Spectroscopic properties of triarylcorroles

Corrole is a tetrapyrrolic macrocycle which differs from porphyrin for the lack of a *C-meso* position, replaced by a direct pyrrole-pyrrole link; in this way it has a molecular frame similar to the corrin skeleton of vitamin B₁₂. The absence of a methine bridge leads to a reduced symmetry of the ring, from D_{4h} to C_{2v}.

In the numbering system of corroles (Figure 2.1), position 20 has been omitted, in order to retain the same numbering scheme of porphyrins for the inner core nitrogen atoms.

The disposition of the amino and imino nitrogens in the inner core is determined according to the calculation performed by Dyke^[2], even if there is no real difference in energy among the possible tautomers because of the fast NH tautomerism, as reported by Ghosh and Jynge^[3].

The steric repulsion between inner protons causes a deviation from planarity, with the pyrrole A tilted out from the macrocycle plane, as shown by X-ray analysis^[4]. However corroles have an unexpected flexibility of molecular structure, which retains a quite planar conformation even if all the peripheral positions are substituted.

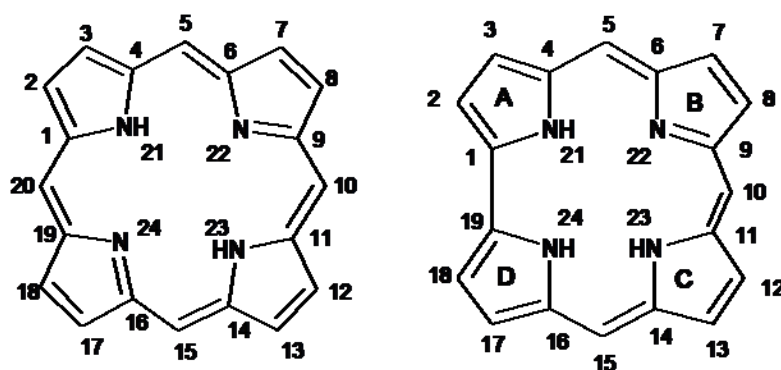


Figure 2.1 – Structure and numeration of porphyrin and corrole

Corroles have a 20 π electrons system; according to Hückel's rule only 18 electrons participate to the formation of aromatic system, as occurs for porphyrins. The effects of the typical current ring, together with the inhomogeneous electronic distribution, affect both nuclear magnetic resonance and electronic spectra of corroles. In the ¹H NMR spectra β -pyrrolic protons resonate at low-field, usually in the range between 7 to 9 ppm.

Moreover, while fully symmetric porphyrins show one singlet for pyrrolic protons, corroles have 4 doublets, each of them referred to two protons.

These signals appear in this order moving from low to high field: $(H_{2,18}) > (H_{7,13}) > (H_{3,17}) \approx (H_{8,12})$, even if the presence of other substituents may affect their chemical shifts.

A broad singlet resonating at high field (around -2 ppm) belongs to the inner protons, although this signal is usually not observed due to the rapid tautomeric exchange.

The electronic spectra of corroles are dominated by transitions occurring within the aromatic system of the macrocycle, although the spectrum is not as well resolved as porphyrin one because of the low symmetry of corrole. UV-vis spectrum can be considered as a confirmation of the aromatic character of corrole.

Free base of A₃ corroles show strong absorption band ($\epsilon = 120000 \text{ M}^{-1}\text{cm}^{-1}$) in the blue side of the visible spectrum (around 415 nm), which is considered to arise from a combination of the second $\pi \rightarrow \pi^*$ transition and its vibrational components; weaker absorption bands occur in the region 550-670 nm ($\epsilon = 10000\text{-}15000 \text{ M}^{-1}\text{cm}^{-1}$). At the same way of porphyrins these are called Soret and Q bands (Figure 2.2).

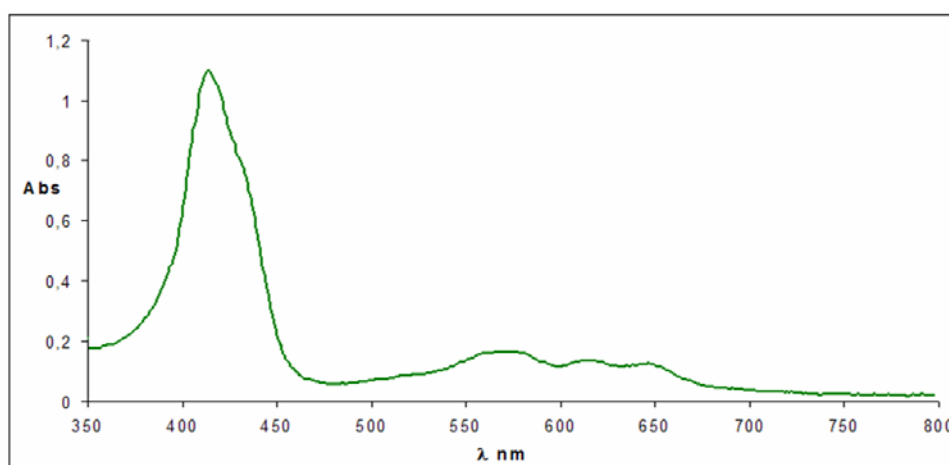


Fig. 2.2 – UV-vis spectrum of 5,10,15-triphenylcorrole

Other two elements affect UV-vis spectrum of corrole, making it so different with respect to porphyrin one. The first one is the relevant changes in the optical bands upon variation of the substituents on the phenyl groups in corroles than in

the corresponding porphyrins. Second, corrole exhibits significant solvent-dependent absorption bands.

Corroles display an intense luminescence band (Figure 2.3) around 670-710 nm; lifetime is in the nanoseconds region with a very small Stokes shift^[4] and a quantum yield of 0.07-0.08; this band could be assigned to the singlet of the lowest $\pi \rightarrow \pi^*$ transition observed in the absorption spectrum. In all cases the excitation spectrum matches the absorption curves.

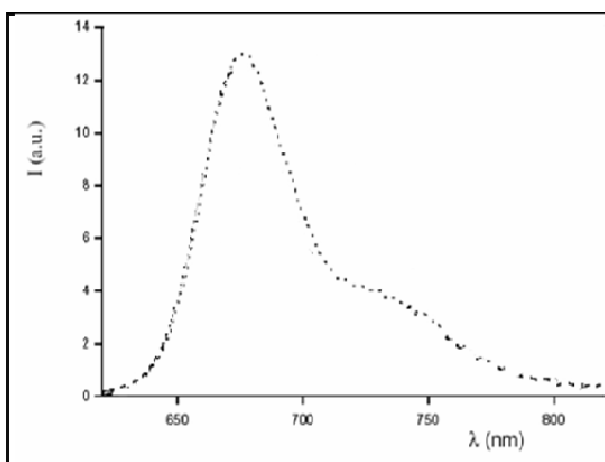


Figure 2.3 – Emission band for triarylcorrole

For triphenylcorrole noticeable changes are observed in intensity and position of the bands on changing the nature of the solvent and in particular fluorescence quantum yield decreases when dielectric constant of solvents increases.

2.1.2 Corrole: acid-base equilibrium^[5]

With respect to porphyrins, corroles show an enhanced tendency both to the protonation and deprotonation process, so much so pH range in which neutral form exist is reduced.

Corrole is more acidic than porphyrin, so free base forms monoanionic species even in dilute basic solutions; monoanion is still aromatic, and retains Soret band in electronic absorption spectrum.

Corrole also reacts with dilute acids to generate monoprotated species; aromatic character is retained in monocation, showing that protonation occurs in the inner nitrogen atom.

Absorption spectrum dramatically changes with disappearance of Soret band, after the addition of strong acidic solution, because in such a case the

protonation occurring at position 5 (or 15) results in the interruption of π system (Figure 2.4).

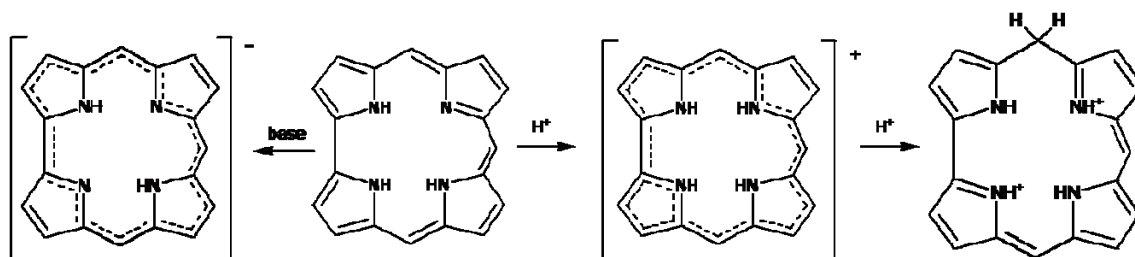


Fig. 2.4 - Acid-base equilibrium of free base corrole

Both $[\text{TPCorH}_4]^+$ and $[\text{TPCorH}_2]^-$ show a splitting of the Soret band, with a slight red shift (5-6 nm) of the main peak, while the second one is located around 440 nm (Figure 2.5).

Q bands are replaced by a strong band at 630 nm for anion and 660 nm for cation, with weaker transitions at shorter wavelengths.

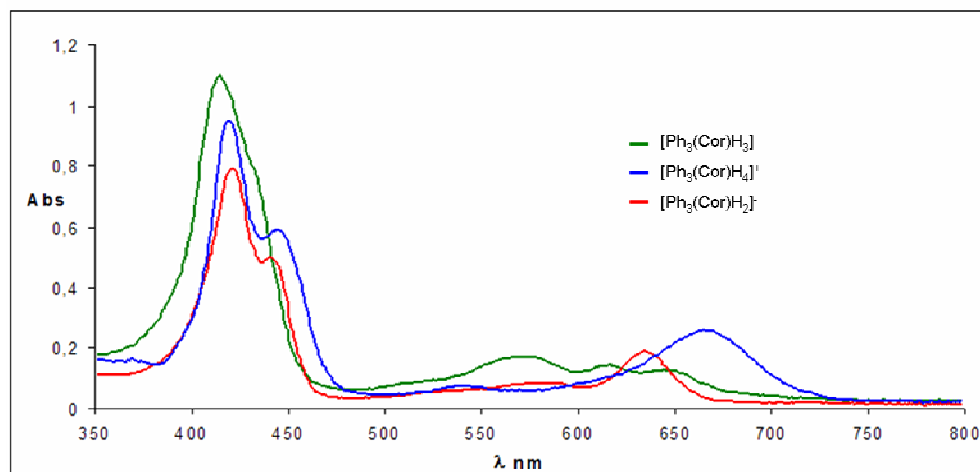


Fig. 2.5 – Absorption spectra of neutral, cationic and anionic TPCorH₃

2.2 *Synthetic procedures for meso-triarylcorroles*

Interest about corroles chemistry has intensely grown up in the last decade, when more affordable synthetic routes have been developed.

Until 1999 procedures leading corroles required several synthetic steps to obtain conveniently functionalized pyrroles and for the following cyclization to corrole. Unfortunately these procedures are usually time consuming and several isomers are afforded if unsymmetrical pyrroles are used.

A summary of procedures till now elaborated includes^[6]:

- tetramerization of 2-substituted pyrrole;
- condensation of pyrrole and aldehydes;
- syntheses from bipyrrrolic units;
- syntheses from *a,c*-biladienes;
- syntheses by macrocycle ring contraction.

Situation radically changed in 1999 when Gross^[7] and Paolesse^[8] groups independently reported two novel methods for synthesis of triarylcorroles from readily available pyrrole and arylaldehydes; however, while Gross procedure is fitted for strong electron-withdrawing aldehydes, (pentafluoro, 2,6-difluoro, 2,6-dichloro-benzaldehyde), Paolesse procedure has a more general scope and can be used for a wide range of aromatic aldehydes.

This procedure is quite similar to Rothmund method for arylporphyrins synthesis, modified in order to promote corrole formation: reaction of a three fold excess of pyrrole with aryl-aldehyde in refluxing acetic acid, leads to the concomitant formation of corrole and a lower amount of porphyrin, which represents the unique drawback of this procedure. As a consequence, the overall yield is reduced due to an inefficient separation; indeed corrole and porphyrin have a quite similar R_f factor.

It was quite surprising that the easy and quick synthetic methodology developed by Rothmund, has been tested in corroles chemistry more than half a century after its optimization for porphyrin syntheses.

As a result of the synthetic efforts to optimize corroles synthetic procedures, a wide range of substituted macrocycles has become available for the chemists, allowing more detailed studies about the peculiar behaviour of that macrocycle.

More recently, further important development occurred: Paolesse^[4] in 2003 and Gryko^[9] in 2006 elaborated two more efficient procedures for triarylcorroles synthesis.

Paper published in 2003 introduced two general procedures, with or without solvent, elaborated with the aim to avoid concomitant formation of corrole and porphyrin.

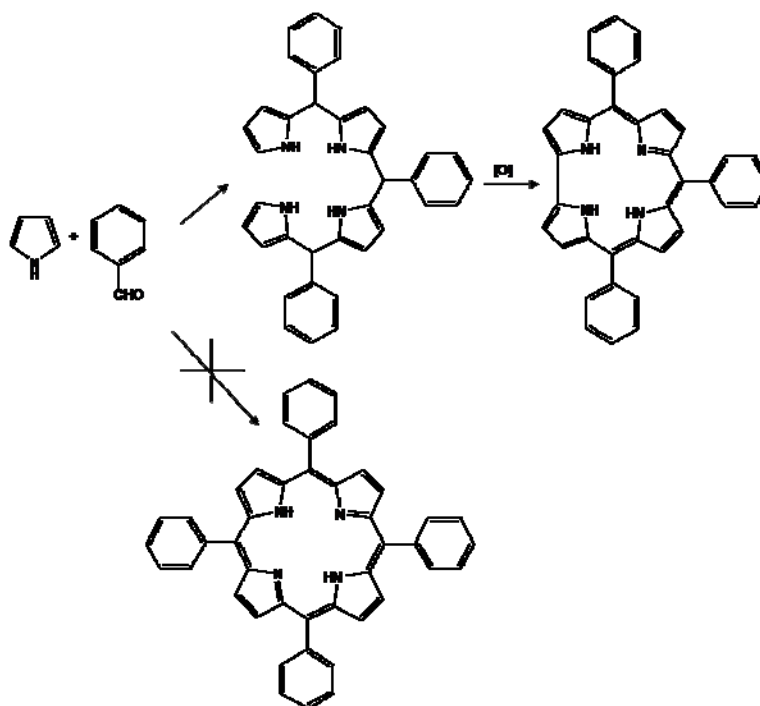
To achieve this goal condensation of pyrrole and aldehyde should be driven toward the formation of bilane, the linear precursor of corrole instead of porphyrinogen, the ring closed precursor of porphyrin.

A ten fold excess of pyrrole and aldehyde (80 mmol vs. 8.3 mmol) were mixed at room temperature under argon atmosphere for 15 minutes, and after TFA (0.2 mmol) addition, mixture was stirred for further 15 minutes, then eluted with 30 mL of CH₂Cl₂ and stirred for 1 further hour (Scheme 2.1).

Dilution with solvent increases the formation of bilane from pyrrolic fragments; final step, oxidative ring closure, was carried out with chloranil (6.4 mmol) in 15 minutes.

That procedure was tested with a number of different aldehydes, to explore the success of this route when reagents bearing different substitution pattern were exploited.

The results obtained showed good generality for the use of several aldehydes; moreover it was possible to synthesize fully substituted corrole. Most remarkable feature of this method, porphyrins formation was reduced to trace levels.



Scheme 2.1 - One step procedure reported by Paolesse

Gryko approach starts from the results obtained by Kral^[10], which reported a novel procedure for dipyrromethanes synthesis: it is based on the different solubility of pyrrole and aldehyde, either soluble in H₂O, and dipyrromethanes which is not soluble, so it forms a white suspension. Optimized Kral method employs a 6 fold excess of pyrrole versus aldehyde, in order to arrest the reaction to dipyrromethane level.

Kral mentioned that by the addition of polar, water-miscible solvent (MeOH, DMF, MeCN, THF, 2-PrOH were tested, but the first one was chosen as reference system), product becomes soluble in that solvents mixture, and it could further reacts, leading to formation of poly-condensate. Gryko starting point was a careful optimization of pyrrole-aldehyde and water-organic solvent ratios to force reaction toward longer pyrrolic compound like bilane (tetrapyrane), which is the corrole precursor instead of dipyrromethane.

In the published procedure for the synthesis of A₃ corroles, 10 mmol of pyrrole and 5 mmol of aldehyde were dissolved in 200 mL of methanol, followed by the addition of the same volume of water and of a catalytic amount of HCl; immediately a white precipitate is formed, then mixture become dark pink because of the formation of oligo-pyrrolic products; after stirring for three hours, the following work up leads to an orange solution (bilane and other polypyrrolic derivatives) which was diluted with chloroform, and oxidized with chloranil.

After purification corroles are obtained in good yield; obviously, the reaction results depend on the typology of aldehyde chosen; when benzaldehyde or other aryl-aldehydes bearing substituents without strong electron releasing or withdrawing effects were used the reaction worked very well, and gave corroles in good yields.

Unfortunately also porphyrins and oligo-pyrrolic compounds were obtained as by-products, leading to a tedious and difficult separation process.

2.3 *Metallocorroles*^[11]

2.3.1 Synthesis and properties of metallocorroles

The ability of corrole to acts as a trianionic chelating system, together with reduced dimension of the cavity, strong influence coordination skills of the macrocycle. Geometries and mainly oxidation states of metal ions inserted in the corroles are usually different from those of porphyrins. The syntheses of metallocorroles were reported some years after the discovery of the corresponding free base, and the majority of the periodic table elements has been successfully incorporated in early studies.

The two basic routes leading to metallocorroles involve a cyclization of *a,c*-biladiene derivatives under the templating effect of a metal ion, and the introduction of a metal into the free base corrole.

The cyclization of *a,c*-biladiene with a metal salt is the most direct approach, but it can not be used with all metals, because some of those are able to catalyze the cyclization of open chain without concomitant coordination, giving the corresponding free base corrole. If the reaction is carried out in presence of an appropriate metal carrier, it affords the corresponding corrole complex in good yield.

When simple methodologies for the preparation of corroles were introduced, direct metallation of corrole became the most frequently employed method, by the same synthetic techniques developed in porphyrins chemistry. The metallation method depends by the availability and the stability of the starting material and by the stability of the product.

When the aim of the synthesis is to obtain a metallocorrole with a specific axial ligand, a stepwise approach is preferable, in which a stable metallocorrole is first synthesized and isolated, after which it is converted into the desired product.

2.3.2 Bonding geometries of metallocorroles

Corroles coordination chemistry is less reach, in terms of geometries, as that of porphyrins which could form hepta- and octa-coordinated monometallic systems, mononuclear bimetallic complexes or even trinuclear types.

Known types of coordination geometries for metallocorroles are briefly summarized below and in scheme 2.2.

➤ *Type A: Square planar.* It is common with metallocorroles and can be found with compounds having the following metals: Mn, Fe, Co, Ni, Cu, In, As, Sb, Bi.

➤ *Type B: Square pyramidal.* It occurs in complexes with Cr, Mo, Mn, Fe, Co, Rh, Ge, Sn, or P ions when neutral (pyridine) or charged (Cl^- , OH^-) ligands occupy the axial position. In the case of Pd and Zn corroles, the structure is described as being a divalent anionic complex with a pyridinium ion as axial ligand. Ni and Cu corroles have no reported examples for this type of coordination, but their ionic reduced form could be considered to have a pyramidal coordination.

➤ *Type C: Octahedral.* This coordination is frequently seen in porphyrins but is rather rare in corroles and can be found only in derivatives containing Rh ($\text{L} = \text{benzonitrile}$) and P (V) ($\text{L} = \text{H}^-$, CH_3 , C_6H_5).

➤ *Type D: Square pyramidal.* A separate group collects metallocorroles with this geometry but with an oxo or acetato moiety acting as a bidentate ligand. Sn ($\text{L} = \text{AcO}^-$), Re and P ($\text{L} = \text{O}$) have been reported to exhibit type D coordination.

➤ *Type G and H.* Large ions can attain high coordination numbers with a cis or trans configuration of the ligands and a structure of type G or H is possible.

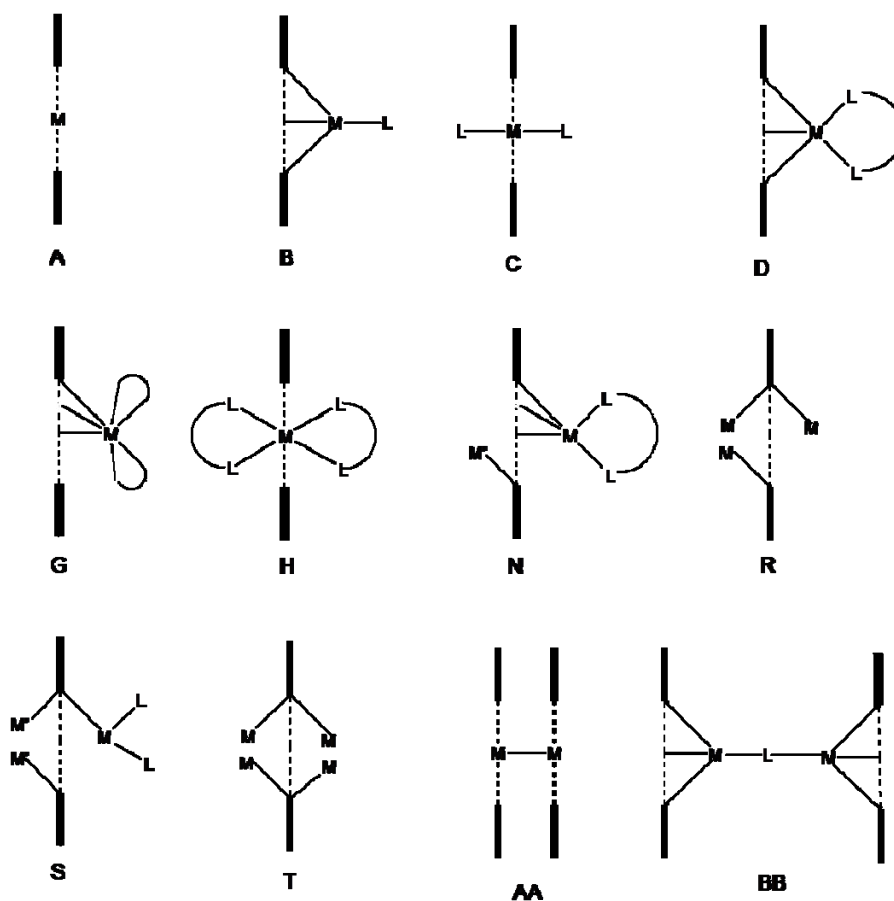
➤ *Type N: Bimetallic.* It has been found only in V and Ti corroles, that have one metal replaced by hydrogen; in this case the corrole ligand acts as a bidentate ligand through two of its pyrrole.

➤ *Type R and T.* Type R is represented by the free-base corrole itself, whereas the type T can be assigned to the protonated free-base corrole.

➤ *Type S.* This structure is considered to be a possible intermediate in porphyrin and corrole metallation reactions, but forms a stable, isolated compound only in corroles, which provides another example of how the trianionic corrole is distinguished from the divalent porphyrin macrocycle. The only representative for this type of arrangements is the Rh (I) dicarbonyl complex.

➤ *Type BB: Monometallic binuclear.* Only one example of a binuclear corrole complex of type BB is now known, which is the μ -oxo-bis(octaethylcorrolato)iron.

➤ *Type AA: Bimetallic binuclear.* The formation of π - π dimers, representing type AA, was shown to occur in solution on electrochemical oxidation of neutral corroles of the type Metal-octaalkylcorrolate.



Scheme 2.2 – Geometries of metallocorrolates

Results and discussion

2.4 Reactivity of triarylcorroles: from functionalization to new isomers

Some chemical-physical properties of corroles make their chemistry different and intriguing by comparison with more investigated porphyrins.

In the last decade corrole chemistry has been subject of a several studies, which have expanded our knowledge about their behaviour, and explained several details concerning their reactivity, promoting exploitation of corrole in different fields of research, such as medicine^[12] or material sciences^[13].

Functionalization of corroles is an inescapable starting point to realize derivatives having more elaborated molecular scaffold, which properties are fitted on various aims; to obtain these results, corroles features are tuned by inserting various substituents on *meso*- or β positions.

Peculiar reactivity of corrole is pointed out by the different and often unexpected results obtained when a reaction is carried out on this macrocycle, using the same conditions previously tested for the functionalization of porphyrins. A plausible explanation comes from the lower symmetry of corroles, which causes an inhomogeneous distribution of the π -electron density.

Formyl and bromine substituents are two useful tools to modify porphyrins^[14] structure; the reactions for the insertion of these group have to be carried out on metal complexes for several reason. When Vilsmeier formylation is carried out on porphyrins, metalation prevents the protonation of the core occurring under the reaction condition, which deactivate the macrocycle toward Vilsmeier

reagent. Insertion of a metal ion is also a needed step in the bromination process, because in this way the symmetry of the macrocycle increases, making possible the functionalization of all the β -pyrrolic positions, and also because the substrate is protected from the decomposition.

Furthermore, before the optimization of demetalation process of corrole complexes, many reactions have been tested on corrole free base, presuming that the high electron density of this macrocycle would allow the course of the reaction. With great fulfillment of the scientists, the formation of unusual products confirmed corrole peculiar reactivity.

Either β -octamethylcorrole^[15], or *meso*-triphenylcorrole^[16] showed high regioselectivity when reacted under the condition for formylation process. In the first case, the functionalization occurs on the 10 position, even if the others two positions (5 and 15) were available for the attack of formyl group. More surprisingly, the characterization of the product pointed out that the substituent connected to the ring was not a formyl moiety, as would be logical to suppose, but a dimethyl-aminomethene group (**1b**, Fig. 2.6); moreover, the interruption of the aromaticity proceeded together with the functionalization.

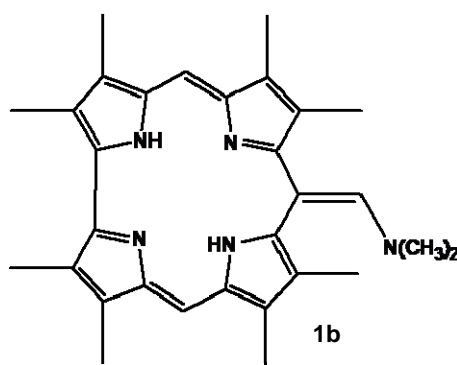


Fig. 2.6 – Product of formylation on Me₈CorH₃

Products of formylation on triphenylcorrole^[16], confirmed the tendency of this macrocycle to give regioselective products: although four different mono-formylated isomers could be obtained, the main product was the 3-substituted

derivative. This behaviour is probably due to the higher electron density on positions 3 (and 17) with respect to the others ones.

Also a third and unusual product was isolated and characterized; it did not result to be a bisformylated derivative, but a completely different product (**2b**, Fig. 2.7), which presents the functionalization of the inner core, with the formation of a C-C bond.

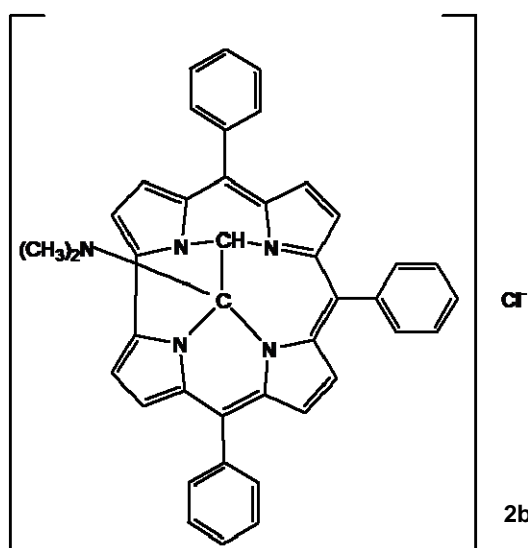


Figure 2.7 – Product of formylation on $TPCorH_3$

We noticed the interruption of the aromaticity also when bromination of corrole free base was attempted^[17]. Although this reaction leads to an extensive decomposition of the starting material, a substituted product has been isolated; following characterization showed the formation of fully brominated derivative. The strong tendency of corrole to be oxidated, and presence of an excess of brominating (and oxidating) agent, drove the formation of an isocorrollic species, characterized by the interruption of the conjugation pathway and by a tautomeric shift of the internal proton, as well as occurred in formylation of β -alkylcorrole.

We assumed for $Br_8TPCorH_2$ (**3b**) the structure drawn in figure 2.8.

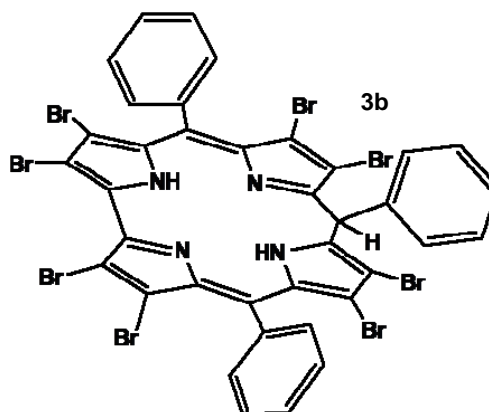


Fig. 2.8 – Structure of $Br_8TPCorH_2$

Formation of **3b**, with the displacement of one inner proton can be explicated with the attempt of the corrole ring to reduce the steric strain induced by the NH protons and by bromine substituents.

2.4.1 Isocorrole: unexpected product from oxidative synthetic step^[18]

Porphyrins and corroles are the most investigated compounds in the family of the polypyrrolic macrocycles, but a wide range of different isomers have been so far synthesized. However, while easy and quick one-step procedures for corroles^[4,9] and porphyrins^[19] syntheses have been developed, the chemistry of others porphyrinoids has not yet received the same rapid growth. Porphyrins isomers are, as the name implies, tetrapyrrolic macrocycles, that consist of a $C_{20}H_{14}N_4$ skeleton, with a N_4 coordination site and $18-\pi$ electrons in a cyclic, fully conjugated path. These compounds are usually named “porphyrin” and their name concludes the name of bridging meso-carbons given in parentheses, starting with the highest number and going around the ring toward the next highest number.

Porphycene (**4b**) [porphyrin (2.0.2.0)], corrphycene (**5b**) [porphyrin (2.1.0.1)], hemiporphycene (**6b**) [porphyrin (2.1.1.0)] and isoporphycene (**7b**) [porphyrin (3.0.1.0)] are some of isomers that have been already studied^[20] (Fig. 2.9).

Research on these compounds has been limited because of the difficult synthetic pathways leading to these porphyrin isomers. Indeed several synthetic steps are required, starting from convenient functionalized pyrroles, bipyroles or dipyrromethanes^[21].

This event led us to consider about the opportunity to get those porphyrins isomers, a field that is still in its infancy, directly from porphyrins or corroles by adequate reaction, a more straightforward way with respect to the specific and dedicated synthetic routes so far adopted.

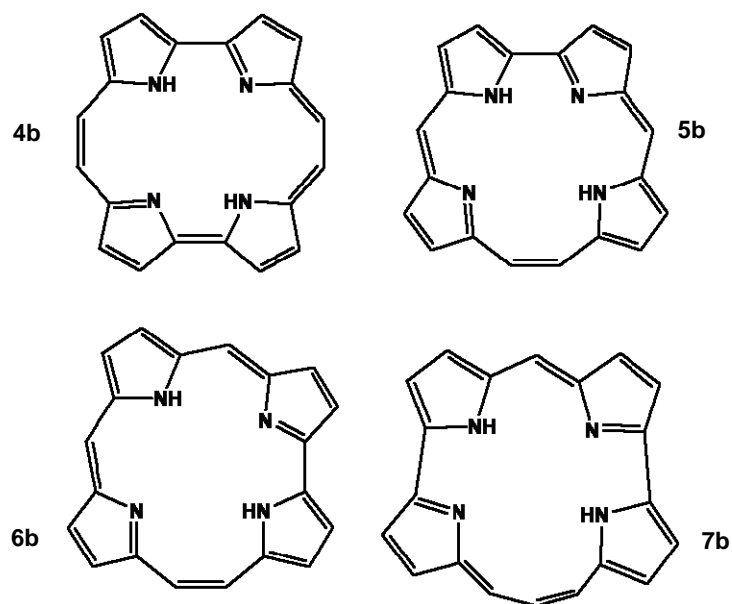


Fig. 2.9 – Porphyrin isomers

We focused our attention on isocorrole^[22], in which one of three *meso* carbons of the aromatic tetrapyrrolic macrocycle is sp^3 hybridized and two inner NH protons, rather than three, are present in an antipodal position; although the name isocorrole has been used in the past to indicate also corrole analog

[porphyrin 0.2.0.1]^[23] (**8b**), the term isocorrole is more appropriate to indicate the isomers **9b** (Fig. 2.10).

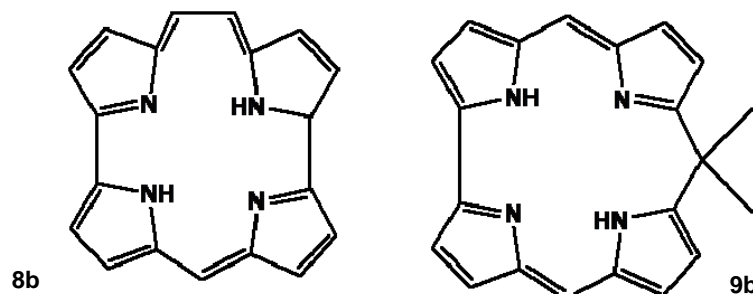


Fig. 2.10 – Compounds usually named isocorrole

So far only two examples of isocorrole have been published in literature: Vogel and co-workers reported^[22] the preparation of Ni(II) complex of 2,3,17,18-tetraethyl-7,8,10,10,12,13-hexamethylisocorrole as a result of cyclization of the *a,c*-biladiene hydrobromide using Ni(AcO)₂ in methanol, followed by chloranil for the ring closure reaction; however this is not a general procedure, because the same authors did not obtain the 2,3,7,8,12,13,17,18-octaethyl-10,10-dimethylisocorrolate Ni(II), due probably to the steric hindrance between peripheral ethyl groups. The first example of free base isocorrole has been reported by Setsune^[23] et al., a bis(azafulvene) derivative of *gem*-dimethyldipyrromethane reacted with 2,2'-bipyrrrole to give a mixture of *gem*-dimethylisocorrole and higher homologues.

The above reported syntheses of isocorrole require the preparation of difficult to obtain precursors, and probably for this reason further investigations on isocorroles have not yet been conducted.

A facile synthetic route to isocorrole would use the corrole macrocycle as a more convenient starting material, since new expeditious synthetic routes to triarylcorroles have been reported^[4,9], making this type of macrocycle readily accessible.

One of the key features of corrole is its easy oxidation to generate π -cation radicals; this feature seems to be interesting for the formation of isocorrole, considering that the first example of an isoporphyrin was observed upon reaction of oxidized [TPPor]Zn with methanol^[24]. We envisioned the application of such a route in the case of corrole (Fig. 2.11), using a strong oxidative system as DDQ-Sc(OTf)₃ where the function of scandium salt is to enhance the oxidizing ability of the quinone.

A toluene solution of TPCorH₃ with scandium triflate and DDQ (1:5:5 ratio) under nitrogen was complete in about 5 min, as indicated by UV-visible spectrophotometry. TLC indicated the formation of two main reaction products, as well as significant decomposition of the starting material.

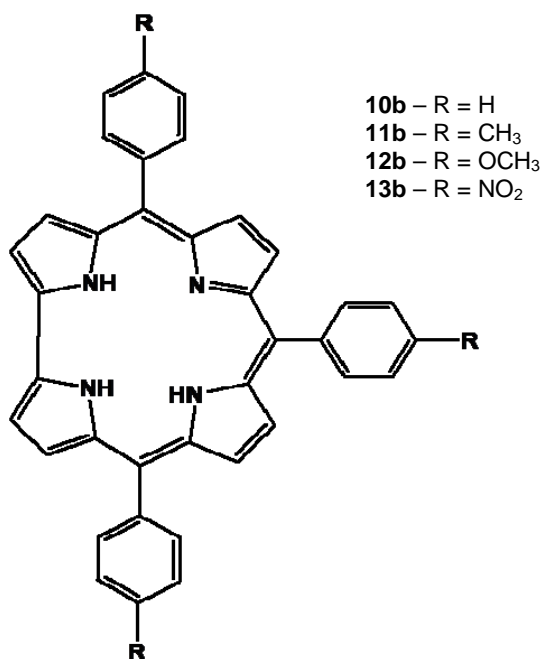


Fig. 2.11 – Aryl-corroles used for isocorrole synthesis

Chromatographic separation (silica gel, CHCl₃/hexane 1:1) afforded two fractions, that were re-crystallized from CHCl₃/methanol.

The ¹H NMR spectrum (Fig 2.12) of the first yellow-green fraction (obtained in 20% yield) displayed the β -pyrrolic proton resonances shifted upfield with respect to those of TPCorH₃: this feature, along with the presence of a signal at

15 ppm, characteristic of NH protons not affected by the ring current, strongly suggested the formation of a non-aromatic structure.

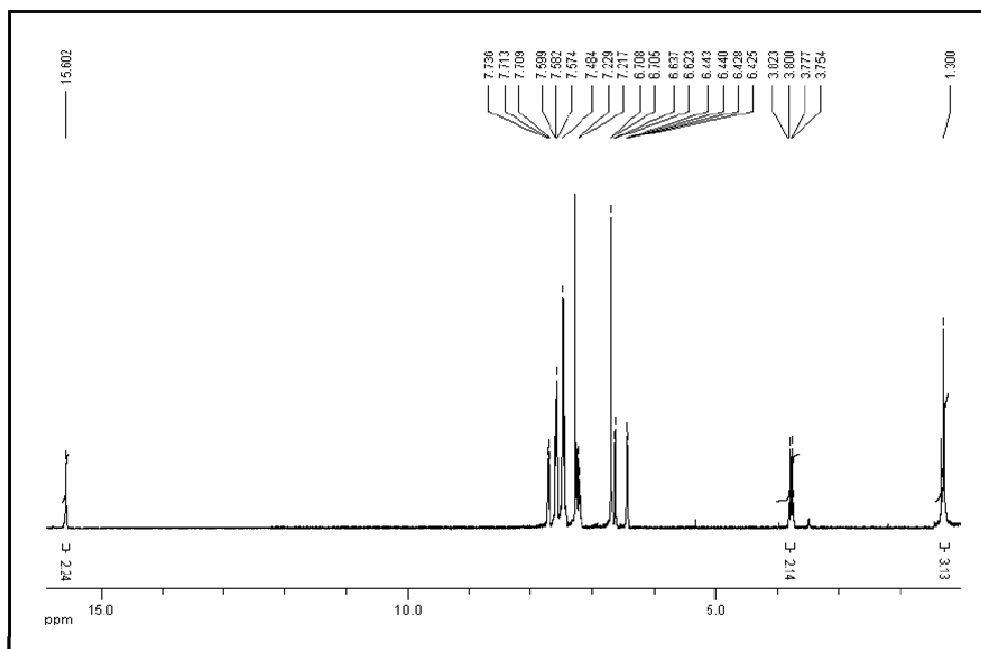


Fig 2.12 – ¹H NMR of 10-ethoxyl-isocorrole

This hypothesis was corroborated also by the UV-visible spectrum of the compound and by mass analysis. Finally the macrocycle was unambiguously characterized as isocorrole **14b** by X-ray crystallography (Figure 2.13).

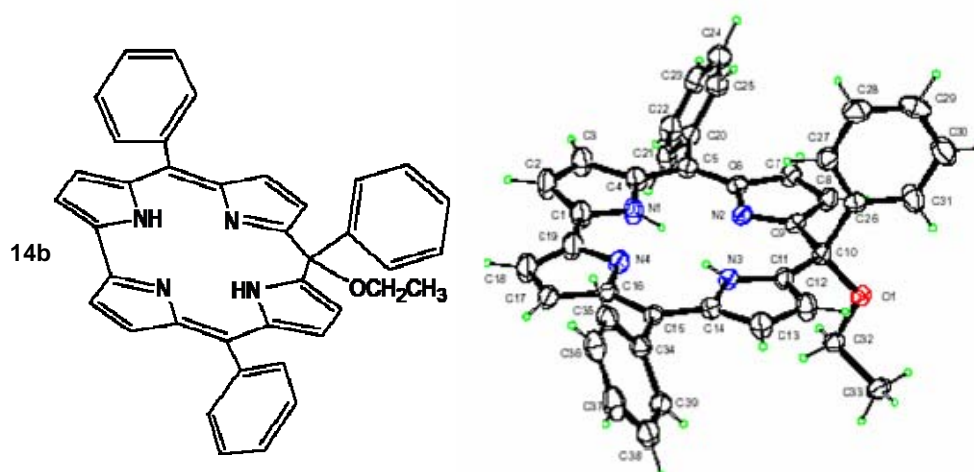


Fig 2.13 – Structure and X-ray of 14b

In this structure an ethoxy group is inserted at the 10 position, resulting in the interruption of the aromatic conjugation. The source of the ethoxy group was the ethanol used for stabilization of the CHCl_3 , the solvent employed in the reaction work-up.

The ^1H NMR spectrum of the second fraction also confirmed the non-aromatic character of this reaction product, as well as lower symmetry than compound **14b**. However, this product was obtained in very low amount (less than 5% yield) and always contaminated with traces of other fraction collected, which did not allow its complete characterization.

With these first results in mind, we carried out the reaction in methanol rather than in toluene, since methanol has the advantage of dissolving all the reagents, and because it could act as nucleophile. We also decided to carry out the reaction on TTCorH_3 , in order to have additional information on the symmetry of the products by NMR, using the resonances of the peripheral methyl groups, and to improve product solubility and chromatographic separation.

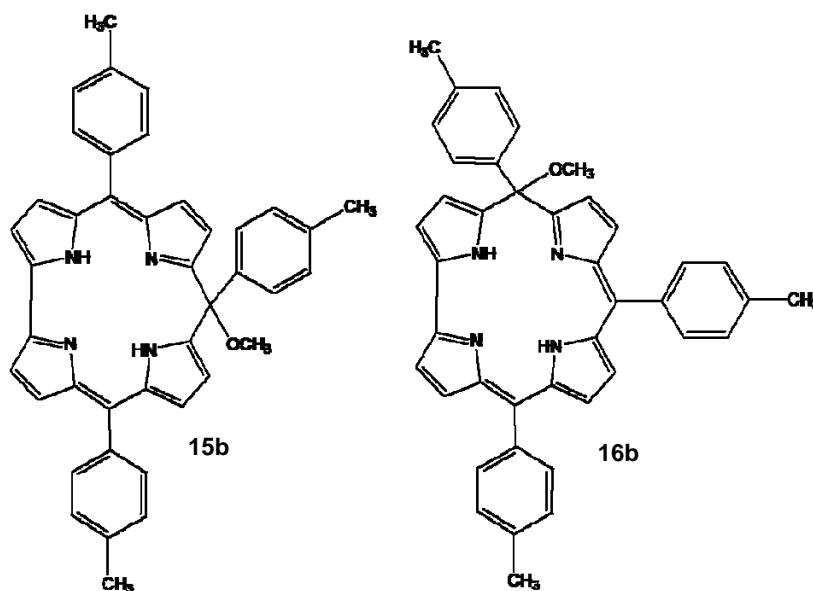


Fig. 2.14 –The two isocorrole isomers collected

Considering the extensive decomposition of starting material, along with the observation previously reported that DDQ can induce overoxidation of

triphenylcorroles^[25], we carried out the reaction using one equivalent of DDQ and without Sc(OTf)₃, obtaining the two products (**15b**, **16b** Fig. 2.14) in 74% overall yield.

The first fraction collected was characterized as the expected 10-substituted isocorrole, bearing a methoxyl group on meso positions. The higher yields obtained under these conditions allowed the chromatographic separation and isolation of the second reaction product. The UV-vis spectrum (Fig. 2.15) shows for this compound a broadened absorption band around 410 nm and weaker absorption at 650-750 nm; all the absorption bands are blue-shifted respect to those of **15b**. ¹H NMR analysis displays two different resonances for the inner NHs and the spread of the signals of the β-pyrrolic protons.

This result indicated the formation of the less symmetric isocorrole **16b**, where the addition of the methoxy group and the consequent interruption of the aromatic conjugation occurred at the 5 position. To the best of our knowledge, this is the first report of such a regioisomer of isocorrole even though the reactivity of the 5-meso position is not unprecedented; we observed similar behaviour in the case of the reaction of triphenylcorrole with Cl₄, where the ring expansion to hemiporphycene occurred exclusively at the 5-meso position^[18].

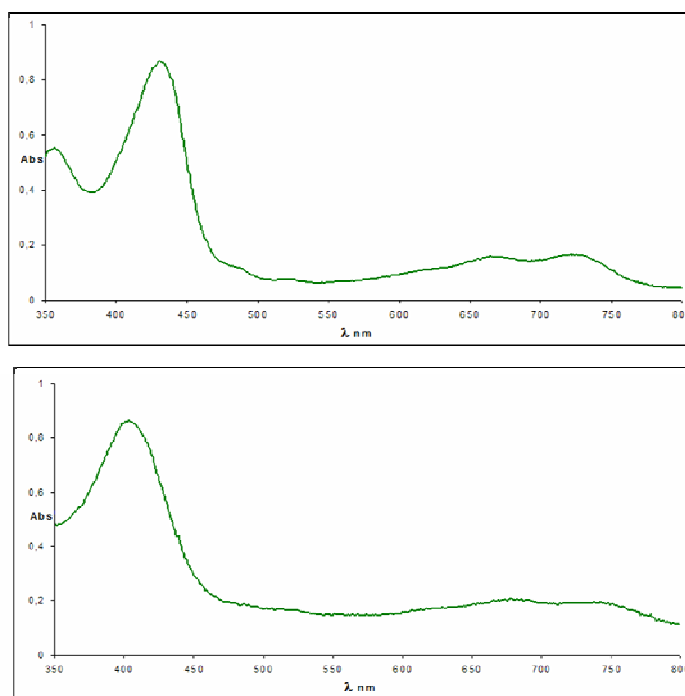
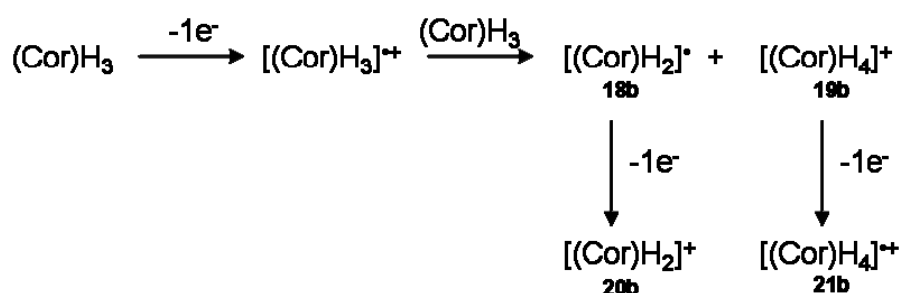


Fig. 2.15 – UV-vis spectra of **15b** (over) and **16b** (below).

To evaluate the influence of the substituents at the corrole periphery on the formation of the isocorroles, we reacted in the same conditions (*p*-OCH₃)TPCorH₃ and (*p*-NO₂)TPCorH₃, which bear *meso*-aryl groups of opposite electronic behaviour. In the case of (*p*-OCH₃)TPCorH₃, bearing electron releasing groups, the corresponding isocorroles were isolated in good yields (75% overall yield), and the 10-isomer (**17b**) was isolated and fully characterized, while in the case of (*p*-NO₂)TPCorH₃, bearing electron withdrawing groups, only traces of the products were obtained along with a mixture of decomposition products.

This results is in good agreement with the hypothesis that the formation of isocorroles occurs after the oxidation of the starting corrole by DDQ, however there is no indication of the reactive intermediate. The stoichiometry of the reaction implies the removal of two electrons and two protons from corrole by DDQ, and the subsequent addition of one molecule of alcohol (or others nucleophilic agents) to give the isocorrole. However the oxidation behavior of corrole is quite complicated and involves the formation of different species, as recently reported by Kadish and co-workers^[26]. The first oxidation step of corrole involves the formation of a radical cation, which, being a strong acid, rapidly loses a proton to give the neutral radical **18b**, while the liberated H⁺ reacts with another molecule of corrole to give the corresponding protonated specie **19b**. The second oxidation can occur on both these species at very close potentials, to give **20b** and the radical corrole dication **21b** (Scheme 2.3).



Scheme 2.3 – Proposed mechanism for isocorrole formation

The potential reactive intermediate can be **18b**, **20b** or **21b**, excluding **19b**, which is stable in MeOH. To obtain further information on the reaction intermediate we used I₂ as the oxidant instead of DDQ, since this reagent was used in the past to obtain **18b** and **19b** from octaethylcorrole^[27]. Under these conditions we observed the immediate formation of a mixture of **18b** and **19b**, evidenced by their characteristic UV-vis spectrum, but no isocorroles were formed. This result indicates that **18b** can be excluded as the reactive intermediate. To respect the other two species, **20b** it is the analogous in the corrole field of the Zn porphyrin dication, which has been reported as the precursor of Zn isoporphyrin^[26], and can afford isocorrole by nucleophilic attack of the alcohol.

However, to investigate **21b** as possible intermediate, we decided to carry out the reaction in the presence of an excess of TFA, therefore having **19b** as the starting material and then **21b** as the oxidation product, following Kadish procedure^[26]. Also in this case the reaction was successful, suggesting that **21b** can be considered as precursor in the formation of isocorroles. This result indicates that both **20b** and **21b** can undergo nucleophilic attack of alcohol to give isocorroles, in a pathway similar to that of porphyrin, where both the dication and the radical cation of porphyrin have been demonstrated to be precursors of the corresponding isoporphyrin^[24,28].

This studies give further insight into the oxidation of the corrole macrocycle and provide a one-step, facile and high-yielding preparation of both 5- and 10-isocorroles. The 5-regioisomer isocorrole preparation has been reported for the first time.

2.5 Metalloporrole: effects of a noninnocent ligand

Inside the rapidly growing scenario of corroles chemistry, one important aspect is still missing: the versatility of functionalization of peripheral positions achieved in the case of porphyrins.

Metalloporphyrins, in fact, are generally used as starting material for several reaction^[14]; metal coordination may be necessary to activate the macrocycle, for example towards electrophilic substitution, or to protect the inner core from protonation, when the reactions are carried out under acidic conditions.

After the functionalization is achieved, porphyrin free base can be obtained by well-defined demetalation protocols^[29]. This approach is more problematic in the case of corroles, because no general procedures for their demetalation have been yet developed, the lack of which can be ascribed to two contrasting features: corrole has better donor properties, but has also a lower stability than porphyrin. Therefore, the interaction between corrole and metal ion does not have a reversible character. More acidic conditions are necessary for the demetalation step, which can result in a corrole modification before the removal of the metal takes place, or even in the decomposition of the macrocycle.

In some cases this problem has been circumvented by carrying out the reaction directly on the corrole free base, taking advantage of its high reactivity. The drawback is the somewhat unpredictable reactivity shown by corrole free-base, which can give interesting products, but somewhat different from what we looked for.

For example, fully bromination of corrole could be achieved in good yield^[30], if metal complexes is used as starting material. Otherwise, reacting corrole free base with brominating agent, degradation or isocorrole formation have been detected.

Metals coordinated to corrole, are also able to drive the regioselectivity of corrole functionalization.

Hexabrominated derivative are elicited when an excess of Br_2 reacted with Ge-corrole^[31], with the functionalization of all β -pyrrolic position excepting 7 and 13 (**22b**, Fig. 2.16)

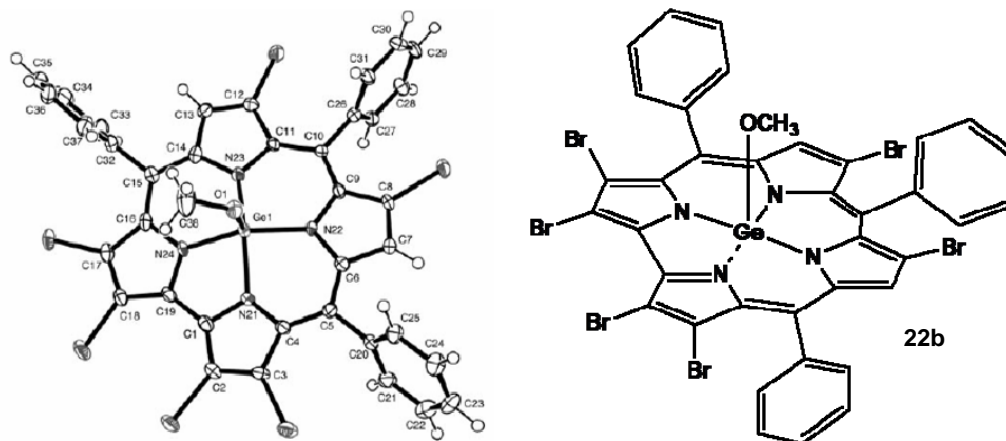
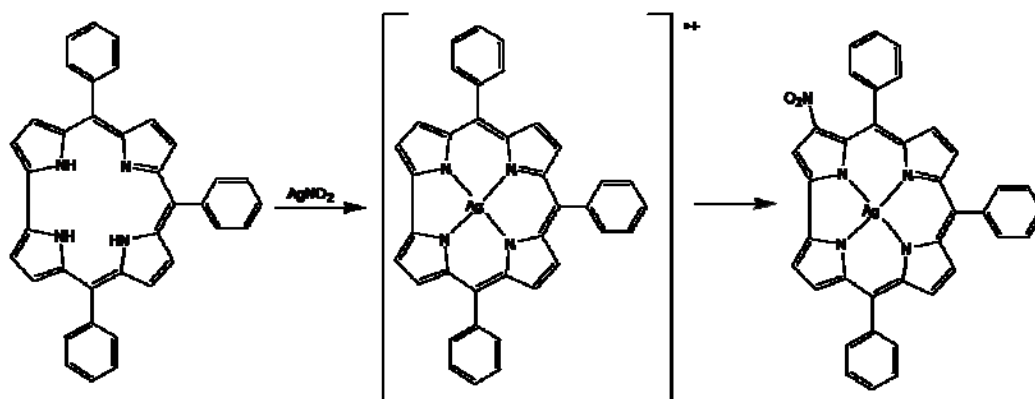


Fig. 2.16 – X-Ray and molecular structure of **22b**

Another useful way to modify tetrapyrrolic macrocycle is represented by the nitration reaction; nitro group is very versatile because it can be used as starting point for further modifications of corrole framework.

Since corrole is a quite sensitive compound, is not possible to use harsh nitrating mixture such as $\text{HNO}_3/\text{H}_2\text{SO}_4$, which would lead to the complete degradation of macrocycle, while others nitrating systems as N_2O_4 , BF_4NO_2 or $\text{Cu}(\text{NO}_3)_2$ in acetic anhydride do not work properly.



Scheme 2.4 – Nitration mechanism for TPCorH_3

We found out^[32] that corrole undergoes nitration when reacted with AgNO_2/I_2 , but insertion of nitro group is accompanied by concomitant metalation of the ring, resulting in the formation of $[(\text{NO}_2)\text{TPCor}]\text{Ag}$ (Scheme 2.4)

Spectroscopic analyses confirmed the regioselective character of the insertion of a nitro group in position 3, which is the most reactive of all β -pyrrolic ones.

Although all these experiments made possible to expand corrole chemistry, the unavoidable necessity to use corrole complexes as starting material for a number of functionalizations, prompted us to optimize a procedure for their demetalation, in order to have back the corresponding free bases of functionalized macrocycle.

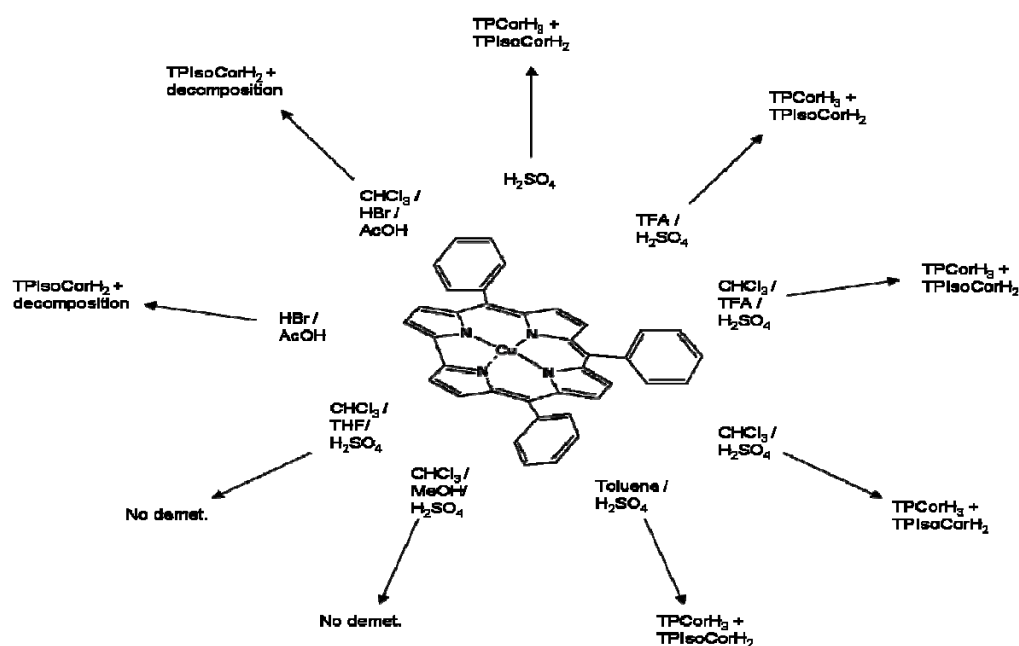
2.5.1 Demetalation of corroles complexes: a starting point towards new synthetic routes

So far, only two examples of corrole demetalation have been reported. The first, reported by Bröring *et al.* in 2001^[33], involves the treatment of the Mn(III) complex of octaethylcorrole with HBr in acetic acid to yield Et_8CorH_3 , quantitatively, within 10 min. Subsequently, Brückner *et al.*^[34] have observed the complete demetalation of silver(III) triarylcorroles in CHCl_3 or CH_2Cl_2 solutions, by using concentrated aqueous HCl in a biphasic system. However, experimental details and yields of these reactions are not available and, furthermore, those are not general demetalation procedure efficient on different corroles. Moreover, it should be considered that these metal complexes are not the best choices for synthetic purposes. Manganese derivative, in fact, need the use of high boiling solvents for their preparation and its paramagnetism prevents the exploitation of NMR spectroscopy for product characterization. Silver corroles have not yet been reported in the case of B-alkyl corroles and, in addition, their suspected liability in several reaction conditions, limits their potential exploitation. In this contest, should be find a metal complex for corroles that could be compared to

Zn, Ni or Cu complexes of porphyrins: these are in fact the most utilized metal derivative in the functionalization chemistry of the above-mentioned macrocycles.

Among these metals, Zn is not useful in the case of corrole, since the corresponding metal complex is not stable; Ni complexes are paramagnetic and more difficult to prepare.

For these reasons, our attention has been focused on the study of the potential exploitation of copper corrole for the substitution of the macrocycle peripheral positions: in fact, copper corrolates can easily be prepared, present good stability and versatility, and they are diamagnetic, allowing their characterization via NMR spectroscopy.



Scheme 2.5 – Demetalating systems tested

The aim of this work was to find a general protocol for the demetalation of copper corrolates, and then a further investigation with other metal complexes of corrole. $[\text{TPCor}]_{\text{Cu}}$ was chosen as a model compound to find and optimize a demetalation procedure; the first attempt was to employ the HBr/AcOH method, which has been reported by Bröring to be successful in the case of Mn corrole

derivatives^[33]. We were able to observe the formation of the corrole cation following the reaction progress by UV-vis spectroscopy, but the reaction work-up showed a significant decomposition of the starting macrocycle and the presence of several reaction by-products. Attempts to improve the reaction yields by dilution of the acid mixture with CHCl_3 were not successful and these results led us to turn our attention to other demetalation systems. We then decided to use neat H_2SO_4 for $[\text{TPCor}]\text{Cu}$ demetalation and, in this case, we obtained the corresponding TPCorH_3 free base within 5 min. The progress of the reaction was monitored by UV-vis spectroscopy, diluting an aliquot of the reaction mixture in CH_3OH and observing the formation of the corrole cation species. Subsequently, CHCl_3 was added and the organic phase was first washed several times with water and then neutralized with a saturated NaHCO_3 aqueous solution. However, also in this case, TLC analysis of the crude reaction mixture showed the presence of baseline material, due to the decomposition of the starting material in the harsh acidic medium, together with two bands having a lower R_f than the expected corrole free base. A second chromatographic run was necessary to obtain analytically pure compounds; the spectroscopic characterization of these bands indicated a peripheral modification of the corrole skeleton, with the interruption of the aromatic conjugation of the macrocycle. The UV-vis spectrum, showed two bands over 600 nm, while in the ^1H NMR spectrum there were resonances around 15 ppm, characteristic of the NH protons not affected by the ring current and all the β -pyrrolic protons resonated below 7 ppm. All these features were consistent with the formation of two isocorrole isomers, identified as (10-OH)TPIsoCorH₂ (**23b**) and (5-OH)TPIsoCorH₂ (**24b**) (Fig. 2.17) substituted respectively at the 10 and 5 position. These compounds had the typical spectroscopic pattern that we have recently observed in the preparation of isocorrole by oxidation of corrole with DDQ^[21].

The plausible pathway for the isocorrole formation during the demetalation reaction is probably due to the easy oxidation of the corrole ring to give a π -

radical cation, which can be then attacked by a molecule of water to both *meso*-positions, to give the detected isocorrollic species.

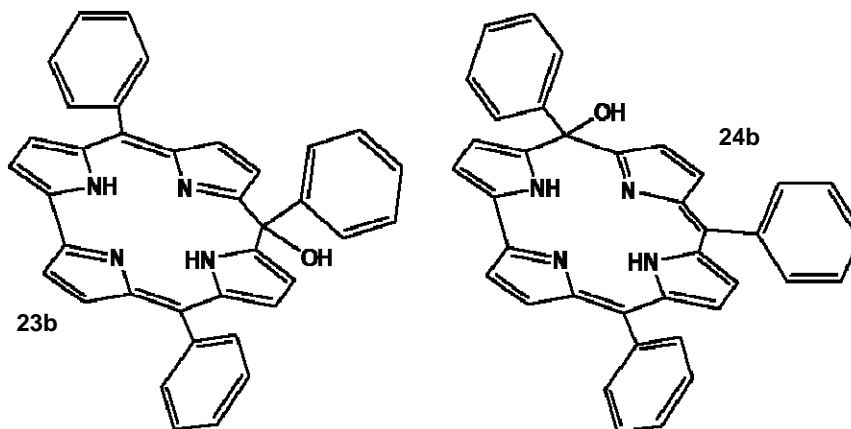


Fig 2.17- Hydroxy-Isocorroles **23b** and **24b**

Although H_2SO_4 was successful in the [TPCor]Cu demetalation, both the isolation of isocorroles and the decomposition of the starting material significantly affected the reaction yields; the search for more satisfying acidic mixtures was still necessary and for this reason we turned our attention towards other acidic media, as reported in table 2.1.

First, we tested the acidic mixtures mostly used in the case of copper porphyrins, such as TFA/ H_2SO_4 in a 10:1 ratio^[35]. The formation of the corrole cation was immediate in this case as well, but the yield of the reaction was just slightly improved with respect to the one carried out in neat sulfuric acid, and in addition, we observed the formation of isocorrole.

The dissolution of [TPCor]Cu in an acidic mixture CHCl_3 /TFA (1:1) and then the addition of neat H_2SO_4 (in a 1:10 ratio with TFA) gave similar results, without significant improvement in the reaction yields. Attempts to reduce the isocorrole formation carrying out the reaction under an inert atmosphere did not give significant results; all these unsuccessful led us to use milder acidic media for the demetalation reaction, to reduce the decomposition of the starting material

and to avoid as much as possible the oxidation of the corrole ring, with the aim of increasing reaction yields.

Acidic mixture	TPCorH ₃	Secondary products
H ₂ SO ₄	yes	TPIsoCor ^a
TFA/H ₂ SO ₄	yes	TPIsoCor ^a
CHCl ₃ /TFA/H ₂ SO ₄	yes	TPIsoCor ^a
CHCl ₃ /H ₂ SO ₄	yes	TPIsoCor ^b
Toluene/H ₂ SO ₄	yes	TPIsoCor ^b
CHCl ₃ /CH ₃ OH/H ₂ SO ₄	no	
CHCl ₃ /THF/H ₂ SO ₄	no	
HBr/AcOH	yes	TPIsoCor + decomposition products
CHCl ₃ /HBr/AcOH	yes	TPIsoCor + decomposition products

^a TPCorH₃/TPIsoCorH₂ ratio 1:1. ^b Traces

Table 2.1 – Comparison of acid mixtures for [TPCor]Cu demetalation

Thus, we decided to add neat H₂SO₄ dropwise to a CHCl₃ solution of [TPCor]Cu, in order to add a more controlled amount of acid: we used UV-vis spectroscopy to observe the immediate formation of the corrole cation. The reaction work-up was carried out as for the reaction with neat sulphuric acid, but in this case, we obtained the corresponding triphenylcorrole free base in good yields, with only trace formation of isocorrole species. The reaction was also successful using toluene instead of chloroform as the solvent^[36], leading to similar yields of the corrole free base after the removal of the metal ion and only traces of the side product. It was surprising to note that, the reaction was not successful when we tried to obtaining a homogeneous reaction media by addition of CH₃OH or THF as co-solvent to the CHCl₃/H₂SO₄ mixture. In this case, we observed the immediate formation of the protonated corrole after the

acid addition by UV-visible spectrum, but the reaction unexpectedly turned back after the reaction work-up resulting in a novel complex formation.

A plausible explanation is that in the biphasic system, the metal ion is extracted from the organic solvent, making the demetalation reaction irreversible.

These interesting results led us to study the scope of the $\text{CHCl}_3/\text{H}_2\text{SO}_4$ procedure, extending this approach both to copper β -alkyl corroles and to other metal corrole complexes; the results obtained are reported in table 2.2.

Complexes	Demetalation ($\text{CHCl}_3/\text{H}_2\text{SO}_4$, 10:1 vol)	Yield, %
[TPCor]Cu	yes	83
[TTCor]Cu	yes	78
[OMCor]Cu	yes	93
[Et ₄ Me ₄ Cor]Cu	yes	89
[TPCor]Co(PPh ₃)	no ^a	-
[OMCor]Co(PPh ₃)	no ^b	-
[TPCor]Mn(Cl)	yes	80
[Et ₂ Me ₆ Cor]Mn(Cl)	yes	91
[TPCor]Fe(Cl)	yes	72
[Et ₄ Me ₄ Cor]Fe(Cl)	no	-
[TPCor]Ge(Cl)	no	-
[Et ₄ Me ₄ Cor]Ge(Cl)	no	-

^a Dimer formation. ^b Functionalization

Table 2.2 – Demetalation reaction products and corresponding yield

The demetalation was successful in the case of copper β -alkyl corrole complexes; the procedure worked also for manganese meso-aryl and β -alkyl

corrolates and showed a partial achievement for iron complexes, for which it was possible to remove the iron in the case of [TPCor]Fe(Cl), while it did not succeed when the metal ion was coordinated to β -alkylcorroles.

No demetalation was obtained for Ge and Co derivatives; however, in the latter case, we observed the formation of different products. When the demetalation protocol was tested on [TPCor]Co(PPh₃), we observed the slow formation of dimeric species by coupling at the β -pyrrolic position, as shown by mass spectrum of the mixture of products, which we were unable to separate by chromatography. The presence of such dimeric species can be attributed to the formation of radical species by oxidation of the starting complex and similar derivatives have already been reported by Gross and coworkers for the pentafluorophenylcorrole complex^[37].

[Me₈Cor]Co(PPh₃) was not demetalated, even in neat H₂SO₄, but methyl groups were slowly oxidized to the corresponding 3,17-diformyl complex (**25b**, Fig. 2.18).

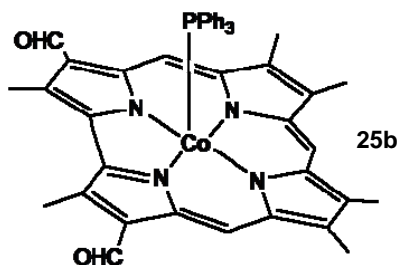


Fig. 2.18 – Molecular structure of 25b

The formation of this compound is not unprecedented in acidic condition, because we obtained the same complex during our study on the corrole formylation by reaction with TFA/trimethylorthoformate^[15]. Furthermore, in this case, the formation of such a species can be attributed to the oxidation of [Me₈C]Co(PPh₃) in the acidic conditions and in fact the same compound was obtained by DDQ oxidation of the same complex^[38]. The success obtained in the case of copper corrole derivatives led us to extend the study to the corresponding

β -octabromo derivatives. In fact, these compounds are particularly interesting as starting materials for further functionalizations of the corrole ring, considering that β -bromination of corrole lead to extensive decomposition of starting material^[17].

The developed $\text{CHCl}_3/\text{H}_2\text{SO}_4$ methodology was also tested for the demetalation of $[\text{Br}_8\text{TPCor}]\text{Cu}$. In this case, the reaction was also successful and it was possible to obtain the corresponding octabromocorrole free base, although an appreciable amount of isocorrole derivative $\text{Br}_8(10\text{-OH})\text{TPIsoCH}_2$ was also formed.

It is interesting to note that this compound was identical to the product that we obtained by the direct bromination of TPCorH_3 using NBS as the brominating reagent^[17]. Different results confirmed the hypothesis about the isocorrole formation: for example, in the ^1H NMR spectrum, it was possible to observe the OH resonance at 3.95 ppm, which can be slowly exchanged with an ethoxy group when the compound is stored in a CHCl_3 /ethanol solution. The absence of the molecular peak in the mass spectrum is due to the lability of the OH substituents in these conditions, as already observed for the β -unsubstituted isocorroles. Finally, the formation of the corresponding corrole complex by reaction with Co(II) acetate and PPh_3 is a general feature for isocorroles, as confirmed by the reaction of $(10\text{-OH})\text{TPIsoCorH}_2$ and $(5\text{-OH})\text{TPIsoCorH}_2$, which readily give the corresponding corrole complexes after Co(III) ion coordination. Although we were unable to completely avoid the formation of isocorrole species, following this approach, it was possible to obtain the fully brominated $\text{Br}_8\text{TPCorH}_3$, impossible to obtain by direct bromination of TPCorH_3 . The UV-vis spectrum of $\text{Br}_8\text{TPCorH}_3$ showed a red shifted Soret-like band at 451 nm, as expected for the fully substituted pattern; after interaction with triethylamine and trifluoroacetic acid, the corresponding monoanion and monocation were formed. While the monocation showed a splitted Soret-like band, it is interesting to note that the deprotonation of $\text{Br}_8\text{TPCorH}_3$ induced a slight blue-shift to the main absorption

band. Since we have already reported the exploitation of $[\text{Br}_8\text{TPCor}]\text{Cu}$ as starting material for the preparation of the fully substituted undecarylcorrole copper complexes by a Suzuki cross-coupling with boronic acids^[39], it was natural to test the demetalation reaction with these derivatives, using $[(4\text{-ClPh})_8\text{TPCor}]\text{Cu}$, as the model compound. The demetalation of $[(4\text{-ClPh})_8\text{TPCor}]\text{Cu}$ in $\text{CHCl}_3/\text{H}_2\text{SO}_4$ mixture afforded the corresponding free base in appreciable yields, while the competitive formation of the isocorrollic form was not observed. The ^1H NMR characterization showed a multiplet of signals around 7 ppm corresponding to the aromatic protons, while in the FAB-MS spectrum it was possible to observe the molecular peak and the fragmentation pattern, with the consecutive loss of several 4-Cl phenyl β -substituents. We are interested to this reaction, because it opens the way to the preparation of undecasubstituted corroles, which are difficult to obtain by the Rothmund condensation of 3,4-disubstituted pyrrole and benzaldehydes.

Experimental section

Reagents

Reagents and solvents (Sigma-Aldrich, Fluka and Carlo Erba Reagenti) were of the highest grade available and were used without further purification.

Materials

Silica gel 60 (70 -230 mesh) and neutral alumina (Brockmann Grade III) were used for column chromatography.

Silica gel 60 (Merck) and neutral alumina 60 F₂₅₄, both on aluminium support, were used for TLC.

Instruments

¹H NMR spectra were recorded with a Bruker AV 300 (300 MHz) spectrometer, using CDCl₃ as solvent. Chemical shifts are given in ppm relative to tetramethylsilane (TMS).

Routine UV-vis spectra were recorded in CH₂Cl₂ on a Varian Cary 50 Spectrophotometer.

Mass spectra (FAB) were recorded on a VG Quattro Spectrometer using *m*-nitrobenzyl alcohol (NBA, Aldrich) as a matrix in the positive-ion mode.

2.6 Syntheses of meso-Arylcorroles

2.6.1 General procedure for syntheses of Triarylcorroles (10b, 11b, 12b)

A solution of pyrrole (5.6 mL, 80 mmol) and arylaldehyde (8.3 mmol) was degassed by bubbling nitrogen for 10 minutes, before the addition of TFA (16 μ L, 0.2 mmol). The mixture was stirred for 15 minutes at r.t. and then diluted with CH_2Cl_2 (30 mL). The reaction mixture was left at r.t. for 1 h; chloranil (1.57 g, 6.4 mmol) was then added and the mixture stirred for a further 15 min. The solvent and the residual pyrrole were removed under reduced pressure. The purification details are described for each case as follows.

2.6.2 Purification of 5,10,15-Triphenylcorrole (10b)

Residue was dissolved in CH_2Cl_2 and chromatographed on silica gel with CH_2Cl_2 as eluent, checking the fractions via UV-vis spectrophotometry. The first green fraction containing corrole was collected, the solvent evaporated under vacuum and the residue crystallized from $\text{CH}_2\text{Cl}_2/\text{CH}_3\text{OH}$ (Yield 21%). The spectroscopic data obtained for the title compound are in agreement with those in the literature^[17].

2.6.3 Purification of 5,10,15-Tris-(4-methylphenyl)corrole (11b)

Residue was dissolved in CH_2Cl_2 and chromatographed on silica gel with CH_2Cl_2 as eluent. The green fraction containing corrole was collected, the solvent evaporated under vacuum and the residue crystallized from $\text{CH}_2\text{Cl}_2/\text{CH}_3\text{OH}$ (Yield 15%). The spectroscopic data obtained for the title compound are in agreement with those in the literature^[17].

2.6.4 Purification of 5,10,15-Tris-(4-methoxyphenyl)corrole (**12b**)

Residue was dissolved in CH₂Cl₂ and purified by chromatography on neutral alumina deactivated with 5% of water eluted CH₂Cl₂. The fraction containing corrole was collected, the solvent evaporated under vacuum and the residue crystallized from CH₂Cl₂/hexane (Yield 8%). The spectroscopic data obtained are in agreement with those in the literature^[17].

2.6.5 Synthesis of 5,10,15-Tris-(4-nitrophenyl)corrole (**13b**)

Pyrrole (4.2 mL, 60.6 mmol) and 4-nitrobenzaldehyde (3.05 g, 20.2 mmol) were dissolved in 250 mL of acetic acid. The solution was refluxed under stirring and the course of the reaction was monitored by UV-vis spectroscopy; after 3 hours the mixture was cooled and solvent removed under reduced pressure.

Residue was dissolved in CH₂Cl₂ and chromatographed on silica gel plug eluted with CH₂Cl₂. Fractions containing corrole were combined and chromatographed again on silica gel with CH₂Cl₂ as eluent. The fractions containing corrole were collected, the solvent evaporated under vacuum and the residue crystallized from CH₂Cl₂/CH₃OH (Yield 20%). The spectroscopic data obtained are in agreement with those in the literature^[17].

2.7 Syntheses of β -Alkylcorroles

2,3,7,8,12,13,17,18-octamethylcorrole (**26b**), 8,12-diethyl-2,3,7,13,17,18-hexamethylcorrole (**27b**) and 2,3,17,18-tetraethyl-7,8,12,13-tetramethylcorrole (**28b**) have been synthesized starting from corresponding biladiene dihydrobromide, obtained following published method^[1]. Biladiene (0.5 g, ~ 1 mmol) was dissolved in 100 mL of methanol and chloranil (0.5 g, 0.2 mmol) was

added. The course of the reaction was monitored via UV-vis spectrometry. After the disappearance of the typical signal of starting material, reaction was quenched with hydrazine solution and solvent evaporated. Residue was dissolved with CH_2Cl_2 , washed three times with water and dried over Na_2SO_4 . Chromatographic purification (alumina oxide 5%, CH_2Cl_2) followed by crystallization (CH_2Cl_2 /hexane) afforded the corresponding corroles free base (Yields ~ 55%). Spectral data correspond to those reported in literature^[6].

2.8 Syntheses of Triarylisocorroles

2.8.1 Synthesis of 5,10,15-Triphenyl-10-ethoxyl-isocorrole (14b)

A solution of triphenylcorrole **10b**, 50 mg (0.095 mmol) in toluene, 40 mL, was placed in 100 mL round-bottomed flask; 108 mg (0.48 mmol) of DDQ and 243 mg (0.48 mmol) of $\text{Sc}(\text{OTf})_3$ were added and the mixture was heated at 50 °C under nitrogen. The progress of the reaction was monitored by UV-vis spectroscopy. After 5 minutes the reaction was complete; the solvent was then evaporated and the product purified by chromatography on silica gel, eluting with a mixture CHCl_3 /hexane (1:1). Recrystallization from CHCl_3 / CH_3OH (1:2) of the first fraction eluted, afforded the isocorrole **14b** in a 20% yield (11 mg; 0.019 mmol).

^1H NMR (CDCl_3 , 300 MHz): δ ppm 15.60 (s, 2 H, NH), 7.72 (m, 2 H, phenyl), 7.59 (m, 4 H, phenyl), 7.48 (m, 6 H, phenyl), 7.21 (m, 3 H, phenyl), 6.70 (s, 4 H, β -pyrrole), 6.63 (d, $^1J = 4.0$ Hz, 2 H, β -pyrrole), 6.43 (d, $^1J = 4.2$ Hz, 2 H, β -pyrrole), 3.79 (q, 2 H, $-\text{CH}_2\text{CH}_3$), 1.30 (t, 3 H, $-\text{CH}_2\text{CH}_3$). UV-vis (CH_2Cl_2): λ max, nm ($\epsilon \times 10^{-3}$, $\text{M}^{-1} \times \text{cm}^{-1}$): 350 (29.8), 432 (48.3), 668 (6.8) 720

(7.5). MS (FAB): m/z (%): 525 (-OCH₂CH₃, 100). C₃₉H₃₀N₄O required C, 82.08; H, 5.30; N, 9.82. Found C, 82.23; H, 5.42; N, 9.65.

2.8.2 Syntheses of 5,10,15-Tris-(4-methylphenyl)-10-methoxyl-isocorrole (**15b**) and of 5,10,15-Tris-(4-methylphenyl)-5-methoxyl-isocorrole (**16b**)

In a 100 mL round-bottomed flask, with a stirring bar, tris-(4-methylphenyl)corrole **11b**, 50 mg (0.088 mmol), was dissolved in 30 mL of MeOH and 19.8 mg of DDQ were added; the mixture was stirred at room temperature and the reaction monitored by UV-vis spectroscopy. After 5 minutes the disappearance of the absorptions of the starting material, confirmed the oxidation of the corrole and the formation of the desired compounds. The solvent was evaporated and the products purified by chromatography on silica gel, by using CHCl₃/hexane (1:1) as the eluent: this procedure allowed the isolation of the isocorroles in 74% overall yield. Subsequent preparative TLC on silica plate (CHCl₃/hexane 1:1, eluent), afforded a first fraction corresponding to the isomer **15b**, while the second fraction was characterized has the product substituted in 5 position (**16b**). Recrystallization from CHCl₃/CH₃OH (1:2), afforded products **15b** and **16b** in a 21% (11 mg; 0.018 mmol) and 43% (23 mg; 0.038 mmol) yield, respectively. Spectroscopic data for **15b**: ¹H NMR (CDCl₃, 300 MHz,): δ ppm 15.62 (s, 2 H, NH), 7.59 (d, ¹J = 8.4 Hz, 2 H, 10-phenyl), 7.48 (d, ¹J = 8.1 Hz, 4 H, 5- and 15-phenyl), 7.26 (d, ¹J = 8.1 Hz, 4 H, 5- and 15-phenyl), 7.06 (d, ¹J = 7.8 Hz, 2 H, 10-phenyl), 6.69 (m, 4 H, β -pyrrole), 6.64 (d, ¹J = 4.5 Hz, 2 H, β -pyrrole), 6.40 (d, ¹J = 4.2 Hz, 2 H, β -pyrrole), 3.50 (s, 3 H, 10-OCH₃), 2.46 (s, 6 H, 5- and 15-phenyl-CH₃), 2.28 (s, 3 H, 10-phenyl-CH₃). UV-vis (CH₂Cl₂): λ max, nm ($\epsilon \times 10^{-3}$, M⁻¹ × cm⁻¹) 357 (29.5), 434 (47.8), 670 (6.7) 725 (7.2). MS (FAB): m/z (%): 567 (-OCH₃, 100). C₄₁H₃₄N₄O required C, 82.25; H, 5.72; N,

9.36. Found C, 82.51; H, 5.49; N, 9.27. Spectroscopic data for **16b**: ^1H NMR (CDCl_3 , 300 MHz): δ , ppm 16.21 (s, 1 H, NH), 15.84 (s, 1 H, NH), 7.59 (d, $^1\text{J} = 8.1$ Hz, 2 H), 7.42 (d, $^1\text{J} = 7.8$ Hz, 2 H, phenyl), 7.27 (m, 6 H, phenyl), 7.07 (d, $^1\text{J} = 8.1$ Hz, 2 H, phenyl), 6.95 (d, $^1\text{J} = 4.5$ Hz, 1 H, β -pyrrole), 6.84 (d, $^1\text{J} = 4.5$ Hz, 1 H, β -pyrrole), 6.56 (m, 2 H, β -pyrrole), 6.51 (d, $^1\text{J} = 4.5$ Hz, 1 H, β -pyrrole), 6.30 (m, 1 H, β -pyrrole), 6.14 (m, 1 H, β -pyrrole), 6.02 (m, 1 H, β -pyrrole), 3.43 (s, 3 H, 5- OCH_3), 2.46 (s, 3 H, phenyl- CH_3), 2.44 (s, 3 H, phenyl- CH_3), 2.30 (s, 3 H, phenyl- CH_3). UV-vis (CH_2Cl_2): λ max, nm ($\epsilon \times 10^{-3}$, $\text{M}^{-1} \times \text{cm}^{-1}$) 404 (37.04), 673 (5.69), 736 nm (4.62). MS (FAB): m/z (%): 567 (- OCH_3 , 100). $\text{C}_{41}\text{H}_{34}\text{N}_4\text{O}$ requires C, 82.25; H, 5.72; N, 9.36. Found C, 82.48; H, 5.54; N, 9.21.

2.8.3 Syntheses of 5,10,15-Tris(4-methoxyphenyl)-10-methoxyl-isocorrole (**17b**)

In a 100 mL round-bottomed flask, with a stirring bar, tris(4-methoxyphenyl)corrole **12b**, 50 mg (0.081 mmol), was dissolved in 30 mL of MeOH and 18.3 mg of DDQ were added; the mixture was stirred at room temperature and the reaction monitored by UV-vis spectroscopy. After 5 minutes the disappearance of the absorptions of the starting material confirmed the formation of the desired compounds. The solvent was evaporated and the products purified by chromatography on silica gel, by using CHCl_3 as the eluent: this procedure allowed the isolation of the isocorroles in 75% overall yield. Subsequent preparative TLC on silica plate ($\text{CHCl}_3/\text{CH}_3\text{OH}$ 5%) afforded a first green fraction corresponding to the isomer bearing methoxyl group on position 10. Recrystallization from CHCl_3 /hexane (1:2), afforded product in a 21% (11 mg; 0.018 mmol) yield. Spectroscopic data for **17b**: ^1H NMR (CDCl_3 , 300 MHz): δ ppm 15.62 (s, 2 H, NH), 7.62 (d, $^1\text{J} = 8.4$ Hz, 2 H, 10-phenyl), 7.53 (d, $^1\text{J} = 8.1$ Hz, 4 H, 5- and 15-phenyl), 6.98 (d, $^1\text{J} = 8.1$ Hz, 4 H, 5- and 15-phenyl),

6.77 (d, $^1J = 7.8$ Hz, 2 H, 10-phenyl), 6.71 (d, $^1J = 3.7$ Hz, 2 H, β -pyrrole), 6.64 (d, $^1J = 3.8$ Hz, 2 H, β -pyrrole), 6.59 (d, $^1J = 3.8$ Hz, 2 H, β -pyrrole), 6.52 (d, $^1J = 3.7$ Hz, 2 H, β -pyrrole), 3.90 (s, 6 H, 5- and 15-phenyl-OCH₃) 3.75 (s, 3 H, 10-OCH₃). UV-vis (CH₂Cl₂): λ max, nm ($\epsilon \times 10^{-3}$, M⁻¹ × cm⁻¹) 371 (29.5), 437 (46.8), 670 (6.4) 727 (7.1). MS (FAB): m/z (%): 615 (-OCH₃, 100). C₄₁H₃₄N₄O₄ required C, 76.14; H, 5.3; N, 8.66. O, 9.9. Found C, 76.31; H, 5.39; N, 8.81; O, 9.49.

2.9 Syntheses of Metalloporroles

2.9.1 Synthesis of [5,10,15-Triarylcorrolates]Cu

TPCorH₃ (**10b**) or TTCorH₃ (**11b**), were dissolved in CHCl₃ and a three fold excess of Cu(AcO)₂ in CH₃OH was added. The mixture was heated to reflux for about 2 hours, and the progress of the reaction monitored by UV-vis spectroscopy. Upon completion, the solvent was removed under reduced pressure, residue dissolved with a few mL of CHCl₃ and purified by chromatography (silica gel, CHCl₃ as eluent). Fractions corresponding to corrole complex were collected and crystallized by CH₂Cl₂/CH₃OH. Yields and spectroscopic data correspond to those reported^[32].

2.9.2 Synthesis of [2,3,7,8,12,13,17,18-Octaalkylcorrolates]Cu

Me₈CorH₃ (**26b**) or Et₄Me₄CorH₃ (**28b**), were dissolved in CHCl₃, a four fold excess of Cu(AcO)₂ in CH₃OH was added and mixture refluxed for 2 hours. Reaction was monitored by UV-vis spectroscopy; after complex formation, the solvent was removed and residue purified by chromatography (alumina 5%,

CH₂Cl₂ as eluent). Crystallization by CH₂Cl₂/hexane afforded corresponding Cu-complexes. Yields and spectroscopic data correspond to those reported^[11].

2.9.3 Synthesis of [5,10,15-Triphenylcorrolato]Co(PPh₃)

TPCorH₃ (**10b**) was dissolved in CHCl₃ and a saturated solution of Co(AcO)₂ and triphenylphosphine in methanol was added. The mixture was refluxed under stirring and the course of the reaction monitored by UV-vis spectroscopy and TLC; after 1 h no starting material was detected. The solvent was evaporated under vacuum, the resulting residue was chromatographed on silica gel with CH₂Cl₂ as eluent, and crystallized by CH₂Cl₂/CH₃OH. Yield and spectroscopic data correspond to those reported^[17].

2.9.4 Synthesis of [2,3,7,8,12,13,17,18-Octamethylcorrolato]Co(PPh₃)

Me₈CorH₃ (**26b**) was dissolved in CHCl₃ and a saturated solution of Co(AcO)₂ and triphenylphosphine in methanol was added. The mixture was refluxed under stirring and the course of the reaction was monitored by UV-vis spectroscopy and TLC; after 2 h the reaction was complete. The solvent was evaporated under vacuum and the resulting residue was purified by chromatography on alumina deactivated with 5% of water and CH₂Cl₂ as eluent. Crystallization by CH₂Cl₂/CH₃OH afforded the corresponding complex. Yield and spectroscopic data correspond to those reported^[11].

2.9.5 Synthesis of [5,10,15-Triphenylcorrolato]MnCl

TPCorH₃ (**10b**) was dissolved in DMF and an excess of MnCl₂ was added. Mixture was refluxed under inert atmosphere for 1 hour, monitoring the progress by UV-vis spectroscopy. After the appearance of the absorption peaks of the complex, solvent was removed and residue purified by chromatography (alumina deactivated with 5% of water, CH₂Cl₂ as eluent). Crystallization by CH₂Cl₂/hexane afforded Mn-complex. Yield and spectroscopic data correspond to those reported^[40].

2.9.6 Synthesis of [8,12-Diethyl-2,3,7,13,17,18-hexamethylcorrolato]MnCl

Corrole Et₂Me₆CorH₃ (**27b**) was dissolved in DMF together with the stoichiometric amount of Mn(AcO)₂ and refluxed, under nitrogen, for 2 h. When UV-vis spectroscopy indicated complex formation, the solvent was evaporated under vacuum and the residue chromatographed on Florisil, using diethyl ether as eluent. Pure Mn complex was obtained by recrystallization from diethyl ether/hexane (1:2). Yield and spectroscopic data correspond to those reported^[11].

2.9.7 Synthesis of [5,10,15-Triphenylcorrolato]FeCl

TPCorH₃ (**10b**) was dissolved in DMF and an excess of FeCl₂ was added. Mixture was refluxed under inert atmosphere for one hour, and monitored by UV-vis spectroscopy. After the appearance of absorption bands of iron complex, solvent was removed under reduced pressure. Residue was chromatographed on alumina (deactivated with 5% of water) eluted with CH₂Cl₂; two fractions were collected, corresponding to the monomeric and dimeric form of iron corrole

complex. The fractions were combined, washed with HCl 1M dried over Na₂SO₄ anhydrous and crystallized with CH₂Cl₂/hexane. Yield and spectroscopic data correspond to those reported^[41].

2.9.8 Synthesis of [2,3,17,18-Tetraethyl-7,8,12,13-tetramethylcorrolato]FeCl

Et₄Me₄CorH₃ (**28b**) was dissolved in DMF together with the stoichiometric amount of FeCl₂ and refluxed, under nitrogen, for 2 h, monitoring the course of the reaction by UV-vis spectroscopy. When spectroscopy showed the reaction was complete, solvent was evaporated in a vacuum and the residue chromatographed on Florisil, using diethyl ether as eluent. Pure Fe complex was obtained by recrystallization from diethyl ether/hexane (1:2). Yield and spectroscopic data correspond to those reported^[11].

2.9.9 Synthesis of [5,10,15-Triphenylcorrolato]GeCl

TPCorH₃ (**10b**) was dissolved in anhydrous DMF under nitrogen atmosphere and a four fold excess of GeCl₄ was added; the mixture was refluxed for about two hours, monitoring the progress of the reaction by UV-vis spectroscopy. When analysis showed the complete conversion of corrole free base in the corresponding metal complex, the solvent was evaporated and the product purified by chromatography on silica gel; the first fraction, eluted with CHCl₃ was the μ -oxo dimer, while the second fraction, eluted with CHCl₃/CH₃OH 5%, was the germanium methoxide complex; corresponding chloride derivative was obtained by treating the collected fractions with HCl 4M. Residue was crystallized by CH₂Cl₂/hexane. Yield and spectroscopic data correspond to those reported^[31].

2.9.10 Synthesis of [2,3,17,18-Tetraethyl-7,8,12,13-tetramethylcorrolato]GeCl

Et₄Me₄CorH₃ (**28b**) was dissolved in anhydrous DMF under nitrogen atmosphere and a four fold excess of GeCl₄ was added; the mixture was refluxed for about two hours, monitoring the progress of the reaction by UV-vis spectroscopy. After the appearance of the typical complex absorption bands, the solvent was evaporated and the product purified by chromatography on alumina (deactivated with 5% of water) with CHCl₃ as eluent. Residue was crystallized by CH₂Cl₂/hexane. Yield and spectroscopic data correspond to those reported^[11].

2.10 General procedures for demetalation process

2.10.1 CHCl₃/H₂SO₄ method

Concentrated H₂SO₄ (1 mL) was added to a chloroform solution (10 mL) of the metal corrole complex (0.2 mmol). The progress of the demetalation reaction was monitored by UV-vis spectroscopy, by diluting an aliquot of the reaction mixture in CH₃OH. The immediate formation of the corrole cation was observed and, after 5 min, distilled water (50 mL) was added and the organic phase extracted by adding chloroform (50 mL). The organic mixture was washed twice with distilled water, then neutralized twice with an aqueous NaHCO₃ solution and dried over sodium sulfate. Chromatography on silica gel (eluent: CH₂Cl₂/hexane 1:1) and crystallization from CH₂Cl₂/hexane afforded the corresponding corrole free base (the yields are reported in Table 2.2), identical to an authentic specimen prepared according to literature methods^[6,11,42-45].

2.10.2 H₂SO₄ method

The metal corrole complex (0.2 mmol) was dissolved in concentrated H₂SO₄ (5 mL) and the reaction was carried out as above. Chromatographic separation on silica gel (eluent: CH₂Cl₂/hexane 1:1) afforded two main fractions; the first one, crystallized from dichloromethane/hexane, was the corrole free base, identical to an authentic specimen prepared according to literature methods^[6,11,42-45]. The second band was separated into two fractions of isomeric isocorrole species after a further chromatographic separation (silica gel, eluent: CH₂Cl₂/hexane 1:1.5).

2.10.3 HBr/HOAc method

HBr/HOAc method. The metal corrole complex (0.2 mmol) was dissolved in 20 mL of a HBr/HOAc (30%) solution. The reaction was carried out as above and chromatography on silica gel (e CH₂Cl₂/hexane 1:1) afforded several fractions, difficult to separate. Further separation was not attempted, due to the overall low yields of the reaction.

References

1. Johnson, A.W.; Kay, I.T. *J. Chem. Soc.*, **1965**, 1620.
2. Dyke, J.M.; Hush, N.S.; Williams, M.L.; Woolsey, I.S. *Mol. Phys.*, **1971**, *20*, 1149.
3. Ghosh, A.; Jynge, K. *Chem. Eur. J.*, **1997**, *3*, 823.
4. Paolesse, R.; Marini, A.; Nardis, S.; Froiio, A.; Mandoj, F.; Nurco, D.J.; Prodi, L.; Montalti, M.; Smith, K.M. *J. Porphyrins Phthalocyanines*, **2003**, *7*, 25.
5. Johnson, A.W. In “*Porphyrins and Metalloporphyrins*”; Smith, K.M., Ed.; Elsevier: Amsterdam, **1975**; p. 729.
6. Paolesse, R. In “*The Porphyrin Handbook*”, Vol. 2, Kadish K.M., Smith K.M., Guillard R. (Eds.) Academic Press: San Diego, **2000**; pp 201-232.
7. Gross, Z.; Galili, N.; Saltsman, I. *Angew. Chem. Int. Ed.*, **1999**, *38*, 1427-1429.
8. Paolesse, R.; Jaquinod, L.; Nurco, D.J.; Mini, S.; Sagone, F.; Boschi, T.; Smith, K.M. *Chem. Comm.*, **1999**, 1307-1308.
9. Koszarna, B.; Gryko, D.T. *J. Org. Chem.*, **2006**, *71*, 3707-3717.
10. Král, V.; Vašek, P.; Dolenský, B. *Collect. Czech. Chem. Comm.*, **2004**, *69*, 1126-1136.
11. Erben, C. In “*The Porphyrin Handbook*”, Vol. 2, Kadish K.M., Smith K.M., Guillard R. (Eds.) Academic Press: San Diego, **2000**; pp 233-300.
12. Luguay, R.J.; Fronczek, F.R.; Smith, K.M.; Vicente, M.G.H. *Tetrahedron Lett.*, **2005**, *46*, 5365-5368.
13. Radecki, J.; Stenka, I.; Dolusic, W.; Dehaen, W. *Electrochim. Acta*, **2006**, *51*, 2282-2288.

14. Jaquinod, L. In "*The Porphyrin Handbook*", Vol. 1, Kadish K.M., Smith K.M., Guillard R. (Eds.) Academic Press: San Diego, **2000**; pp 201-232.
15. Paolesse, R.; Jaquinod, L.; Senge, M.O.; Smith, K.M. *J. Org. Chem.*, **1997**, *62*, 6193-6198.
16. Paolesse, R.; Nardis, S.; Venanzi, M.; Mastroianni, M.; Russo, M.; Fronczek, F.R.; Vicente, M.G.H. *Chem. Eur. J.*, **2003**, *9*, 1192.
17. Paolesse, R.; Nardis, S.; Sagone, F.; Khoury, R.G. *J. Org. Chem.*, **2001**, *66*, 550-556.
18. Nardis, S.; Pomarico, G.; Fronczek, F.R.; Vicente, M.G.H.; Paolesse, R. *Tetrahedron Lett.*, **2007**, *48*, 8643-8646.
19. Lindsey, J. In "*The Porphyrin Handbook*", Vol. 1, Kadish K.M., Smith K.M., Guillard R. (Eds.) Academic Press: San Diego, **2000**; pp 45-118.
20. Vogel, E. *Pure & Appl. Chem.*, **1996**, *68*, 1355-1360.
21. Sessler, J.L.; Gebauer, A.; Vogel, E. In "*The Porphyrin Handbook*", Vol. 2, Kadish K.M., Smith K.M., Guillard R. (Eds.) Academic Press: San Diego, **2000**; pp 1-54.
22. Hohlneicher, G.; Bremm, D.; Wytko, J.; Bley-Escrich, J.; Gisselbrecht, J.P.; Gross, M.; Michels, M.; Lex, J.; Vogel, E. *Chem. Eur. J.*, **2003**, *9*, 5636.
23. Setsune, J.I.; Tsukajima, A.; Watanabe, J. *Tetrahedron Lett.*, **2006**, *47*, 1817.
24. Dolphin, D.; Felton, R. H.; Borg, D. C.; Fajer, J. *J. Am. Chem. Soc.*, **1970**, *92*, 743.
25. Geier III, G. R.; Forris Beecham Chick, J.; Callinan, J. B.; Reid, C. G.; Auguscinski, W. P. *J. Org. Chem.*, **2004**, *69*, 4159.
26. Shen, J.; Shao, J.; Ou, Z.; E, W.; Koszarna, B.; Gryko, D. T.; Kadish, K. M. *Inorg. Chem.*, **2006**, *45*, 2251.
27. Giselbrecht, J.-P.; Gross, M.; Vogel, E.; Will, S. *J. Electroanal. Chem.*, **2001**, *505*, 170.
28. Shine, H. J.; Padilla, A. G.; Wu, S.-M. *J. Org. Chem.*, **1979**, *44*, 4069.

29. Fuhrhop, J.H.; Smith, K.M. In "Porphyrins and Metalloporphyrins", Smith K.M. (Ed.) Elsevier: Amsterdam, **1975**; pp. 757-910.
30. Wasbotten, I.H.; Wondimagegn, T.; Ghosh, A. *J. Am. Chem. Soc.*, **2002**, *124*, 8104-8116.
31. Nardis, S.; Mandoj, F.; Paolesse, R.; Fronczek, F.R.; Smith, K.M.; Prodi, L.; Montalti, M.; Battistini, J. *Eur. J. Inorg. Chem.*, **2007**, 2345-2352.
32. Stefanelli, M.; Mastroianni, M.; Nardis, S.; Licoccia, S.; Fronczek, F.R.; Smith, K.M.; Zhu, W.; Ou, Z.; Kadish, K.M.; Paolesse, R. *Inorg. Chem.*, **2007**, *46*, 10791-10799.
33. Bröring, M.; Hell, C. *Chem. Commun.*, **2001**, 2336-2337.
34. Brückner, C.; Barta, C.A.; Brinas, R.P.; Bauer, A.K. *Inorg. Chem.*, **2003**, *42*, 1673-1680.
35. Smith, K.M. In "The Porphyrin Handbook", Vol. 1, Kadish K.M., Smith K.M., Guillard R. (Eds.) Academic Press: San Diego, **2000**; pp 1-40.
36. Wijesekera, T.; Dupré, D.; Cader M.S.R. Dolphin, D. *Bull. Soc. Chim. Fr.*, **1996**, *133*, 765-775.
37. Mahammed, A.; Giladi, I.; Goldberg, I.; Gross, Z. *Chem. Eur. J.*, **2001**, *7*, 4259-4265.
38. Conlon, M.; Johnson, A.W.; Overend, W.R.; Rajapaksa, D.; Elson, C.M. *J. Chem. Soc., Perkin Trans. I*, **1973**, 2281-2288.
39. Scriveranti, A.; Beghetto, V.; Matteoli, U.; Antonaroli, S.; Marini, A.; Mandoj, F.; Paolesse, R.; Crociati, B. *Tetrahedron Lett.*, **2004**, *45*, 5861-5864.
40. Saltsman, I; Mahammed, A.; Goldberg, I.; Tkachenko, E.; Botoshansky, M; Gross, Z. *J. Am. Chem. Soc.*, **2002**, *124*, 7411-7420.
41. Cai, S., Licoccia, S.; D'Ottavi, C., Paolesse, R.; Nardis, S.; Bulach, V.; Zimmer, B.; Shokhireva, T.K.H.; Walker, F.A. *Inorg. Chem. Acta*, **2002**, *339*, 171-178.
42. Gryko, D.T. *Eur. J. Org. Chem.*, **2002**, 1735-1742.

43. Gryko, D.T. ; Fox, J.P. ; Goldberg, D.P. *J. Porphyrins Phthalocyanines*, **2004**, 8, 1091-1105.
44. Aviv, I ; Gross, Z. *Chem. Commun.*, **2007**, 1987-1999.
45. Nardis, S; Monti, D., Paolesse, R. *Mini-Rev. Org. Chem.*, **2005**, 2, 355-374.

Chapter 3

Triaryl-tetrabenzocorroles: innovative compounds for biomedical applications

Introduction

Photodynamic therapy (PDT) is the oxygen mediated, tumoricidal combination of non-thermal power densities of visible light and non-toxic, light absorbing chemicals. PDT is based on oxidative damage induced by singlet oxygen ($^1\text{O}_2$) to a biological substrates. It has been developed to destroy the unwanted tissue, sparing the normal tissue. The active form of oxygen is generate in situ by energy transfer from a photosensitizers to molecular oxygen. Due to their many-sided properties, porphyrin derivatives, has been revealed themselves as good photosensitizers for PDT; some results, concerning the synthesis of novel porphyrinoids, will be discussed in this chapter.

3.1 History of photodynamic therapy

The therapeutic use of light began in 1900, when Raab reported the destruction of living organisms^[1] by using a combination of acridine orange and light. In the 1920s, Policard^[2] noted an inherently enhanced fluorescence of tumor tissues than healthy ones.

For several decades during the 20^o century, research workers attempted to activate endogenous fluorescent molecules in tumor tissue, either to delineate its boundaries more accurately or to kill cancer cells.

Only in 1960 researches on PDT knew a peremptory development, thanks to S. Schwartz and R. Lipson experiments.

Schwartz had isolated a tumor localizing impurity from hematoporphyrin preparations, that was later named hematoporphyrin derivative (HpD), while Lipson was investigating how to detect tumor tissue by observing the intratumoral fluorescence of hematoporphyrin. Unable to obtain good results with this compound, Lipson began to use Schwarz's HpD, noticing that HpD could be used to destroy tumor tissue^[3,4].

Further developments occurred when Dougherty treated tumor-bearing animals with fluorescein and found that it could work as a photosensitizer. At last, in the 1976, Weishaupt identified the cytotoxic product of the photochemical reaction to be singlet oxygen^[5]. Because of fluorescein has remarkable drawbacks, such as the low singlet oxygen quantum yield and a long wavelength absorption in the green portion of the electromagnetic spectrum that does not penetrate deeply the tissue, photosensitizers porphyrin-based were examined, because they are efficient singlet oxygen generators and have absorption maxima shifted on the red portion of the electromagnetic spectrum.

After several years spent isolating and identifying the active fraction of HpD, a purified version called Photofrin® was produced. At this time Photofrin® has been approved for use in the US against early and late stage lung and esophageal cancers and dysplasias with other indication pending^[6].

This drug is also used in several countries, or its use is pending approval.

Since Photofrin® has gained legal status, many works explaining how PDT works, have been published and many new photosensitizers have been created^[7].

3.2 Principles of PDT

3.2.1 Photochemistry of PDT

Singlet oxygen is the cytotoxic agent of PDT; even if it has a series of absorption bands in the ultraviolet, visible and infra-red, and the direct photoexcitation of molecular oxygen^[8] to produce singlet oxygen is also possible, this method is not much interesting due to small yield of $^1\text{O}_2$.

The main way to produce toxic form of oxygen is by an indirect excitation.

Jablonski diagram shows (Fig. 3.1) the photochemical reaction generating $^1\text{O}_2$ from ground state oxygen^[9].

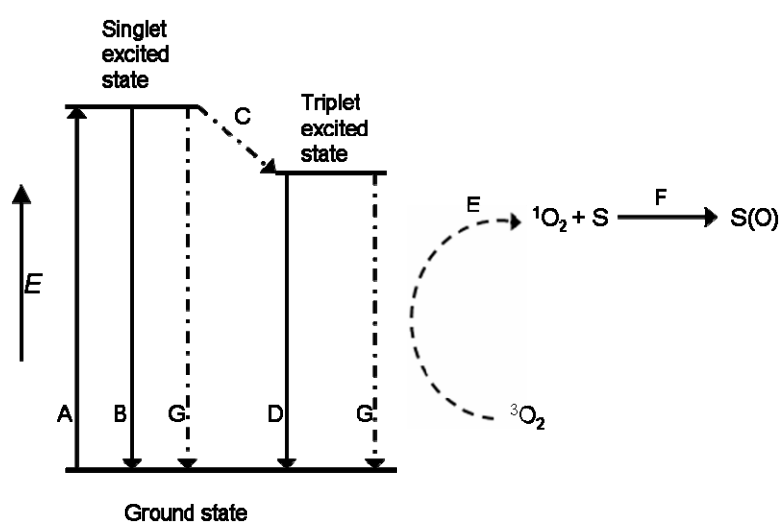


Fig. 3.1 – Jablonski diagram for $^1\text{O}_2$ formation

Illuminating the chromophore with light of the appropriate wavelength, excites it from the ground state S_0 to the excited singlet states S_n (A).

Relaxation of the S_n state, yields to the lowest excited singlet state of the sensitizer S_1 . The chromophores can relax back to the ground state S_0 by emitting a fluorescent photon (B), or to excited triplet states T_1 via intersystem crossing (ISC) (C).

From triplet excited states T_1 the chromophores can relax back to the ground state S_0 by emitting a phosphorescent photon (D), or transferring energy to another molecule via a radiationless transition (E). Radiative triplet to singlet transitions are mechanically forbidden since a change of electron spins is required, however these transitions occur to a very small extent^[10].

Additionally the chromophore can also lose energy through internal conversion or radiationless transitions during collisions with other molecules (G)^[9].

The lifetime of the T_1 state is longer (μs) than that of the S_1 state (ns), allowing this excited state to react in one of two possible ways, named as Type I or Type II mechanism.

Type I mechanism involves hydrogen-atom abstraction or electron transfer between the excited sensitizer and a substrate, yielding an oxidized substrate (S^+) and reduced photosensitizer (P^-). The reduced photosensitizer can react with oxygen to produce superoxide anion (O_2^-), which can then form the highly reactive hydroxyl radical (OH^\cdot)^[11]. The excited photosensitizer ($^3P^*$) can also react with superoxide radical (O_2^\cdot) to produce superoxide anion (O_2^-), which can then create the highly reactive hydroxyl radical (OH^\cdot)^[11] (Fig. 3.2).

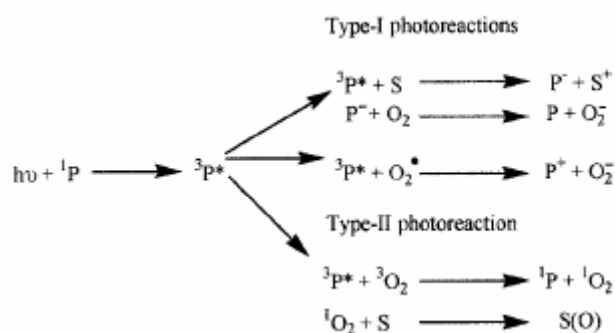
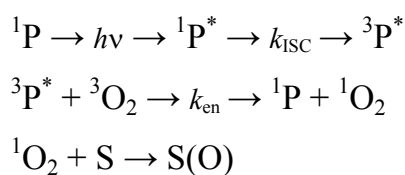


Fig. 3.2 – Type I and II photoreaction

In a Type II mechanism, singlet oxygen is generated via an energy transfer process during a collision of the excited sensitizer with triplet oxygen, as shown in the following scheme:



Where ${}^1\text{P}$ is photosensitizer in the singlet ground state; ${}^1\text{P}^*$ is photosensitizer in the first excited singlet state; ${}^3\text{P}^*$ is photosensitizer in the excited triplet state; k_{ISC} is rate constant for intersystem crossing; k_{en} is rate constant of energy transfer; ${}^3\text{O}_2$ is ground state triplet oxygen; ${}^1\text{O}_2$ is singlet oxygen and $\text{S}(\text{O})$ is an oxygen adduct of a substrate.

In order to have triple to singlet transition, an energy of 94.1 kJ mol^{-1} is required, which corresponds to a radiation with a wavelength of $1274 \text{ nm}^{[12]}$ (Fig. 3.3).

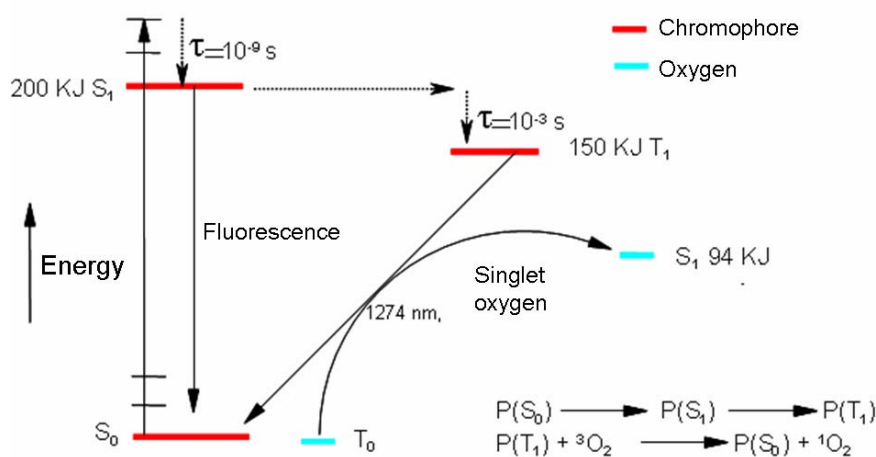


Fig. 3.3 – Photophysical process for singlet oxygen generation

Each photosensitizer molecule can typically produce 10^3 - 10^5 molecules of ${}^1\text{O}_2$, before being degraded through photobleaching by ${}^1\text{O}_2$ or by some other process. In absence of oxygen or any chemical reaction, the lifetime τ of an excited sensitizer is related to the rate constant of the monomolecular deactivation processes by:

$$\tau_T = \frac{1}{k_{\text{dec}}^T} = \frac{1}{k_{\text{phosp}} + k_{\text{isc}}^T}$$

For the triplet state, and

$$\tau_S = \frac{1}{k_{\text{dec}}^S} = \frac{1}{k_{\text{fluor}} + k_{\text{ic}} + k_{\text{isc}}^S}$$

for the singlet states. In presence of oxygen the observed quenching rate of the triplet sensitizer is given by:

$$k_{\text{obs}} = k_{\text{dec}}^T + k_q[\text{O}_2]$$

where k_q is the rate constant characterizing bimolecular quenching by oxygen and is expressed as the sum of oxygen dependent rate constants namely of energy transfer, electron transfer and enhanced intersystem crossing.

Since diffusion controlled k_q is of the order of 10^9 - $10^{10} \text{ M}^{-1}\text{s}^{-1}$, the determination of the correct value of k_{dec}^T is extremely sensitive to traces of oxygen.

The quantum yield of the singlet oxygen formation Φ_Δ , depends on the quantum yield of the triplet states Φ_T , according to:

$$\Phi_\Delta = \Phi_T S_\Delta S_q$$

Where S_Δ is the fraction of the triplet molecules quenched by oxygen and yielding $^1\text{O}_2$, and is given by:

$$S_\Delta = \frac{k_{\text{et}}}{k_q}$$

where k_{et} is the rate constant of energy transfer leading to the formation of $^1\text{O}_2$ ($^1\Delta_g$) and $^1\text{O}_2$ ($^1\Sigma_g$), and S_q is the fraction of oxygen dependent triplet deactivations:

$$S_q = k_q \frac{[\text{O}_2]}{k_q[\text{O}_2] + k_{\text{dec}}^T}$$

The denominator represents all pathway of triplet deactivations; if $k_{\text{dec}}^{\text{T}} \ll k_{\text{q}}[\text{O}_2]$, then $S_{\text{q}} \approx 1$ and Φ_{Δ} becomes equal to $\Phi_{\text{T}}S_{\Delta}$ ^[13,14].

3.2.2 Singlet oxygen

Singlet oxygen, is a highly reactive form of oxygen that is produced by inverting the spin of one of the outermost electrons. In the ground state the outermost electrons are distributed according to Hund rule in the P_x and P_y antibonding orbitals^[15]; since the orbitals are degenerated and the electrons spins are aligned, the quantum numbers of each electron are identical, so they are forced to occupy separate orbitals according to Pauli exclusion principle^[12].

Due to the interaction with excited photosensitizers, the spin of one electron inverts, allowing them to pair together into one of the π_{2p}^* antibonding orbitals, forming the species $^1\text{O}_2$ ($^1\Delta_g$); if the electron inverts its spin continuing to occupy the same orbital, the more reactive species of singlet oxygen $^1\text{O}_2$ ($^1\Sigma_g$) will be formed (Fig.3.4).

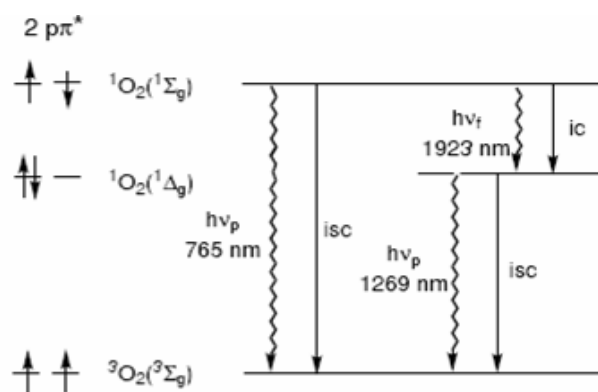


Fig. 3.4 – Energy levels for singlet and triplet oxygen

The lifetime of singlet oxygen is in the range 10-100 μs in organic solvents, which means that the activity is restricted to a spherical volume 10 nm in diameter, centered at its point of production.

In an aqueous environment singlet oxygen lifetime is reduced to 2 μs , because the energy of oxygen-hydrogen stretching in water molecules is closely equal to the excited states energies of $^1\text{O}_2$. Because singlet oxygen reacts so rapidly, PDT-induced damage is highly localized to a region no larger in diameter than the thickness of a cell membrane.

Singlet oxygen can be consumed in two competing ways: physical quenching of $^1\text{O}_2$ by a quencher (bimolecular) or deactivation proceeding by vibrational excitation of solvent molecules (monomolecular).

The second way is the chemical oxidation of a molecule by $^1\text{O}_2$.

Quenching and oxidation of substrates in the ground state are spin allowed reaction; the fraction of $^1\text{O}_2$ molecules that react with the substrate S to oxidize substrate S_{ox} is:

$$f_r = \frac{k_r[\text{S}]}{k_r[\text{S}] + k_d + k_p[\text{Q}]}$$

where k_r is the rate constant of oxidation reaction, k_p the rate constant of physical quenching by a quencher Q, and k_d the rate constant of deactivation in the absence of S and Q. If no quencher is present, the quantum yield of the oxidized substrate Φ_r is given by:

$$\Phi_r = \Phi_{\Delta} f_r = \Phi_{\Delta} \frac{k_r[\text{S}]}{k_r[\text{S}] + k_d}$$

When $k_r[\text{S}] \gg k_d$, the above equation simplifies to $\Phi_r = \Phi_{\Delta}$; in this case all the singlet oxygen available is consumed in a reaction with substrate^[16].

3.3 Photosensitizers

3.3.1 Properties of photosensitizers

There are several groups of UV-vis absorbing molecules that have shown the ability to generate singlet oxygen. A good photosensitizer should exhibit the following properties:

- ✓ Maximum absorption in the region 600-800 nm^[17-19]. The incident intensity of light is reduced by absorption of chromophores in tissues or by scattering, which efficiency increases as the wavelength is decreased. One of the main components of biological systems is water, that absorbs wavelength above 800 nm. Consequently the window for optimum penetration lies between 600 and 800 nm, that means in the red portion of the spectrum. The upper limit of the wavelength to produce ¹O₂ depends by the energy necessary for the ¹O₂ formation ($\lambda < 1270$ nm, $\Delta E > 94.1$ kJ mol⁻¹)
- ✓ Minimum absorption in the region 400-600 nm^[13,20,21]. In this region there is the maximum distribution of daylight, so photosensitizers absorbing in this region enhance photosensitivity of the skin, which is a side effect of PTD. Photosensitization of the skin has been the major drawback of first generation sensitizers based on HpD.
- ✓ High quantum yields of ¹O₂. The quantum yields Φ_{Δ} vary in the range 0.3-0.8 for most sensitizers, but it shouldn't be overestimated because depending on other factors, such as interaction with surrounding molecules, aggregation of the sensitizer, oxygen depletion and side reactions.
- ✓ Photostability. A sensitizer should be stable against photodegradation and against oxidation by ¹O₂ or other reactive oxygen species generated in situ. Photobleaching plays an important role in decreasing skin sensitization.
- ✓ Non-toxic and phototoxic. Low dark toxicity is a desirable factor to avoid unnecessary strain in the organism prior to irradiation. The overall destructive

photodynamic effect of the sensitizers on biological material is called phototoxicity.

- ✓ Specific retention in the malignant tissue. The specific retention of a sensitizers in the malignant tissue is a consequence of different kinetic of sensitizers removal from the malignant and the healthy tissue. The concentration difference is adjusted within several hours after sensitizers administration and depends by its nature. Effectual removal of the sensitizer from the healthy tissue precludes its photodynamic damage^[22].
- ✓ Fluorescence. Fluorescence of the sensitizer enables detection of the sensitizer distribution in vivo. To retain both function of the sensitizer, fluorescence and $^1\text{O}_2$ production, the ratio Φ_f/Φ_{ISC} should be optimized^[13].
- ✓ Solubility. Sufficient solubility of the sensitizer in aqueous media is important for direct intravenous application and transportation to the intended target location.

3.3.2 Photophysic of photosensitizers

Porphyrins, chlorins and bacteriochlorins are among the most common photosensitizers for in vivo PDT. There are several reasons that played a key role for the diffusion of these macrocycles as drugs. The ability to selectivity localize in a variety of tumors^[23], along with the low-dark toxicity of porphyrin derivatives, prompted their initial choice as very promising photosensitizers.

Porphyrinoid based compounds have many others useful features: different synthetic procedures have been developed, making easy the preparation of number of differently functionalized compounds. Moreover the chemical stability, the ability to form complexes with a wide variety of different metal ions, the affinity for serum proteins and their favorable pharmacokinetic properties: these are some of the essential requirements for a good photosensitizer.

Finally porphyrins and related compounds are attracted scientists attention for their photophysical properties, because they are able to absorb the light in the red portion of the spectrum; this is the light that could penetrate deeper in the tissue^[24].

Porphyrins, are fully conjugated compounds with an 18 π electrons aromatic systems; chlorins and bacteriochlorins which retain the same molecular frame, differ for the presence, respectively, of one and two reduced double bond (Fig. 3.5).

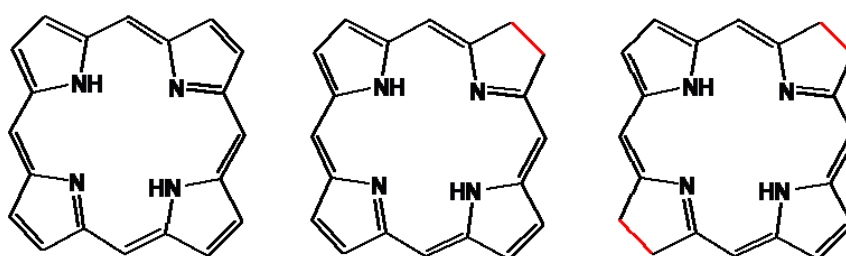


Figure 3.5 – Structure of porphyrin, chlorin and bacteriochlorin

The main absorption band of these macrocycles, named Soret band, is located around 400 nm; unfortunately radiation with that wavelength does not penetrate deeply in the tissue (Fig. 3.6).

More useful for PDT are the weaker absorption bands named Q bands, located around 630 nm for porphyrins, 650 nm for chlorins and 710 nm for bacteriochlorins.

The different absorption spectra can be explained assuming that the π electrons in the aromatic ring behave as particles in one dimensional square well potential, which is a region of length L , bounded on each side by an infinitely high potential energy barrier.

Below is shown the solution of Schrödinger equation, where h is Plank's constant, n is the energy state of the electron, m its mass, and L the length of confining region.

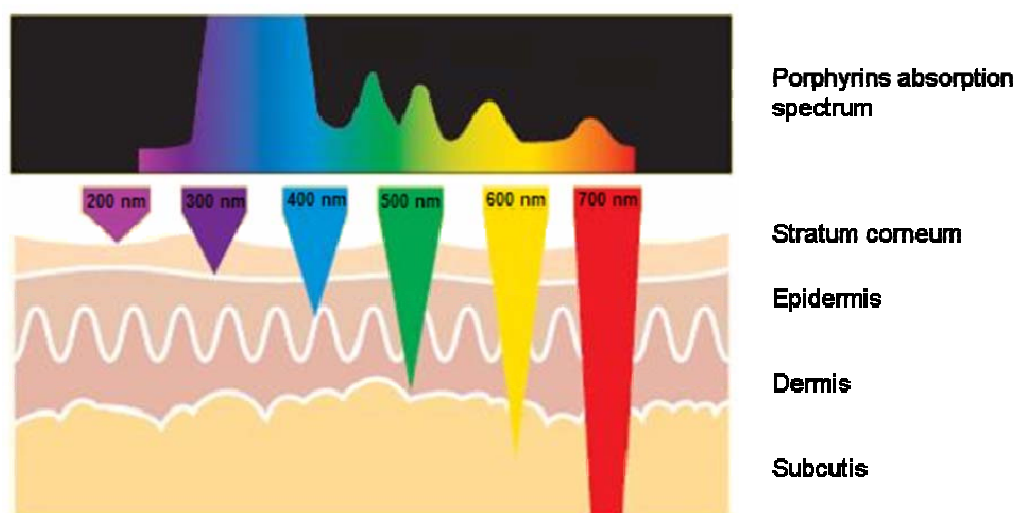


Fig. 3.6 – Wavelength of light and skin penetration

The term $E(n, N)$ is a perturbation to the energy levels due to electron-electron interactions when there is more than one electron in the box, and N in the number of additional particles.

$$E_n = \frac{h^2(n+1)^2}{8mL^2} + E(n, N) \quad n = 0, 1, 2, \dots; N = 1, 2, 3, \dots$$

The perturbation term is equal to zero if only one electron is in the box, but raises the energy of the levels as the number of electrons increases, so the energy required to excite one electron from the ground state ($n=0$) to an excited state ($n=9$) is greater when more of one electron ($N>1$) is confined in the potential well. Since the energy of light is inversely proportional to the wavelength, blue shifted radiation requests to excite the single particles.

Porphyrins, chlorins and bacteriochlorins have respectively 22, 20 and 18 π electrons confined in the same region of space. Therefore the absorption maxima of porphyrins are more blue shifted than chlorins one, and so on for bacteriochlorins.

3.4 Biological mechanism of action

Originally was thought that PDT could destroy tissues by damaging cells which had accumulated enough photosensitizer and had received enough light to produce lethal amount of singlet oxygen. Nevertheless, understand how this technique works, is still a target of the research.

The cytotoxic species generated intracellularly upon activation of sensitizers, cause death of tumor cells by necrosis and/or apoptosis (programmed cell death)^[25,26].

Porphyrin induces apoptosis primarily by mitochondrial damage^[27], and this damage usually occurs rapidly, probably as a result of a cascade-like process, leading to a rapid loss of treated tissue^[28].

In porphyrin-based sensitizers can also occur DNA damage^[29], because cell nucleus is considered a target in PDT, and porphyrins have the ability to promote DNA cleavage^[30] and RNA modification^[31].

Another important mechanism of tumor necrosis is the damage to the tumor vasculature, thus starving the tumor of oxygen and nutrients^[32].

In the initial phase after irradiation, plasma membranes and membranes of mitochondria and lysosomes start to disintegrate, which causes depletion of ATP and liberation of phospholipids, leading to the release of several vasoactive and inflammatory mediators^[33]; these substances initiate an acute inflammation and edema, and the following hemorrhaging creates areas of local hypoxia and a necrotic process by nutrient privation.

The mechanism for porphyrins tumor selectivity is not yet completely understood, but important roles are those of their affinity towards plasma protein, especially with low density lipoproteins^[34], the high content of macrophages in tumor cells^[35], and the lower pH intracellular^[36].

LDL receptor sites are abundantly expressed on the membranes of proliferating tumor cells, and can be internalized by endocytosis; hydrophobic

porphyrins, which form aggregates in aqueous solution, are ingested by macrophages, or by passive diffusion through the plasma membrane.

Hydrophilic porphyrins show low affinity for binding to LDL, but bind strongly albumin^[37].

There are several localization where porphyrins tend to accumulate inside the cell, but the main sites are the lysosomes, the mitochondria, the endoplasmatic reticulum, the Golgi apparatus, and sometimes the nuclei of tumor cells.

Also the hydrophobicity and the charge play an important role: cationic compounds are reported to accumulate in mitochondria^[38], due to the highly negative electrochemical potential of the inner mitochondrial membrane, while anionic compounds target cell lysosomes, which have a low internal pH^[39].

In general, porphyrin sensitizers display multiple localization sites within the cell, which might account for their effectiveness in tumor cell destruction. In addition to the direct effects on tumor cells, PDT also induces indirect effects mediated by damage to the tumor vasculature or by modulation of the immune system^[40,41].

Results and discussion

3.5 PDT: porphyrinoids in the service of medicine

In paragraph 3.3.1 have been roughed out main properties that a good sensitizer should have. Porphyrinoids are endowed of a large chemical versatility and variety of properties, fulfilling the requirements for tumors and other diseases treatment.

Since the preparation of a purified form of hematoporphyrin derivative^[4], several compounds have been developed, with the aim to improve tumor-selectivity and photosensitizing properties. A short account about the progress in this field of research is next given.

3.5.1 Exploitation of porphyrin derivatives in PDT^[42]

Hematoporphyrin was the first tetrapyrrolic macrocycle experimented in PDT; it was isolated from the hemoglobin using concentrated sulfur acid. However it was not possible to obtain pure Hp after the work-up because of its high reactivity, which led to the formation of phototoxic oligomeric components. Not reacted Hp, classified as first-generation photosensitizers together with other Hp derivatives, is a good photosensitizer, but it can not be used in PDT because of the short retention time.

After the improvement of production procedure, a product called hematoporphyrin derivative was obtained; this compound as know with the

commercially name of Photofrin[®], is a mixture of hematoporphyrin monomer, dimer and oligomers, but the latest one is the main fraction after purification by HPLC.

The treatment of Hp with 5% sulfuric acid in acetic acid causes acetylation and elimination of hydroxyethyl groups; the product of this reaction is the “HpD Stage I”, which mainly contains HpD Stage I but also not reacted Hp. In the following basification the acetoxyethyl groups can be hydrolyzed back to hydroxyethyl or eliminated to vinyl groups, giving “HpD Stage II”. This product is not purified Hp but a mixture of monomeric and oligomeric porphyrins (Fig. 3.7)

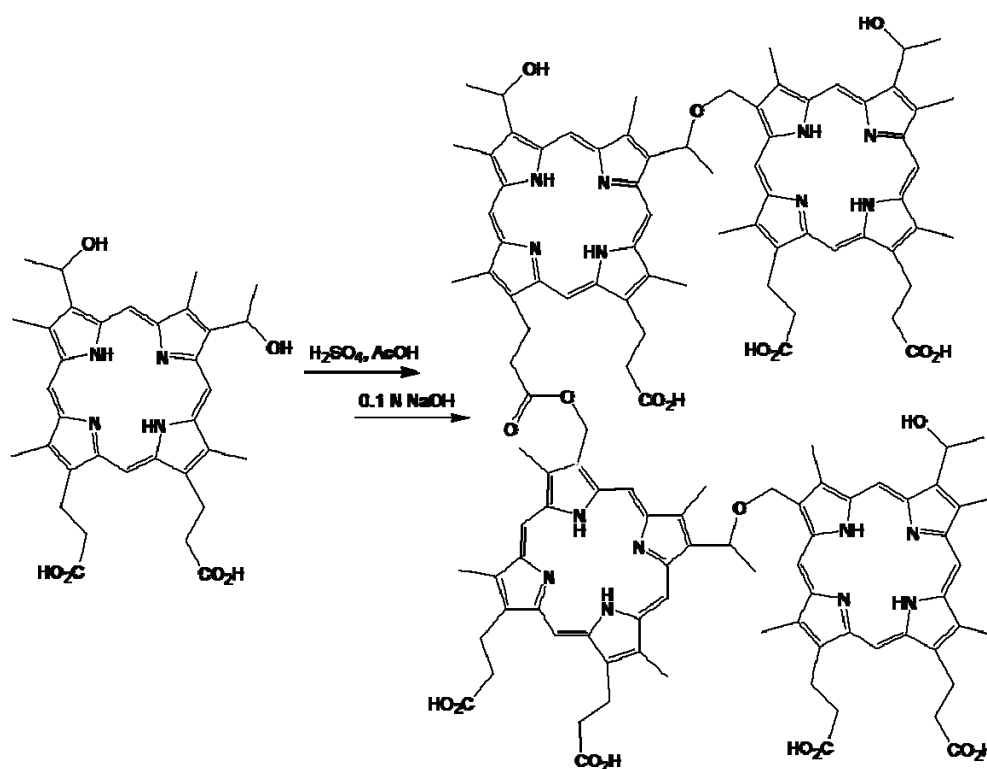


Fig 3.7 – Hp and oligomers in HpD

Among the drawbacks of HpD, its absorption spectrum is probably the most serious limitation, because the weakness of the bands able to absorb light with long wavelengths. Thus the research steered to photosensitizers with better photophysical features.

Synthetic porphyrins, phthalocyanines, texaphyrins, chlorins and bacteriochlorin, belonging to the group of second-generation photosensitizers, present a red-shifting of absorption bands, also then the ability to produce $^1\text{O}_2$ with larger yield.

While in the first generation photosensitizers naturally occurring β -alkyl porphyrins were used, the second generation was based on synthetic derivatives: macrocycles bearing meso aryl substituents.

Tetrakis-(4-sulfonatophenyl)porphyrin (**1c**) and tetrakis-(3-hydroxyphenyl)porphyrin (**2c**) showed to be tens times more effective as photosensitizers. A further advantage of tetrapyrroles functionalized with sulfonato moieties, is their hydrophilicity; the sulfonic group has low pK_a value and remains in anionic form throughout the physiological pH range. In this way it does not need any carrier to avoid the self-aggregation process that would occur in aqueous system. Unfortunately, a neurotoxicity in mice after exposure to high doses of porphyrins has been reported^[43], so its experimentation ceased.

Since larger is the aromatic system stronger is the absorption at longer wavelength, phthalocyanines (**3c**) and naphthalocyanines, which have respectively benzene and naphthalene rings fused on pyrrolic positions; have been experimented. They also differ from porphyrins because carbons of methine bridges are replaced with nitrogens.

Because these compounds absorb strongly, they can be used in small doses, up one order of magnitude lower. Anyway the high hydrophobicity and the difficult synthetic pathway represent serious limitations to their exploitation as drugs.

The reduction of one or two double bonds in the peripheral positions, leads to the formation of chlorin and bacteriochlorin (if it has two antipodal double bonds reduced) or isobacteriochlorin (two adjacent reduced double bonds). Also these derivatives show a red-shift of absorption spectra, as explained in paragraph 3.3.2.

Moreover, many others macrocycles have been tested in studies concerning PDT, such as porphyrin isomers (porphycene **4c** and texaphyrin **5c**) or the natural or partially synthetic second-generation photosensitizers (chlorin prepared from protohemin or bilirubin, chlorophylls).

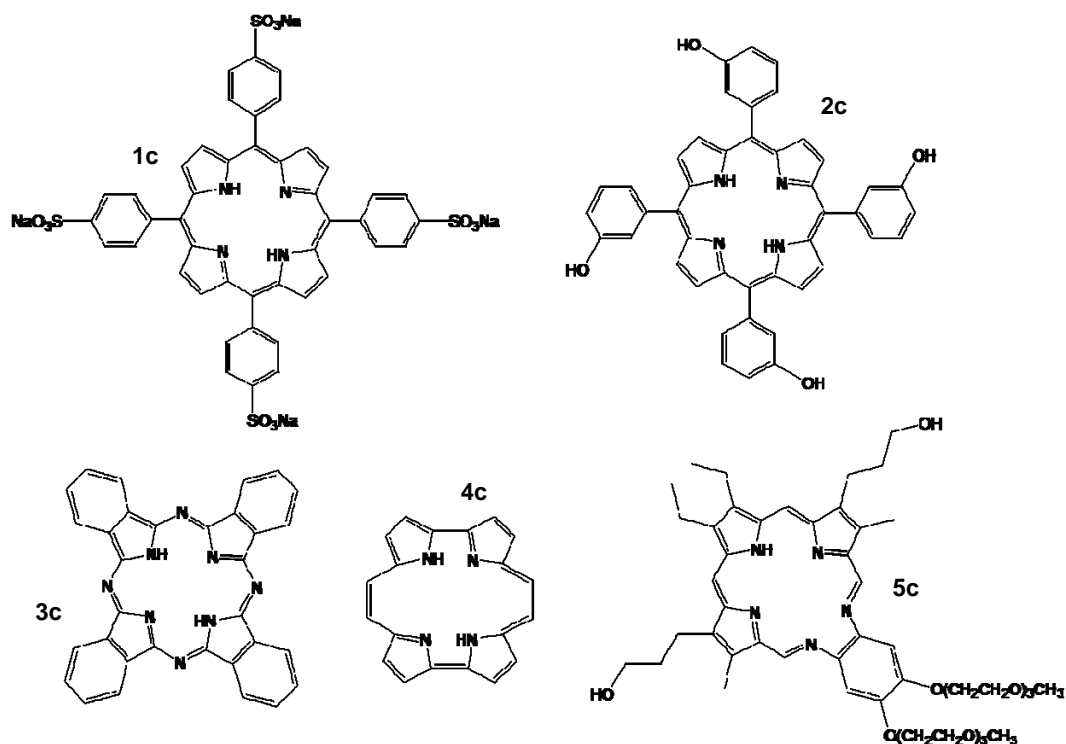


Fig. 3.8 – Tetrapyrrole exploited in PDT

3.5.2 Benzoporphyrins

Chemical modification of synthetic porphyrin macrocycles at the peripheral position have attracted intense interests for a number of years. Thank to development of new methodologies for easy access to functionalized porphyrins, above all meso aryl derivatives, the tedious total synthesis of porphyrins can be avoided, and a variety of new macrocycle can be efficiently synthesized. Among the chemical modifications, the functionalization of tetrapyrroles at their β -pyrrolic positions is particularly attractive, because of the potential applications

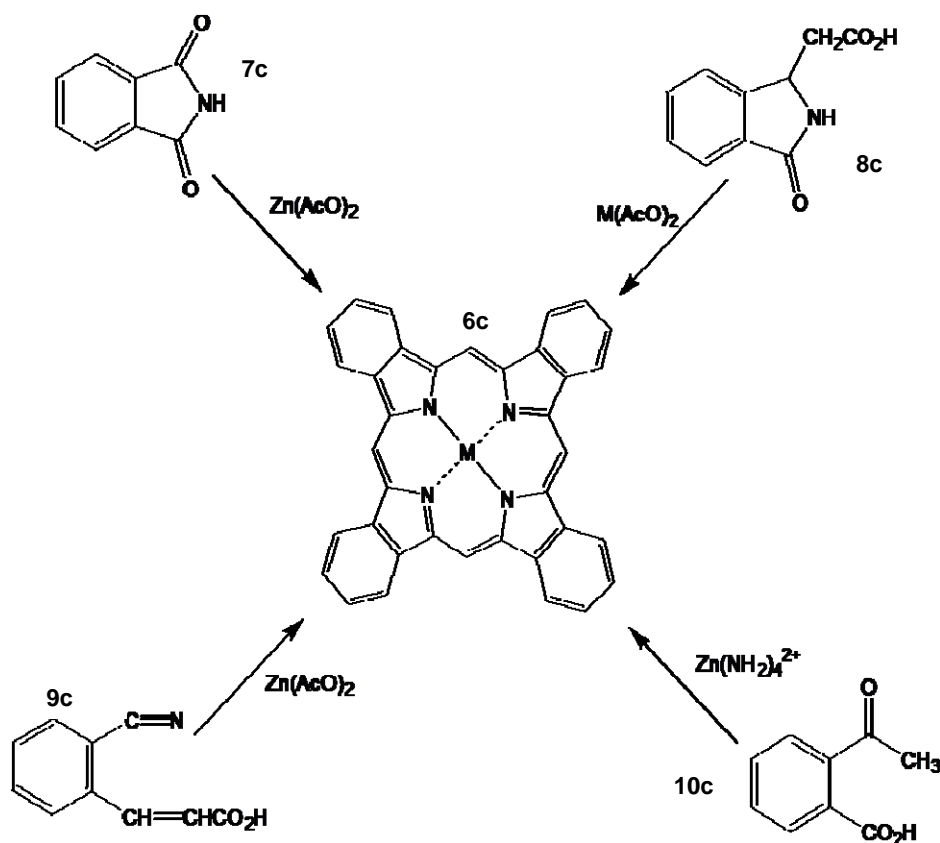
involving addition of new bonds to directly conjugate the porphyrin macrocycle^[44].

The extension of π -conjugated systems is interesting because the potential applications of such a kind of compounds, either in the medicinal area and in material science^[45,46]. The most obvious method to extend the π -conjugation of porphyrins is by fusing aromatic subunits at the β -pyrrolic positions. In this way porphyrins are converted in the corresponding benzoporphyrins (TBPorH₂), that are chemically stable compounds, endowed with useful chemical, physical and spectroscopic properties. Among those, their absorption spectra are significantly shifted to the infrared region; while maximum absorption band of porphyrins falls around 420 nm, and other bands exist between 500 and 650 nm, TBPorH₂s have absorbance in the near IR region, which allows deep light penetration into tissue, making them as suitable photosensitizers for PDT. They have similar physical properties compared with phthalocyanines, which is one of the most widely studied organic pigments, having many applications in industry as dyes, inks, catalysts, electrical conductors and other optical materials. Similarly, TBPorH₂s have found applications as opto-electronic and non-linear optical materials, luminescent markers for oxygen and near-IR labeling dyes.

Benzoporphyrins appeared for the first time on scientific literature when Baker reported their presence in trace amounts in various shale oils and petroleum^[47]. Despite the increasing interests in their synthesis and characterization, researches on tetrabenzoporphyrins have progressed slowly, due to the difficult synthetic access to these compounds, especially for unsymmetrical benzoporphyrins such as the mono- and dibenzoporphyrins.

Helberger first described the syntheses of TBPorH₂ from *o*-cyanoacetophenone and various phthalimidines^[48]. Two main approaches were utilized as synthetic methodologies for tetrabenzoporphyrins syntheses. Since TBPorH₂ resemble phthalocyanines, it was thought to mime the high temperature condensation of phthalimidine derivatives (**7c**) in the presence of a metal salt.

Then, a second approach was developed, adapting the general porphyrin synthesis of condensation of pyrrole (**8c**) with meso-carbon donors^[49]. In this case pyrrole was replaced with isoindole, which however is unstable and not easy to synthesize.



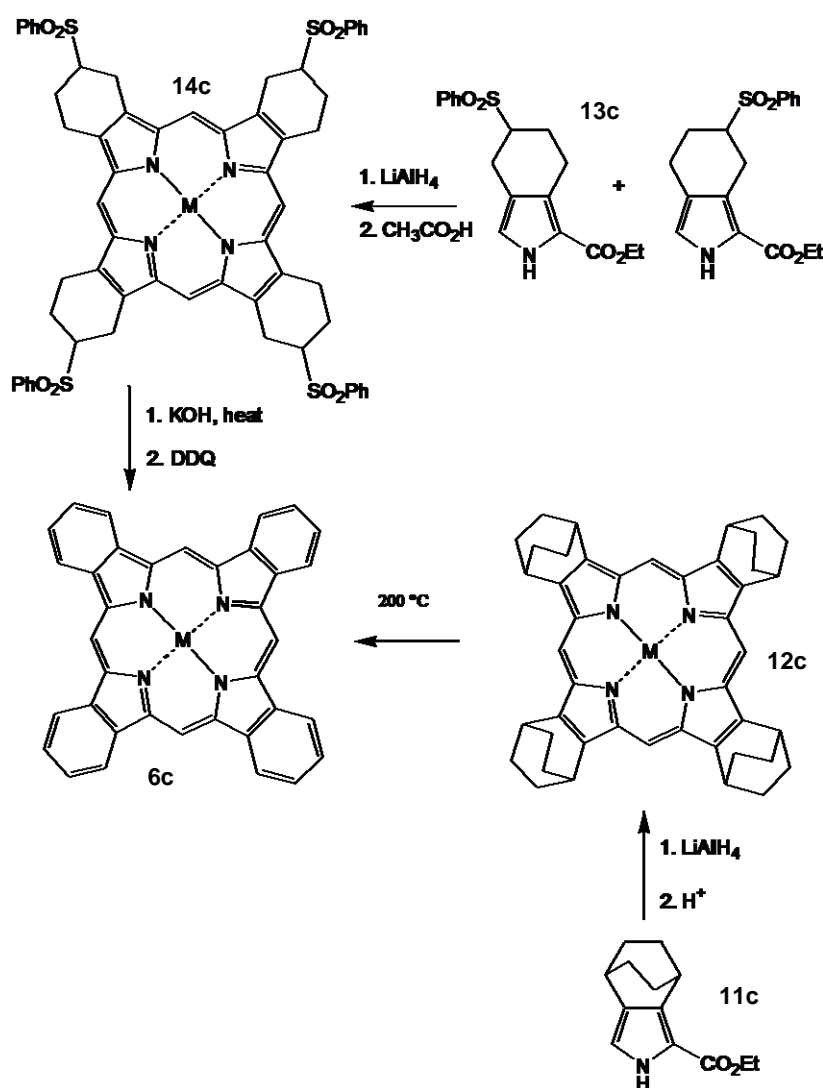
Scheme 3.1 – Procedures for synthesis of symmetrical benzoporphyrins

Improvement of TBPorH_2 synthesis was made by Linstead's group^[50], in which TBPorH_2 were prepared by high temperature condensation of *o*-cyanocinnamic (**9c**) acid in presence of zinc salts^[51], or by using 3-carboxymethylphthalimidine with zinc acetate as template; the yield of this last method was reported to be higher.

Tetrabenzoporphyrin was also isolated by Vogler and Kunkely^[52] after reacting 2-acetylbenzoic acid (**10c**) with zinc acetate as template, while a further

methods employs phthalimide or its potassium salt with sodium acetate or malonic acid in the presence of $\text{Zn}(\text{AcO})_2$ at $360\text{ }^\circ\text{C}$ (Scheme 3.1).

Rothmund condition afforded, in low yield, metalated symmetrical benzoporphyrins from unstable isoindole through inert atmosphere pyrolysis in the presence of metals or metal salts, or from refluxing in a high-boiling solvent (1,2,4-trichlorobenzene or 1-chloronaphthalene). Meanwhile, Ono et al^[53] avoided the use of instable isoindole by generating a masked isoindole (**11c**) reduced with lithium aluminum hydride, before the cyclization reaction. The eventual generation of tetrabenzoporphyrin **6c** from **12c** is obtained through a retro-Diels-Alder reaction by just simply heating at $200\text{ }^\circ\text{C}$.



Scheme 3.2 – Syntheses of benzoporphyrins from different precursor

Recently, Vicente^[54] et al. developed milder and more modern synthetic method starting from pyrrole-fused 3-sulfolene (**13c**) obtained from classical Barton-Zard conditions^[55], which was reduced with LiAlH₄, and then cyclotetramerized in acetic acid; following oxidation was achieved with DDQ.

The products of this reaction were a mixture of isomers of phenylsulfonyl-substituted porphyrins (**14c**), separated in 60% yield.

The elimination of the phenylsulfinate units was achieved under basic condition and subsequent aromatization with DDQ afforded symmetrical benzoporphyrin (Scheme 3.2).

Compared with porphyrins, unsubstituted TBPorH₂ has very poor solubility due to its extended, planar, π -conjugated system, which tends to give high π - π stacking (aggregation). However, substituted benzoporphyrins on *meso* or on β -fused ring positions, have enhanced solubility due to their significantly nonplanar structure; this is an effect of the steric hindrance generated from the substituents.

3.6 Syntheses of Triaryl-tetrabenzocorroles

Corroles photophysical properties are similar and sometime better, to those of porphyrins. Having in mind this fact, we thought to synthesize and characterize suitable corrole derivatives as compounds for biomedical application; in particular our attention was attracted by triaryl-tetrabenzocorrole.

The synthesis and the characterization of these compounds, was the purpose of the research I carried out during the six months spent in the Department of Chemistry of Louisiana State University, under the supervision of professors Maria Graça H. Vicente and Kevin M. Smith.

During this time several synthetic procedures from suitable precursors were tested, in order to point out a good methodology leading to tetrabenzocorrole.

3.6.1 Synthesis of precursor: 4,5,6,7-tetrahydroisoindole

The general synthetic approach for meso aryl-corroles syntheses is one or two steps acid catalyzed condensation between aryl-aldehyde and pyrrole.

In last fifteen years, several easy approachable procedures for corrole preparation have been developed, and some of those, modified where needed, were tested in order to obtain the target molecules of our research.

The main methodologies mimics, of course, those for tetrabenzoporphyrin synthesis. A possible method starts from bicyclooctadiene fused pyrrole, and the final oxidation is accomplished by thermal retro-Diels-Alder reaction^[53]. However the second step requires strong conditions in the retro-Diels-Alder step, making it unsuitable for our purpose.

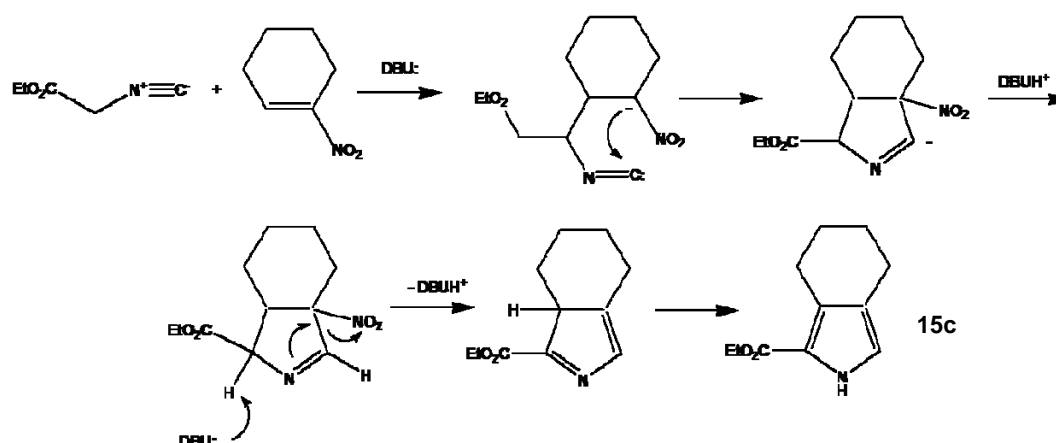
The procedure based on pyrrole-fused 3-sulfolene has been already tested, but corrole was obtained with very small yield.

Since isoindole, that is the most straightforward route to expanded aromatized macrocycles is not a stable compound, we preferred to use a strategy based on a stable isoindole derivative (4,5,6,7-tetrahydroisoindole, **15c**) as precursor for the corrole formation, while the eventual aromatization of fused rings is carried when the macrocycle synthesis is fulfilled.

This pyrrole was easily synthesized from commercially available reagents via Barton-Zard procedure^[56]; it is a condensation reaction between nitro-olefin and ethyl-isocyanoacetate, catalyzed by a bulky base as DBU (Scheme 3.3).

Usually *tert*-butyl- or ethyl-isocyanoacetate are chosen for the reaction; electron-withdrawing substituents on α position is required to protect pyrrole from oxidative polymerization.

Even if the cleavage of *tert*-butyl group and the following work up are easier procedures, we preferred to use ethyl-isocyanoacetate as starting material, because it returns the final product in higher yield and also because it is less expensive.



Scheme 3.3 – Barton-Zard procedure for synthesis of pyrrole

1-Nitro-1-cyclohexene was dissolved in freshly distilled THF under Ar atmosphere, and mixture cooled down at 0°C for 10 minutes, then ethyl-isocynoacetate was added dropwise and mixture stirred for further 10 minutes followed by the dropwise addition of DBU.

After 15 minutes ice bath was removed, and mixture stirred at room temperature for 16 hours, then residue was washed with 10% HCl, and extracted with ethyl acetate.

Brownish oil residue was purified by silica gel chromatography eluted with hexane/ethyl acetate 10/1; final product, appearing as a white solid, was characterized with ¹H NMR spectroscopy (Fig. 3.9).

Deprotection of pyrrole was achieved in two steps: heating pyrrole with an excess of sodium hydroxide in ethylene glycol at 100 °C for 60' leads to the loss of ethyl group, while the decarboxylation of pyrrole was accomplished by raising up the temperature to 200 °C for 30'.

Deprotected pyrrole (**16c**) has to be stored at -20°C in the dark or used as soon as possible in order to avoid its decomposition, pointed out by the changing of color of the solid (from light yellow to black).

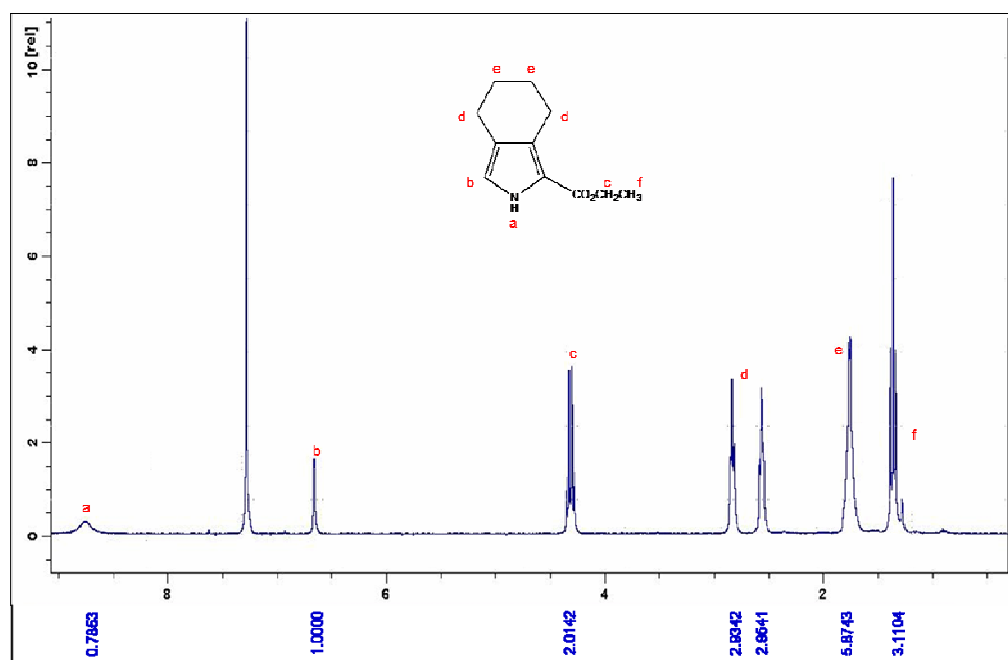


Fig.3.9 – ¹H NMR spectrum of protected tetrahydroisindole

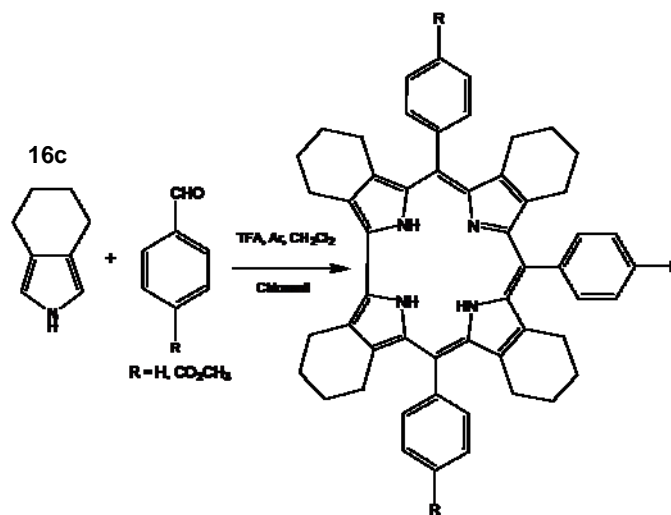
3.6.2 Synthesis of triaryl-tetrabenzocorroles: one step procedure

Modified Rothemund^[57] and Paolesse methods are two powerful tools in the field of corroles chemistry, but the first method is not suitable for our purpose because required to much strong conditions (refluxing acetic acid for two-three hours); the good results mentioned by Paolesse^[58] for one pot synthesis of triarylcorroles, encouraged us to test that procedure in order to get the target compound. In the reported paper an excess of pyrrole versus aldehyde is reacted with TFA as catalyst in neat condition. The main product of this step is bilane, the linear precursor of corrole, whose yield is further increases by the following dilution of the mixture with CH₂Cl₂. Final oxidative ring closure is operated with chloranil or DDQ. We had to fit this procedure on the basis of the different conditions of starting material.

The solventless procedure may work because pyrrole, being liquid at room temperature, acts as solvent at the beginning of the process; our functionalized

pyrrole is solid, so we had to dissolve it together with aryl-aldehyde at once in a few mLs of dichloromethane; reaction mixture was stirred at room temperature under Ar atmosphere, for 5 minutes before the addition of catalyst (TFA).

The remaining steps of the synthetic pathway were similar than those reported on published work (Scheme 3.4). Longer time is requested for the oxidative ring closure carried out with chloranil, because the steric hindrance of β -



Scheme 3.4 – Modified Paolesse method for corrole synthesis

substituents prevents the oxidation of the macrocycle; the course of the reaction was monitored by UV-vis spectroscopy.

The influence of several parameters on the course of the reaction were tested: TFA and $\text{BF}_3 \cdot \text{OEt}_2$ as catalysts, chloranil or the stronger DDQ for oxidative ring closure step, and also the duration of oxidation reaction.

The best results were guaranteed using TFA as catalyst, and reacting bilane chloranil for 12 hours. Spectroscopic analysis (Fig. 3.10) showed the formation of a having a macrocycle structure, more similar to a porphyrin than to a corrole, but it was not possible to purify adequately that product for a further characterization.

Either benzaldehyde and methyl-4-formylbenzoate (*p*-carboxymethyl-benzaldehyde) were tested with this approach, to explore the influence of substituents on phenyl rings, but both the cases we did not obtain the corrole.

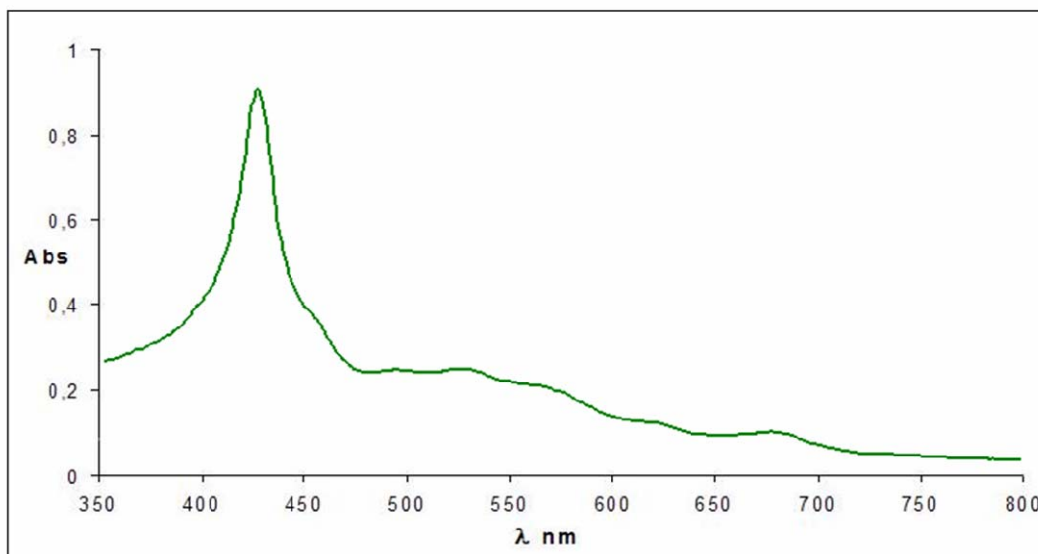


Fig. 3.10 – UV-vis spectrum of reaction mixture from modified Paolesse's method

The reason of the failure has to be pursued in the starting dilution of reagents that may drive the condensation toward the formation of porphyrinogen instead of bilane.

The dilution matter was overcome by operating as close as possible to the original experimental conditions reported by Paolesse. How was possible to mix the reagents without solvent? Having in mind this assumption.

Reaction leading to corroles or porphyrins, starts with an electrophilic substitution of carbonyl group of aldehyde on pyrrole; this reaction has an esothermic character, more prominent in β -alkyl substituted pyrrole. The heat released during the reaction, accomplishes the transition of pyrrole from solid to liquid state, realizing the ideal conditions so that the condensation take place; of course catalyst addiction accelerates the process.

To initiate pyrrole fusion, then completed by TFA addition, the flask was slightly heated.

The dark red color taken on by reaction mixture, likely suggested the polymerization of pyrrole; the apparition of typical absorption bands of

olypyrrole open chain derivatives in the UV-vis spectrum (Fig. 3.11) confirmed this hypothesis.

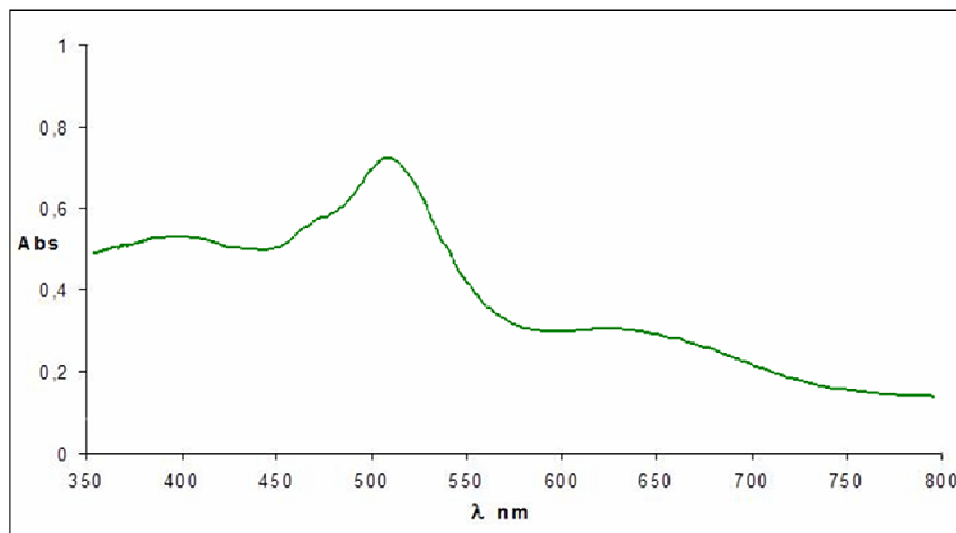


Fig. 3.11 – UV-vis spectrum for corrole synthesis with solventless method

Unfortunately tetrahydroisindole has a very low stability and an high tendency to give unwanted reaction, so we thought to repeat the synthesis with as little catalyst as possible, replacing neat TFA with its vapors. Despite the smallest quantity of catalyst used seemed to restrain the formation of polypyrrolic products, also in this case just traces of corrole were detected, so we were unable to purify and characterize it adequately. A common denominator of all those experiments was the initial high concentration of reagents; to avoid these strong conditions, we tested procedure putted right by Gryko for synthesis of triarylcorrole, that is based on milder conditions.

3.6.3 Synthesis of triaryl-tetrabenzocorroles: two steps procedure

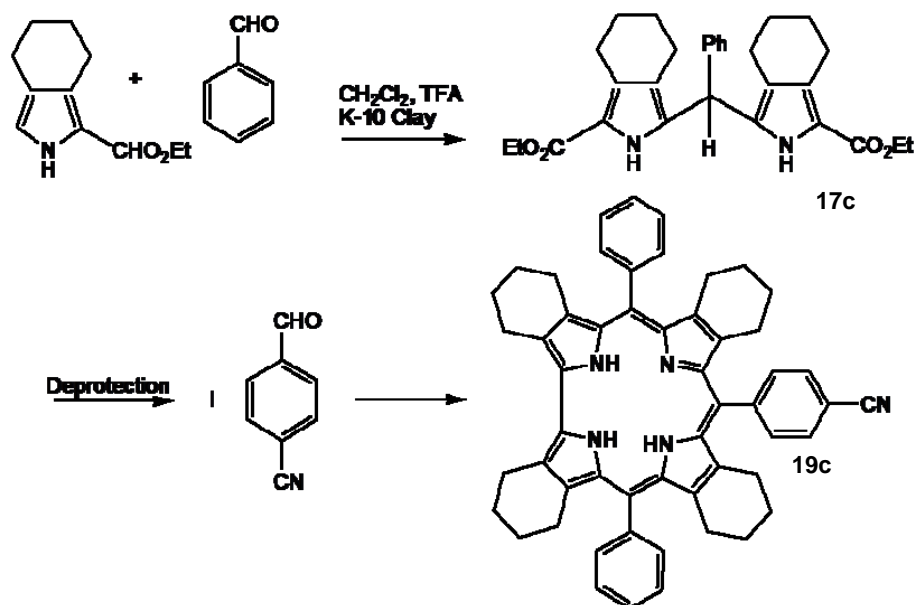
Two years ago, Gryko^[59] reported a new method for A_3 and trans- A_2B corroles syntheses in water-methanol solvents system; the interest for this

procedure is due to the mild reaction conditions, a virtually useful characteristic for the achievement of our target molecule.

A wide range of triarylcorrole have been synthesized with Gryko procedure; among these, we focused our attention on *meso* phenyl monosubstituted tetrapyrrole bearing a nitrile group for two reasons: the good yield (around 50%) reported for this kind of corrole, without any concomitant scrambling product formation. The second reason is given by the versatility of nitrile group, which could be converted in other functional group, and used to link oligopeptide or other molecules with some biological property.

This further functionalization is intriguing because, the different linked oligopeptides, confer to the photosensitizers a larger affinity towards different type of tumor cells, getting better results in terms of specific retention in malignant tissue.

Condensation of pyrrole (Scheme 3.5) with benzaldehyde, in freshly distilled CH_2Cl_2 , with TFA and montmorillonite K-10 Clay as a catalyst, afforded dipyrromethane in 60% yields.



Scheme 3.5 – Procedure for trans- A_2B corroles synthesis

Montmorillonite is a useful acid catalyst in dipyrromethane synthesis, that can be removed simply filtering the mixture before the following work up.

Protecting group was removed with the same procedure used for protected isoindole.

One equivalent of 4-cyanobenzaldehyde and two equivalents of dipyrromethane were dissolved in methanol, then water and concentrated HCl were added, and mixture stirred at room temperature for 1 hour.

The mixture was extracted with chloroform, washed twice with water, diluted with CHCl_3 , and after the addition of chloranil, it was stirred for 90 minutes.

When the UV-vis spectrum appeared compatible with those of corroles, a solution of $\text{Cu}(\text{AcO})_2$ in methanol was added, and the mixture stirred overnight.

We did not try to isolate the free base preferring to work on the metal complex, because one of the most noticeable drawback encountered in the previous experiments, was the hardness of the purification step.

Alkyl substituents on corrole have a weak electron releasing effect, which makes macrocycle core more basic and so easier to be protonated. Since the protonation could enhances the tendency of corrole to decompose, we thought to prevented this unexpected difficulty with the direct metallation of the macrocycle.

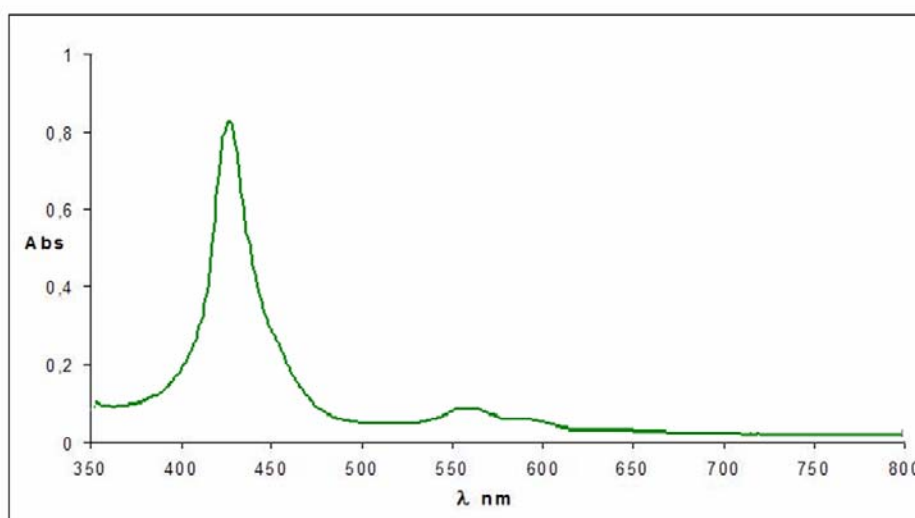


Fig. 3.12 – UV-vis spectrum of reaction mixture for A_2B corrole

Residue was purified with silica gel column eluted with CH_2Cl_2 ; several fractions macrocyclic-like were collected, each of them resulted to be a porphyrins complexes, as shown by the peak of a well shaped Soret band at 425 nm (Fig. 3.12).

Synthesis of A_3 corroles by Gryko method was then explored.

Aryl-aldehyde and pyrrole were dissolved in methanol, followed by the addition of water and HCl; stirring mixture at room temperature for three hours leads to the formation of a dark pink suspension that was extracted with CHCl_3 , washed twice with water and diluted with chloroform.

DDQ was added to oxidized bilane to corrole; DDQ is a stronger oxidant agent than chloranil, and it works also at room temperature, while with chloranil high temperature or longer reaction time are required.

Once more time neither benzaldehyde or methyl-4formylbenzoate (*p*-carboxymethyl-benzaldehyde) gave the wanted product, while better results gave 3-cyano-benzaldehyde, as shown by the UV-vis spectrum of reaction mixture, more similar to that of a corrole with respect to what we observed in the previous experiments.

Solution was divided in two fractions: the first fraction was purified in order to characterize free base of corrole, while the second one was reacted with copper acetate, because the insertion of the metal ion allows a better purification process.

Mixture containing free base was passed on a silica gel column eluted with CH_2Cl_2 - CH_3OH -TEA (98:1:1); we needed base to overcome the protonation of inner imino group that is quite sensitive to protonation on silica gel.

Tris-(3-cyanophenyl)-tetracyclobutanecorrole [(3-CN)BuTPCorH₃], **20c**, Fig. 3.13] was collected as a green fraction,

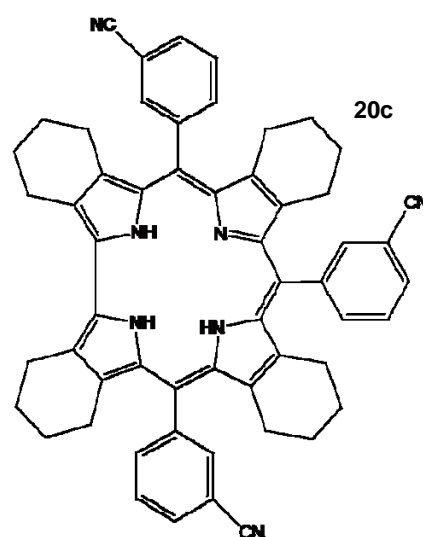


Fig. 3.13 - (3-CN)BuTPCorH₃

crystallized by $\text{CH}_2\text{Cl}_2/\text{CH}_3\text{OH}$ and fully characterized with different spectroscopic techniques.

UV-vis spectra (Fig. 3.14) has a broad Soret band at 434 nm and three Q bands at 525, 576 and 650 nm.

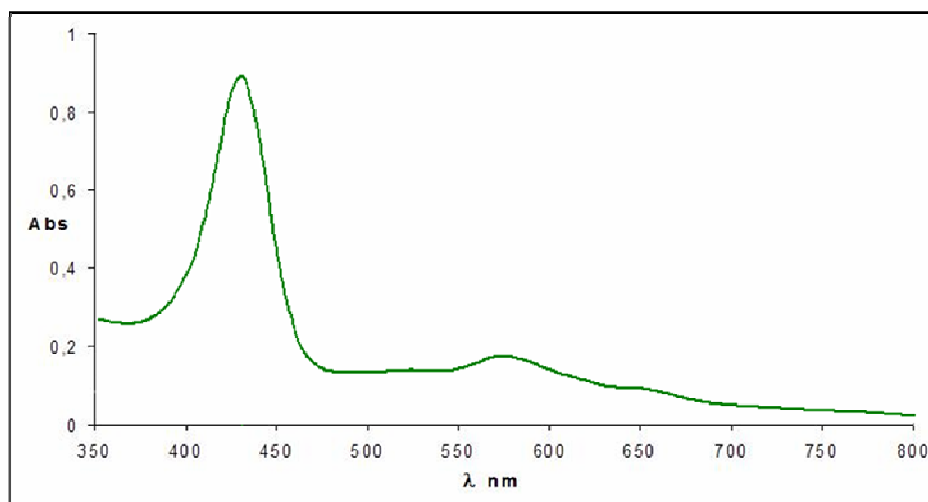


Fig. 3.14 – UV-vis spectrum of **20c**

^1H NMR (Fig. 3.15) has three groups of signals in the aromatics area (phenyls protons). There is a broad singlet at 4.1 ppm; actually it is a set of overlapped signals for the four protons on alkyl substituents closer to the direct bond (between C2 and C18), shifted at lower field because the different electronic density on that side of corrole. The clustered signal in the range 1.2-2.8 ppm can be referred to the others alkyl protons.

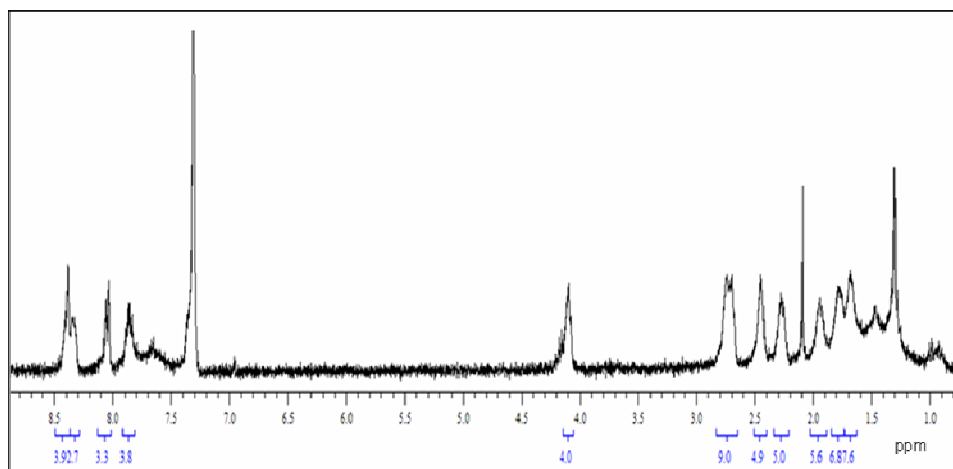


Fig. 3.15 – ^1H NMR of **20c**

MALDI spectrum (Fig. 3.16) give a further confirmation about corrole free base formation.

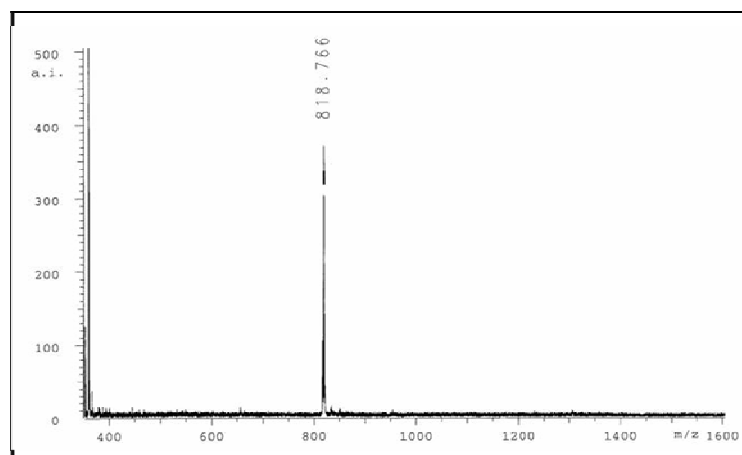


Fig. 3.16 – Mass spectrum of **20c**

Fraction reacted with copper was purified by silica gel column eluted with CH_2Cl_2 ; the red band corresponding to the [(3-CN)BuTPCor]Cu (**21c**) was collected, crystallized by $\text{CH}_2\text{Cl}_2/\text{CH}_3\text{OH}$ and characterized with the same spectroscopic methodologies.

UV-vis spectra (Fig. 3.17) showed a blue-shift of Soret band (414 nm) with respect to the free base, and a decreasing of number of Q bands from three to two; this is due to the higher symmetry of the metal complex.

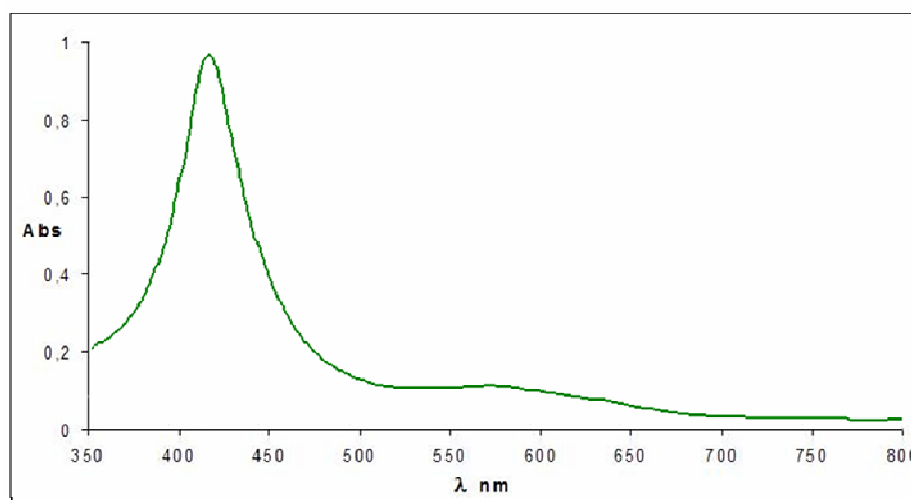


Fig. 3.17 – UV-vis spectrum of **21c**

^1H NMR (Fig. 3.18) doesn't show relevant difference about the number and the chemical shift of signals.

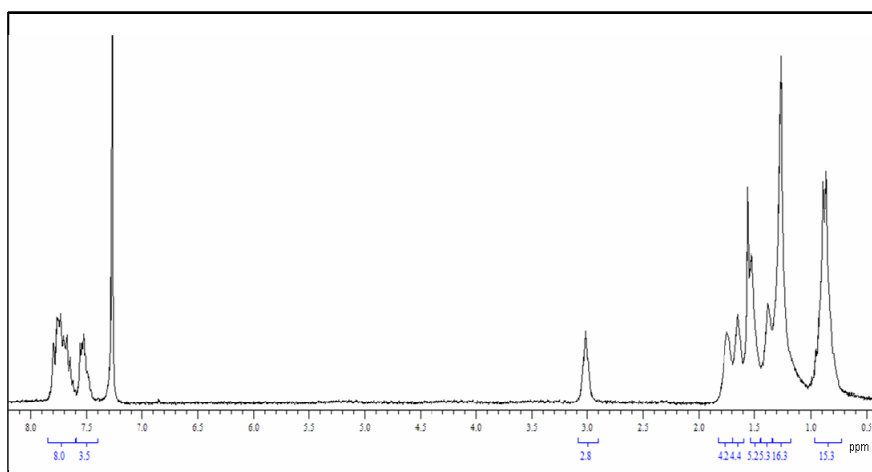


Fig. 3.18 – ^1H NMR spectrum of **21c**

There are a multiplet of peaks between 7.5 and 7.8 ppm corresponding to protons of phenyl rings, while the broad signal at 3 ppm belongs to the methylene protons adjacent to the directly linked pyrrolic unit.

The rest of the signal of alkyl substituents appeared as clustered peaks between 0.8 and 1.8 ppm.

Finally also MALDI (Fig. 3.19) confirmed complex formation.

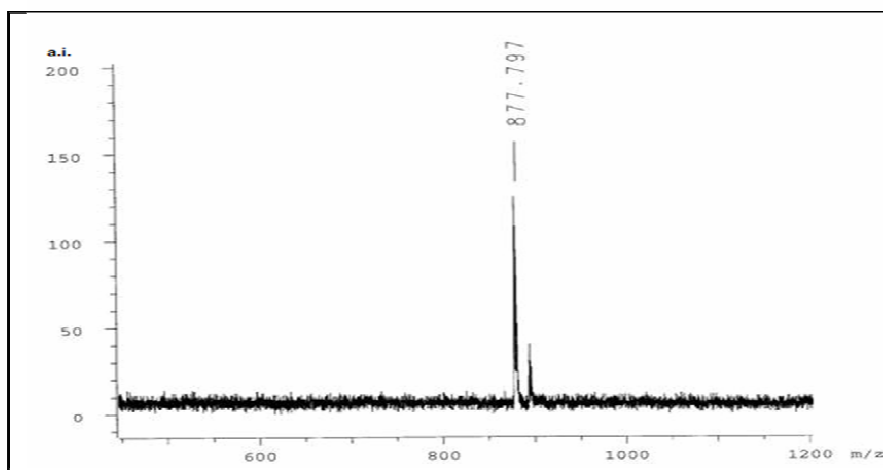


Fig. 3.19 – MALDI spectrum of **21c**

Final aromatization of fused rings were carried out in refluxing toluene for 10 minutes with a ten fold excess of DDQ (each proton: 1.25), monitoring the reaction by UV-vis spectroscopy; mixture was passed on a quick alumina plug eluted with chloroform, then purified again by column chromatography (neutral alumina deactivated with 5% of water; CH_2Cl_2); two green fractions were collected.

First fraction has Soret band (Fig. 3.20) 20 nm shifted toward longer wavelength; the red side of the spectra of [(3-CN)TBCor]Cu is quite similar to that of Cu-tetrabenzoporphyrin, for the presence of a intense absorption band occurring at lower energy with respect to what happen with §simple copper-triarylcorrole. The unique Q band lies at 650 nm; such red shifting is compatible with the presence of an extended aromatic system.

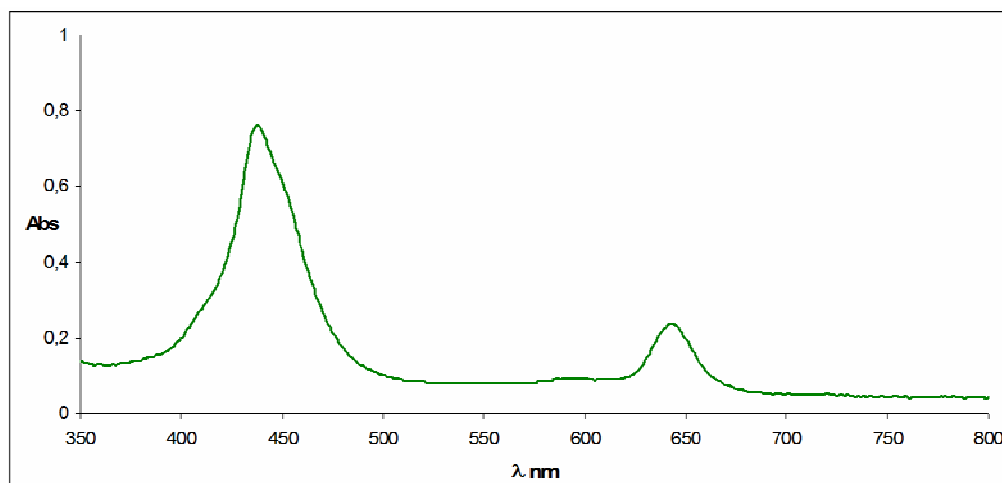


Fig. 3.20 – UV-vis spectrum of [(3-CN)TBCor]Cu

The presence of two kind of aromatic system, whose signals were partially overlapped, made impossible to assign each peak to the proton it comes from; besides the interpretation of NMR (Fig. 3.21) spectrum becomes difficult because there is not any reference signal for the integration process.

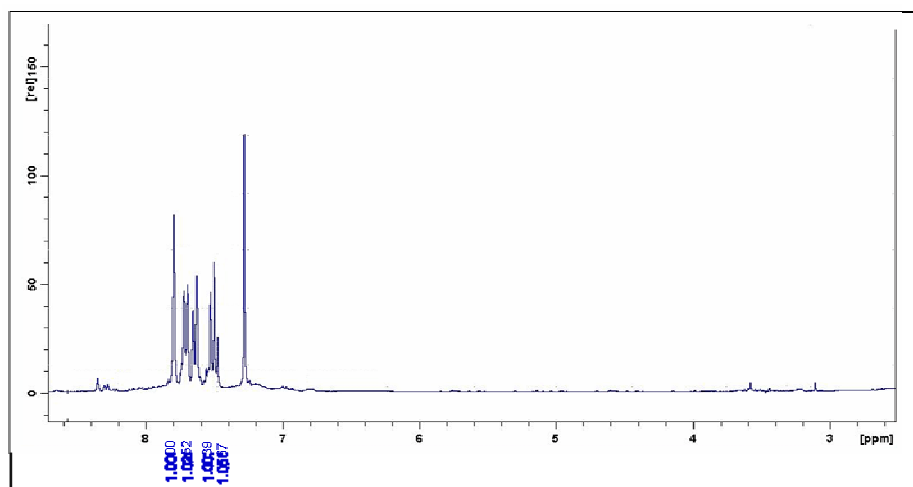


Fig. 3.21 – ^1H NMR spectrum for $[(3\text{-CN})\text{TBCor}]\text{Cu}$

Luckily we made sure about the outcome of the reaction by the result of MALDI analysis (Fig. 3.22), where the unique signal at 862 m/z value confirmed the complete aromatization of peripheral rings.

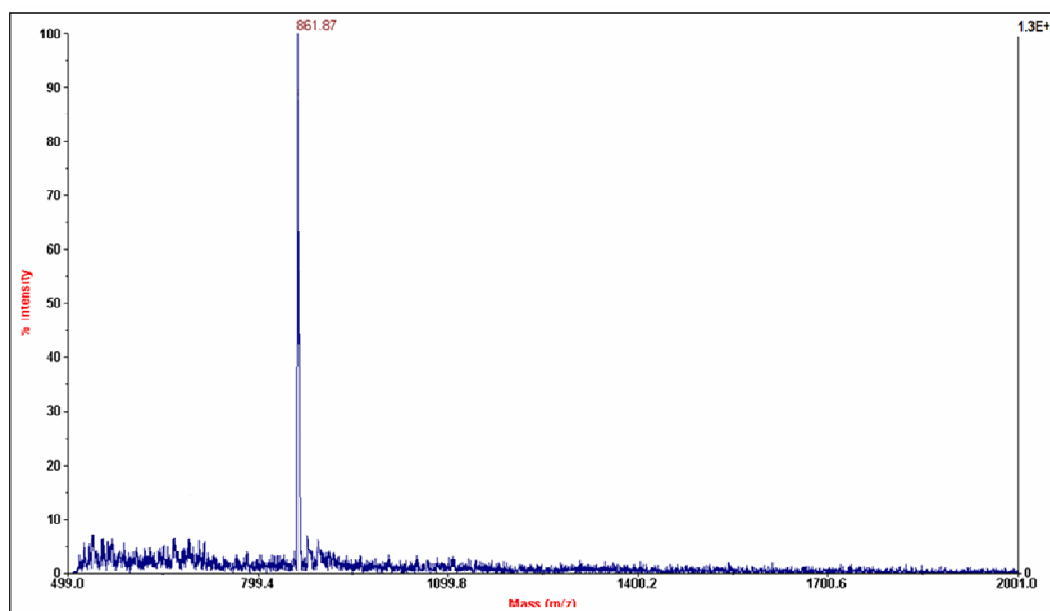


Fig. 3.22 – Mass spectrum for $[(3\text{-CN})\text{TBCor}]\text{Cu}$

Second green fraction collected gave unexpected and intriguing results; UV-vis was quite similar to that of the first collected fraction, while it was no

possible to run ^1H NMR experiment, because the complex had a paramagnetic character; the structure of the compound was pointed out by X-ray crystallography analysis, carried out on a crystal obtained by slow diffusion of methanol in chloroform.

The compound showed a porphyrin framework (**23c**, Fig 3.23), even if not all the *meso* positions had a phenyl group. One *meso* carbon was free of substituent; this compound was probably originated when a reorganization (opening and following ring closure) of the macrocycle took place.

Such structure explains the singlet observed at 12 ppm in ^1H NMR spectrum; signal for proton on methine bridge appears at very low field because it is affected by the magnetic field generated by the macrocycle ring current.

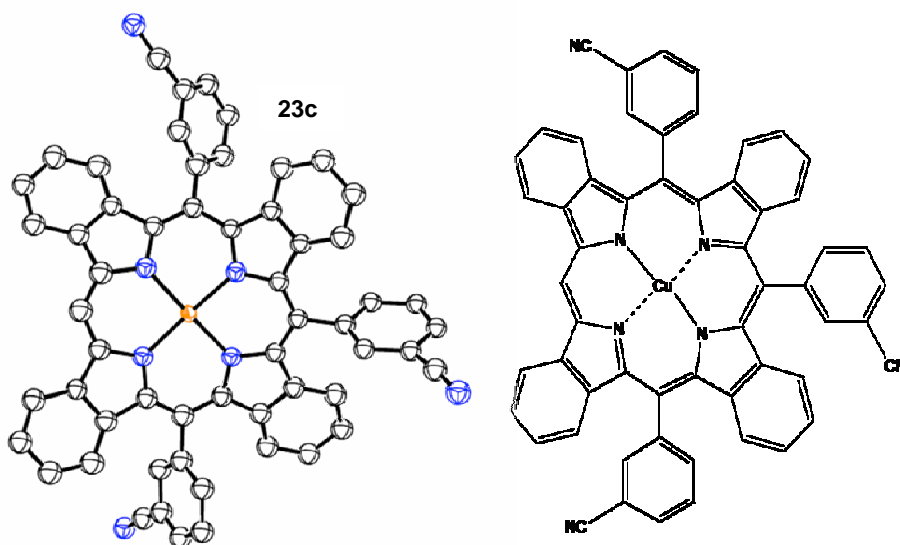


Fig. 3.23 – Crystal structure of **23c**

Porphyrin formation is probably a consequence of the interaction between the nitrile group and a corrole molecule, which undergoes the insertion of carbon atom from $-\text{CN}$ at high temperature or as result of the oxidating action of DDQ.

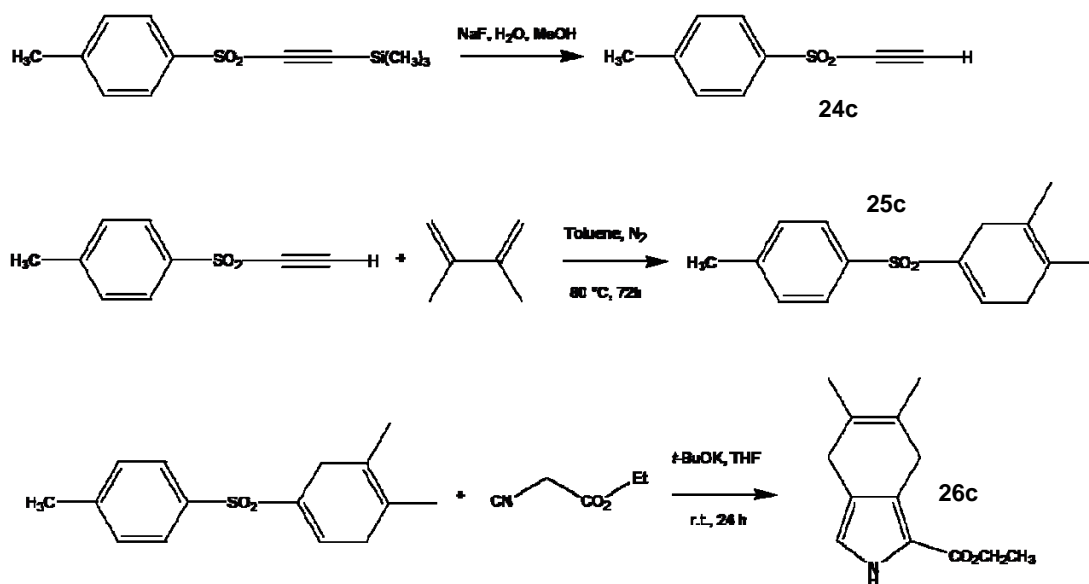
3.6.4 Dihydroisoindole: a closer precursor to tetrabenzocorroles

At the beginning of this chapter different synthetic routes to tetrabenzoporphyrins were illustrated.

While this work was accomplished, an interesting paper by Cheprakov^[60] appeared, relating a new procedure for tetrabenzoporphyrins synthesis.

In that work was surveyed the possibility to obtain TBPorH₂ by a precursor as closer of isoindole as possible, and the only pyrrole derivative suitable for this purpose was the partially oxidized 4,7-dihydroisoindole (**26c**, Scheme 3.6).

The main advantage given by this pyrrole is a facilitated aromatization process, with the target to minimized the decomposition of tetrapyrrolic derivative; even if it could be expected that an unwanted migration of double bond would happen, it does not take place neither in strong basic or acid conditions.



Scheme 3.6 – Synthesis of functionalized dihydroisoindole

Improved stability of this molecule is due to the more acidic and more nucleophilic character of NH group than the reaction centers involved in the double bond migration.

Dihydroisindole has been achieved, in good yield, in several synthetic steps from commercially available [2-(trimethylsilyl)-ethynyl]-*p*-tolyl-sulfone. It was reacted with NaF to remove trimethylsilyl group^[61]; subsequently ethynyl-sulfone (**24c**) was employed as dienophile in Diels-Alder reaction with 2,3-dimethyl-butadiene^[62].

Differently from what Cheprakov did, we choose a substituted butadiene; 1,3-butadiene is liquid at room temperature, so it has to be handle with special device, making very uncomfortable its exploitation; moreover the steric hindrance of methyl groups compiles the diene to assume more reactive *cis* conformation leading to a faster reaction course.

Electron withdrawing sulfone group has the effect of activate the dienophile.

Diels-Alder adduct (**25c**) was used for preparation of 4,7-dihydroisindole (¹H NMR spectrum in figure 3.24, **26c**) by modified^[63] Barton-Zard procedure with ethyl-isocyanoacetate and *t*-BuOK as base.

Protecting group can be removed under the same condition used on tetrahydroisindole, returning as final product, 4,7-dihydro-5,6-dimethyl-isindole. At this time the effectiveness of this compound to form TBCorH₃ is under investigation.

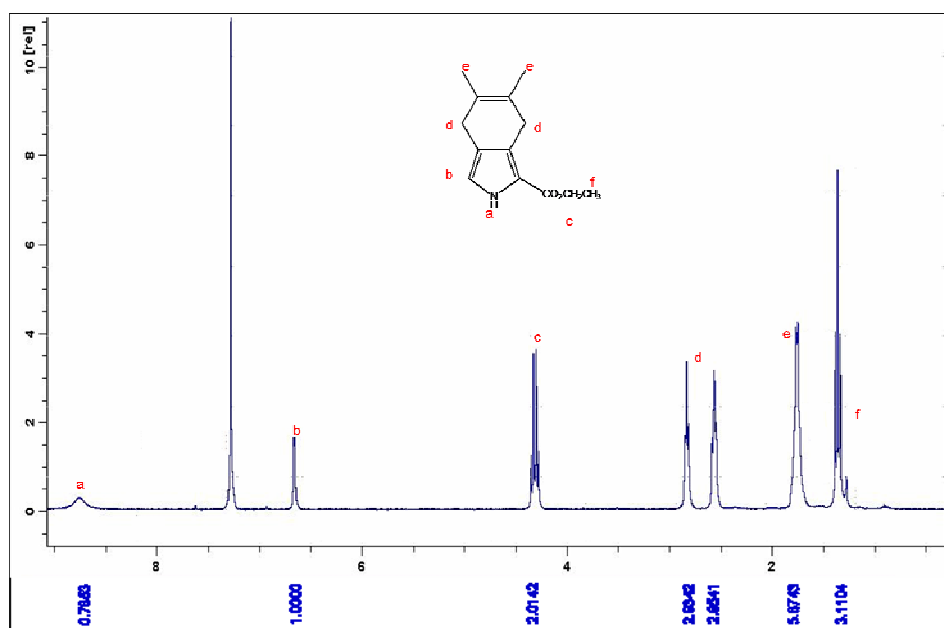


Fig. 3.24 – ¹H NMR spectrum of **26c**

Experimental section

Reagents

Reagents and solvents (Sigma-Aldrich, Fluka, Fisher Scientific and Carlo Erba Reagenti) were of the highest grade available and were used without further purification.

Materials

Silica gel 60 (70-230 mesh) and neutral alumina (Brockmann Grade III) were used for column chromatography

Silica gel 60 (Merck) and neutral alumina 60 F₂₅₄, both on aluminium support, were used for TLC.

Instruments

¹H NMR spectra were recorded with either a Bruker DPX-250 (250 MHz) or a Bruker AV 300 (300 MHz) spectrometers, using CDCl₃ as solvent. Chemical shifts are given in ppm relative to tetramethylsilane (TMS).

Routine UV-Vis spectra were recorded in CH₂Cl₂ on either Perkin Elmer Lambda 35 UV-Vis or a Varian Cary 50 spectrophotometers.

Mass spectra (MALDI-TOF) were recorded on either an Applied Biosystems QSTAR XL, using positive method with dithranol as matrix, or a Voyager-DE STR Biospectrometry workstation, in positive mode, using an α -cyano-4-hydroxycinnamic acid as matrix.

3.7 Synthesis of precursors: tetrahydroisoindole and dipyrromethane

3.7.1 Synthesis of 2-Carboxyethyl-4,5,6,7-tetrahydroisoindole (15c)

To a solution of 1-nitro-1-cyclohexene (2.7 mL, 23.9 mmol) in freshly distilled dry THF (30 mL), were added dropwise ethyl isocyanoacetate (2.7 mL, 23.9 mmol) then DBU (3.6 mL, 23.7 mmol) at 0°C, and the mixture was stirred at room temperature for 15 h. The reaction mixture was then washed with dilute hydrochloric acid (10% HCl, 100 mL), extracted into ethyl acetate (3×100 mL), dried over Na₂SO₄ and solvent evaporated under vacuum. The brown oil residue was purified by chromatography on silica gel eluting with hexane/ethyl acetate 9/1, to give pure yellow crystals of the title pyrrole in a 90% yield (3.00 g, 15.5 mmol).

¹H NMR (CDCl₃, 250 MHz): δ ppm 8.77 (s br, 1H, NH), 6.64 (d, J = 2.7 Hz, α-pyrrole), 4.29 (q, 2H, -CO₂CH₂CH₃), 2.82 and 2.54 (t, 2H each, α-CH₂ cyclobutane), 1.74 (m, 4H, β-CH₂ cyclobutane) 1.34 (t, 3H, -CO₂CH₂CH₃).

3.7.2 Synthesis of 4,5,6,7-Tetrahydroisoindole (16c)

Tetrahydroisoindole **15c** (1.1 g, 5.7 mmol) was suspended in ethylene glycol (80 mL) with NaOH (2 g, 50 mmol). The solution was then heated at 100 °C for 60' to saponify the ethyl ester group, before refluxing at 195 °C for 40' for the decarboxylation. The orange suspension was cooled down and extracted with hexane. The organic layer was dried over Na₂SO₄ and solvent evaporated under vacuum. Residue was purified with a quick silica gel plug eluted with CH₂Cl₂. Yield 65% (449 mg, 3.71 mmol).

^1H NMR (CDCl_3 , 250 MHz): δ ppm 8.27 (s br, 1H, NH), 6.11 (d, $J = 2.7$ Hz, α -pyrrole), 2.39 (t, 2H each, α - CH_2 cyclobutane), 1.52 (m, 4H, β - CH_2 cyclobutane).

3.7.3 Synthesis of 1,9-Dicarboxyethyl-2:3,7:8-dibutane-5-phenyl-dipyrromethane (17c)

Pyrrole **15c** (2 g, 10.32 mmol) was dissolved in 80 mL of freshly distilled CH_2Cl_2 and degassed with Ar for approximately 5'. Montmorillonite K10 Clay (2.1 g) was added and the round bottom flask sealed. TFA (4.0 mL, 51.9 mmol) was added followed by benzaldehyde (0.7 mL, 6.9 mmol). The reaction was allowed to stir under argon for 12 h, before TLC analysis showed completion of the reaction. The mixture was filtered through silica gel plug to remove the excess aldehyde. The filtrate was collected and washed with 100 mL of water and 100 mL of $\text{NaHCO}_3(\text{aq})$. The organic layer was then collected, dried over sodium sulfate and solvent removed under reduced pressure. Recrystallization from CH_2Cl_2 /methanol afforded a beige solid in a yield of 60% (1.47 g, 3.1 mmol).

^1H NMR (CDCl_3 , 250 MHz): δ ppm 7.81 (s br, 2H, NH), 7.52-7.17 (m, 5H, phenyl), 5.43 (s, 1H, 5-meso), 4.22 (q, 4H, $-\text{CO}_2\text{CH}_2\text{CH}_3$) 2.71 and 2.43 (t, 4H each, α - CH_2 cyclobutane) 1.73 (m, 8H, β - CH_2 cyclobutane), 1.33 (t, 6H, $-\text{CO}_2\text{CH}_2\text{CH}_3$).

3.7.4 Synthesis of 2:3,7:8-Dibutane-5-phenyl-dipyrromethane (18c)

Dipyrromethane **17c** (1.5 g, 3.15 mmol) was suspended in ethylene glycol (135 mL) and NaOH (2.83 g, 70.8 mmol) was added. The solution was heated

30' at 100 °C before refluxing at 195 °C for 35'. An orange precipitate was formed on cooling down the hot ethylene glycol solution to room temperature. 50 mL of water were added to the flask to enhance the precipitation and the reaction flask stored at -20 °C for 12 hours. The mixture was then filtered, and the precipitate washed with water before being dried under vacuum.

Yield 55% (0.57g, 1.74 mmol). ¹H NMR (CDCl₃, 250 MHz): δ ppm 7.69 (s br, 2H, NH), 7.42-7.13 (m, 5H, phenyl), 6.35 (s, 2H, α-pyrrole) 5.43 (s, 1H, 5-meso), 2.71 and 2.43 (t, 4H each, α-CH₂ cyclobutane), 1.73 (m, 8H, β-CH₂ cyclobutane).

3.8 Synthesis of Triaryl-tetrabenzocorroles

3.8.1 Synthesis of 5,10,15-Triphenyl-2:3,7:8,12:13,17:18-tetrabutane-corrole - modified Paolesse method

Pyrrole (**16c**) (500 mg, 4.1 mmol) was dissolved in 8 mL of CH₂Cl₂ and let to stir for ten minutes under argon current. Benzaldehyde (83 μL, 0.82 mmol) was added and mixture stirred for further 5 minutes under inert atmosphere, before the addition of TFA (1.6 μL, 0.021 mmol). Reaction was stirred for 10 minutes, diluted with CH₂Cl₂, then let to stir for two hours. After this time, chloranil (161 mg, 0.66 mmol) was added and mixture stirred for 12 hours, monitoring the course of the reaction by UV-vis spectroscopy. When the analysis showed the formation of a compound macrocycle-like (presence of the Soret and the Q bands), together with open chain-derivatives, solvent was removed under reduced pressure and residue purified by chromatography (alumina 5%, CH₂Cl₂). A green fraction was collected, but it was not pure enough for a complete characterization.

3.8.2 Synthesis of 5,10,15-Tris-(4-methyl-carboxylatephenyl)-2:3,7:8,12:13,17:18-tetrabutane-corrole - modified Paolesse method

Pyrrole (**16c**) (500 mg, 4.1 mmol) was dissolved in 8 mL of CH₂Cl₂ and let to stir for ten minutes under argon current. Formyl-4-methylbenzoate (135 mg, 0.82 mmol) was added and mixture stirred for further 5 minutes under inert atmosphere, before the addition of TFA (1.6 μL, 0.021 mmol). Reaction was stirred for 10 minutes, diluted with CH₂Cl₂, then let to stir for two hours. After this time, chloranil (161 mg, 0.66 mmol) was added and mixture stirred for one hour, monitoring the course of the reaction by UV-vis spectroscopy. When the analysis showed the formation of a porphyrinoids derivative (Soret and Q bands), mixed with open chain-derivatives, solvent was removed under reduced pressure and residue purified by chromatography (alumina 5%, CHCl₃). Product macrocycle-like was collected just in traces, and it was not possible to characterize it.

3.8.3 Synthesis of 5,10,15-Triphenyl-2:3,7:8,12:13,17:18-tetrabutane-corrole - Paolesse method

Pyrrole (**16c**) (500 mg, 4.1 mmol) was mixed with benzaldehyde (83 μL, 0.82 mmol), under argon atmosphere and the flask slightly warmed; so that pyrrole melted; TFA vapours were added, and the fusion of the mixture went to completion. Reaction was stirred for 5 minutes, then diluted with 12 mL of CH₂Cl₂ and let to stir for two hours. DDQ (145 mg, 0.64 mmol) was added and mixture stirred for 12 hours, monitoring the course of the reaction by UV-vis spectroscopy. When the analysis showed the formation of a compound macrocycle-like (Soret and Q bands), mixed with open chain-derivatives, solvent was removed under reduced pressure and residue purified by chromatography

(alumina 5%, CH₂Cl₂). A green fraction was collected, but it was not pure enough for a complete characterization.

3.8.4 Synthesis of 10-(4-Cyanophenyl)-5,15-diphenyl-2:3,7:8,12:13,17:18-tetrabutaneacorrole (19c) - Gryko method

Dipyrromethane (**18c**) (330 mg, 1 mmol) and 4-cyanobenzaldehyde (65.5 mg, 0.5 mmol) were dissolved in CH₃OH (50 mL). Subsequently, a solution of HCl_{aq} (36%, 2.5 mL) in H₂O (50 mL) was added, and the reaction was stirred at room temperature for 1 h. The mixture was extracted with CHCl₃, and the organic layer washed twice with H₂O, dried over Na₂SO₄, filtered, and diluted to 250 mL with CHCl₃. Chloranil (369 mg, 1.5 mmol) was added, and the mixture was stirred at room temperature for 90 minutes.

3.8.5 Synthesis of [10-(4-Cyanophenyl)-5,15-diphenyl-2:3,7:8,12:13,17:18-tetrabutaneacorrolate]Cu

To a solution of corrole (**19c**) in chloroform, was added a solution of Cu(AcO)₂ in CH₃OH, and the mixture stirred at room temperature overnight, monitoring the course of the reaction by UV-vis spectrometry. When the formation of a copper complex was evident, solvent was removed under reduced pressure, and passed on a silica gel column eluted with CH₂Cl₂. Several red fractions were collected, but all of them resulted to be copper porphyrin isomers, as pointed out by Soret (425 nm) and Q bands (510 nm, 560 nm).

3.8.6 Synthesis of 5,10,15-Tris-(3-cyanophenyl)- 2:3,7:8,12:13,17:18-tetrabutane-corrole (20c)

Pyrrole (**16c**) (500 mg, 4.1 mmol) and 3-cyano-benzaldehyde (269 mg, 2.05 mmol) were dissolved in CH₃OH (150 mL). Subsequently, a solution of HCl_{aq} (36%, 7.5 mL) in H₂O (150 mL) was added, and the reaction stirred at room temperature for 3 h. The mixture was extracted with CHCl₃, and the organic layer washed twice with H₂O, dried over Na₂SO₄, filtered, and diluted to 700 mL with CHCl₃. Chloranil (1.47 g, 6.0 mmol) was added, and the mixture was stirred at room temperature for 90 minutes, monitoring the course via UV-vis spectrometry.

After the appearance of the typical corrole free base absorption bands, an aliquot (20%) of the reaction mixture was removed and solvent evaporated to dryness. Residue was dissolved with CH₂Cl₂, passed on a silica gel column eluted with CH₂Cl₂-CH₃OH-TEA (98:1:1); a green fraction was collected and crystallized by CH₂Cl₂/CH₃OH, to give the titled corrole with 6% yield.

¹H NMR (CDCl₃, 250 MHz): δ ppm 8.47-8.27 (m, 6 H, phenyl), 8.10-7.99 (m, 3 H, phenyl), 7.92-7.78 (m, 3 H, phenyl), 4.18-4.09 (s br, 4 H, α-CH₂ cyclobutane C2, C18), 2.84-1.32 (m, 28 H, α, β-CH₂ cyclobutane C3, C7, C8, C12, C13, C17). UV-vis (CH₂Cl₂): λ max, nm (ε × 10⁻³, M⁻¹ × cm⁻¹): 434 (133.1), 525 (17.9), 576 (29.1), 650 (15). Em. λ 675 nm (Ex. λ 575). MS (MALDI, M+1): calculated for C₅₆H₄₇N₇ 818.039; found 818.766.

3.8.7 Synthesis of [5,10,15-Tris-(3-cyanophenyl)- 2,3,7,8,12,13,17:18-tetrabutane-corrolate]Cu (21c)

To the mixture containing corrole **20c**, was added a solution of Cu(AcO)₂ in CH₃OH, and it was stirred overnight at room temperature, monitoring the course of the reaction by UV-vis spectrometry. When analysis showed complex

formation, solvent was removed under vacuum; purification by column chromatography (silica gel, CH₂Cl₂) afforded a red fraction that was crystallized by CH₂Cl₂/CH₃OH, to give the titled compound in a 90% yield.

¹H NMR (CDCl₃, 250 MHz): δ ppm 7.83-7.61 (m, 8 H, phenyl), 7.55-7.44 (m, 4 H, phenyl), 3.01 (s br, 4 H, α-CH₂ cyclobutane C2, C18), 1.88-0.72 (m, 28 H, α, β-CH₂ cyclobutane C3, C7, C8, C12, C13, C17). UV-vis (CH₂Cl₂): λ max, nm (ε × 10⁻³, M⁻¹ × cm⁻¹): 414 (131.9), 549 (10.9), 600 (5.1). MS (MALDI, M+1): calculated for C₅₆H₄₄CuN₇ 878.561; found 877.797.

3.8.8 Synthesis of [5,10,15-Tris-(3-cyanophenyl)-2,3,7,8,12,13,17:18-tetrabenzocorrolate]Cu (**22c**)

Corrole **21c** was dissolved in toluene and DDQ was added to the mixture before heating at reflux for 5 minutes. The reaction was followed by TLC (alumina) for the appearance of a green streak at the baseline, and by UV-vis spectrometry for the red shifting of the absorption bands. Once the reaction was complete, the mixture was allowed to cool and filtered through a very short alumina (5%) plug eluted with chloroform, then was purified again on column chromatography (alumina 5%, CH₂Cl₂ then CHCl₃). Two green fraction were collected, crystallized by CH₂Cl₂/CH₃OH. First fraction (**22c**) was obtained in a 22% yield. ¹H NMR (CDCl₃, 250 MHz): δ ppm 7.80-7.47 (m, 28 H, phenyl and fused ring). UV-vis (CH₂Cl₂): λ max, nm (ε × 10⁻³, M⁻¹ × cm⁻¹) 437 (88.7), 641 (24.4) MS (MALDI): calculated for C₅₆H₂₈N₇Cu 862.43; found 861.87. Second fraction (**23c**) UV-vis (CH₂Cl₂): λ max, nm 460, 597, 641. Em. λ 719 nm (Ex. λ 641). MS (MALDI, M+1): calculated for C₅₇H₂₉N₇Cu 875.48; found 877.71.

3.9 *An alternative isoindole as triaryl-tetrabenzocorrole precursor*

3.9.1 Synthesis of Ethynyl *p*-tolyl sulfone (**24c**)

A solution of sodium fluoride (480 mg, 11.93 mmol) in degassed water (10 ml) was added dropwise to a solution of 2-(trimethylsilyl)ethynyl *p*-tolylsulfone (2 g 7.93 mmol) in degassed methanol (16 ml) at 10°C. After complete addition, the resulting suspension was stirred for another 15 min. Water was added and the mixture was extracted with CHCl₃ (3 × 20 ml). The combined organic layers were treated with sodium hydrogen carbonate, washed with brine, and then dried with anhydrous Na₂SO₄. After concentration to dryness, a white product was obtained. Yield 97% (1.4 g, 7.66 mmol)

¹H NMR (CDCl₃, 250 MHz): δ ppm 7.91 (d, 2 H, J = 8.3 Hz, Ts), 7.39 (d, 2 H, J = 8.3 Hz, Ts), 3.44 (s, 1 H, alkynyl), 2.49 (s, 3 H, -CH₃).

3.9.2 Synthesis of 1-Tosyl-[(4,5-dimethyl)-cyclohexa-1,4-diene] (**25c**)

Ethynyl *p*-tolyl sulfone **24c** (1.78 g 9.9 mmol) was dissolved in 30 mL of toluene; 2,3 dimethyl-butadiene (1.12 mL, 9.91 mmol) was added and the mixture stirred at 65 °C for 72 hours under argon atmosphere. The reaction mixture was checked by TLC (silica gel, hexane/ethyl acetate 4/1) exposed to UV lamp (254 nm). Solvent was removed under vacuum and residue purified by silica gel column eluted with hexane/ethyl acetate 4/1. First band collected was characterized as the desired compound. Yield 60% (1.56 g, 5.94 mmol)

¹H NMR (CDCl₃, 250 MHz): δ ppm 7.95 (d, 2 H, J = 6.9 Hz, Ts), 7.36 (d, 2 H, J = 6.5 Hz, Ts), 7.01 (s, 1 H, 2-cyclohexadiene), 2.89 (s br, 2 H, 6-

cyclohexadiene), 2.74 (s br, 2 H, 2-cyclohexadiene), 2.47 (s, 3 H, -CH₃ phenyl), 1.65 (s, 6 H, -CH₃ cyclohexadiene).

3.9.3 Synthesis of 2-Carboxyethyl-5,6-dimethyl-4,7-dihydro-2H-isoindole (26c)

A solution of ethyl-isocyanoacetate (568 μ L, 5.72 mmol) in 8 mL of THF was added dropwise to a stirred suspension of *t*-BuOK (584 mg, 5.2 mmol) in 8 mL of THF at 0 °C under argon. A solution of 1-Tosyl-[(4,5-dimethyl)-cyclohexa-1,4-diene] **25c** (1.5 g, 5.72 mmol) in 8 mL of THF was added dropwise and the resulting mixture was stirred at room temperature. After 4 h the volume of the mixture was reduced by rotary evaporation and 30 mL of CH₂Cl₂ was added. The resulting solution was washed with water and brine and dried over Na₂SO₄. The solvents were removed in vacuum, and the residue was purified on silica gel column (eluent CH₂Cl₂). Yield: 65% (744 mg, 3.39 mmol).

¹H NMR (CDCl₃, 250 MHz): δ ppm 8.82 (s br, 1 H, NH), 6.70 (s, 1 H, α -pyrrole), 4.32 (q, 2 H, -CO₂CH₂CH₃), 3.37 and 3.14 (s, 2 H each, -CH₂ 4,7-indole), 1.79 (d, 6H, J = 7.8 Hz, -CH₃ 5,6-indole) 1.37 (t, 3H, -CO₂CH₂CH₃).

References

1. Raab, O. *Z. Biol.* **1900**, *39*, 524-546.
2. Policard, A. *Compt. Rend. Soc. Biol.*, **1924**, *91*, 1423-1424.
3. Henderson, B.W.; Dougherty, T.J.; Schwartz, S. In “*Photodynamic Therapy: Basic Principles and Clinical Applications*”. Henderson B.W., Dougherty T.J. (eds). Marcel Decker: New York, **1992**; 1–15.
4. Lipson, R.L.; Baldes, E.J.; Olsen, A.M. *J. Natl. Cancer Inst.*, **1961**, *26*, 1–11.
5. Weishaupt, K.R.; Gomer, C.J.; Dougherty, T.J. *Cancer Res.*, **1976**, *36*, 2326–2329.
6. Dougherty, T.J. *J. Clin. Laser Med. Surg.*, **1996**, *14*, 219–221.
7. Pandey, R.K.; Zheng, G. In “*Porphyrins as Photosensitizers in Photodynamic Therapy*”, Vol. 6. Kadish K.M., Smith K.M., Guillard R. (Eds.) Academic Press: San Diego, **2000**.
8. Matheson, I.B.C.; Lee, J. *J. Am. Chem. Soc.*, **1972**, *94*, 3310.
9. Gilbert, A.; Baggott, J. In “*Essential of Molecular Photochemistry*”. CRC press: Boca Raton, **1991**, 1-10.
10. Gilbert, A.; Baggott, J. In “*Molecular Photophysics. Essential of Molecular Photochemistry*”. CRC press: Boca Raton, **1991**, 91-144.
11. Foote, C.S. In “*Porphyrin Localization and Treatment of Tumors*”. Doiron D.R., Gomer Gomer C.J. (eds). Alan R. Liss: New York, **1984**, 3-18
12. Turro, N.J. In “*Modern Molecular Photochemistry*”. University Science Book: California, **1991**; 583-593.
13. Phillips, D. In “*Progress in Reaction Kinetics*”. Kemp, T.J., Donovan R.J., Rodgers, M.A.J. (eds). Vol. 22, **1997**, 175.

14. Bensasson, R.V.; Land, E.J.; Truscott, T.G. In “*Excited States and Free Radicals in Biology and Medicine*”. Oxford University Press, Oxford, **1993**, 101.
15. Gilbert, A.; Baggott, J. In “*Essential of Molecular Photochemistry*”. CRC press: Boca Raton, **1991**, 501-525.
16. Foote, C.S.; Clennan, E.L.; Valentine J.S. In “*Active Oxygen in Chemistry*”. Foote, C.S., Valentine J.S., Greenberg, A., Liebman, J.F. (eds). SEARCH Series, vol. 2, Blackie Academic and Professional: London, **1995**, 105.
17. Boyle, R.B.; Dolphin, D. *J. Photochem. Photobiol. B: Biol.*, **1996**, *64*, 469.
18. Bonnet, R. *Chem. Soc. Rev.*, **1995**, *19*.
19. Stolik, S.; Delgado, J.A.; Pérez, A.; Anasagasti, L. *Photochem. Photobiol. B: Biol.*, **2000**, *57*, 90.
20. Jori, G. *J. Photochem. Photobiol. A: Chem.*, **1992**, *62*, 371.
21. Mac Roberts, A.J.; Brown S.G.; Phillips, D. In: Proceedings of the Ciba Foundation Symposium on Photosensitizing Compounds, vol. 146, Wiley, Chichester, **1989**, p. 4.
22. Henderson, B.W.; Dougherty, T.J. *Photochem. Photobiol.*, **1992**, *55*, 145.
23. Hausman, W. *Biochem. Z.*, **1909**, *14*, 275-278.
24. Spikes, J.D. In “*Porphyryn localization and treatment of tumors*”. Doiron D.R., Gomer C.J., (eds). Alan R. Liss: New York, **1984**; 19-39.
25. Waldman, T.; Zhang, Y.; Dillehay, L.; Yu, J.; Kinzler, K.; Vogelstein, B.; Williams, J. *Nature Med.*, **1997**, *3*, 1034-1036.
26. Mason, M. *Rev. Contemp. Pharmacother.*, **1999**, *151*, 1-18.
27. Luo, Y.; Kessel, D. *Photochem., Photobiol.*, **1997**, *66*, 479-483.
28. Oleinick, N.L.; Evans H.H. *Radiat. Res.*, **1998**, *150* (Suppl.), S146-S156.
29. Rousset, N.; Kerninon, E.; Eleouet, S.; Nell, T.L.; Auget J.L.; Vornax, V.; Carre, J.; Lajat, Y.; Patrice T.; *J. Photochem. Photobiol. B: Biol.*, **2000**, *56*, 118-131.

30. McNair F.I.; Marples, B.; West C.M.; Moore, J.V. *Br. J. Cancer*, **1997**, *75*, 1721-1729.
31. Sessler, J.L.; Sansom P.I.; Kral, V.; O'Connor, D.; Iverson B.L. *J. Am. Chem. Soc.*, **1997**, *119*, 6947-6948.
32. Sitnik, T.M.; Hampton, J.A.; Henderson, B.W. *Br. J. Cancer*, **1998**, *77*, 1386-1394.
33. Fingar, V.H.; *Clin. Laser Med. Surg.*, **1996**, *14*, 323.
34. Kongshaug, M. *Int. J. Biochem.*, **1992**, *24*, 1239-1265.
35. Korbelik, M.; Krosol, G.; Olive, P.L.; Chaplin, D.J. *Br. J. Cancer*, **1991**, *64*, 508-512.
36. Thomas, J.P.; Girotti, A.W. *Photochem. Photobiol.*, **1989**, *49*, 241-247.
37. Villanueva, A.; Jori, G. *Cancer Lett.*, **1993**, *73*, 59-64.
38. Woodburn, K.W.; Vardaxis, N.J.; Hill, J.S.; Kaye A.H.; Phillips D.R. *Photochem. Photobiol.*, **1991**, *54*, 725-732.
39. Geze, M.; Morliere, P.; Maziere J.C.; Smith K.M. *Photochem. Photobiol. B: Biol.*, **1993**, *20*, 23-35.
40. Mason, M.D. *Rev. Contemp. Pharmacother.*, **1999**, *10*, 25-37.
41. Roberts, D.J., Cairnduff, F.; Driver, I.; Dixon, B.; Brown, S.B.; *Int. J. Oncol.*, **1994**, *5*, 763-768.
42. Nyman, E.S.; Hynninen, P.H. *J. Photochem. Photobiol. B: Biol.*, **2004**, *73*, 1-28.
43. Winkelman, J.W.; Collins G.H. *Photochem. Photobiol*, **1987**, *46*, 801-807.
44. Shea, K.M.; Jaquinod, L.; Smith, K.M. *J. Org. Chem.*, **1998**, *63*, 7013.
45. Pandey, R.K.; Zheng, G. In “*The Porphyrin Handbook*”, Vol. 6, Kadish K.M., Smith K.M., Guillard R. (Eds.) Academic Press: San Diego, **2000**; pp 157-230.
46. Chou, J.H.; Nalwa, H.S.; Kosal, M.E.; Rakow, N.A.; Suslick, K.S. In “*The Porphyrin Handbook*”, Vol. 6, Kadish K.M., Smith K.M., Guillard R. (Eds.) Academic Press: San Diego, **2000**; pp 43-132.

47. Baker, E.W. *J. Am. Chem. Soc.*, **1966**, 88, 2311.
48. Helberger, J.H.; *Ann.*, **1937**, 529, 205.
49. Kopranenkov, V.N.; Takhanova, E.A., Lukyanets, E.A. *Zh. Org. Khim.*, **1979**, 15, 642.
50. Barrett, P.A.; Linstead, R.P.; Rundall, F.G.; Tuey, G.A.P. *J. Chem. Soc.*, **1940**, 1079.
51. Linstead, R.P.; Weiss, F.T.; *J. Chem. Soc.*, **1950**, 2975.
52. Vogler, A.; Kunkely, H. *Angew. Chem. In. Ed. Engl.*, **1978**, 17, 760.
53. Ito, S.; Murashima, T.; Uno, H.; Ono, N. *Chem. Commun.*, **1998**, 1661-1662.
54. Vicente, M.G.H.; Tome, A.C.; Walter, A.; Cavaleiro, J.A.S. *Tetrahedron Lett.*, **1997**, 38, 3639.
55. Haake, G.; Struve, D.; Montforts, F.P. *Tetrahedron Lett.*, **1994**, 35, 9703.
56. Barton, D.H.R.; Kervagoert J.; Zard, S.Z. *Tetrahedron*, **1990**, 46, 7587-7598.
57. Paolesse, R.; Jaquinod, L., Nurco, D.J.; Mini, S.; Sagone, F.; Boschi, T.; Smith, K.M. *Chem. Commun.*, **1999**, 1307-1308.
58. Paolesse, R.; Marini, A.; Nardis, S.; Froiio, A.; Mandoj, F.; Nurco, D.J.; Prodi, L.; Montalti, M.; Smith, K.M. *J. Porphyrins Phthalocyanines*, **2003**, 7, 25-36.
59. Koszarna, B.; Gryko, D. *J. Org. Chem.*, **2006**, 71, 3707-3717.
60. Filatov, M.A.; Cheprakov, A.V.; Beletskaya, I. *Eur. Jour. Org. Chem.*, **2007**, 21, 3468-3475.
61. Otten, A.; Namyslo, J.C.; Stoermer, M.; Kaufmann, D.E. *Eur. J. Org. Chem.*, **1998**, 1997-2001.
62. Williams, R.V.; Chauhau, K.; Gadgil, V.R. *J. Chem. Soc., Chem. Commun.*, **1994**, 1739-1740.
63. Arnold, D.P.; Burgess-Dean, L.; Hubbard, J.; Abdur Rahman, M. *Aust. J. Chem.*, **1994**, 47, 969.

List of publications

Publications:

1. F. Dini, E. Martinelli, G. Pomarico, R. Paolesse, D. Monti, D. Filippini, A. D'Amico, I. Lundström, C. Di Natale: “*Chemical sensitivity of self-assembled porphyrin nano-aggregate*”, *Nanotechnology*, **2009**, 20.
2. C. Di Natale, K. Buchholt, E. Martinelli, R. Paolesse, G. Pomarico, A. D'Amico, I. Lundström, A. Lloyd Spetz: “*Investigation of QMB and ChemFET transduction of molecular recognition events in a metalloporphyrin film*”, *Sensors and Actuators B: Chemical*, **2009**, 135, 560-567.
3. M. Stefanelli, D. Monti, V. Van Axel Castelli, G. Ercolani, M. Venanzi, G. Pomarico R. Paolesse: “*Chiral supramolecular capsule by ligand promoted self-assembly of resorcinarene-Zn porphyrin conjugate*”, *Journal of Porphyrins and Phthalocyanines*, **2008**, 12, 1279-1289.
4. F. Mandoj, S. Nardis, G. Pomarico, R. Paolesse: “*Demetalation of corrole complexes: an old dream turning into reality*”, *Journal of Porphyrins and Phthalocyanines*, **2008**, 12, 19-26.
5. S. Nardis, G. Pomarico, F. R. Fronczek, M.G.H. Vicente, R. Paolesse: “*One pot synthesis of isocorroles*”, *Tetrahedron Letters*, **2007**, 48, 8643-8646.

Abstracts:

1. G. Pomarico, D. Monti, S. Nardis, R. Paolesse; *“Tripyridylcorrole derivatives are promising building block for supramolecular assemblies”*, Fifth International Conference on Porphyrins and Phthalocyanines, Moscow, 6-11 July **2008**.
2. G. Pomarico, M. Stefanelli, D. Monti, M. Venanzi, R. Paolesse; *“Kinetic and spectroscopic studies on the self-aggregation of a meso-substituted amphiphilic corrole derivative”*, VIII National Congress of Supramolecular Chemistry, Trieste, 19-22 September **2007**.
3. G. Pomarico, F. Mandoj, S. Nardis, S. Antonaroli, B. Crociani, R. Paolesse; *“Pd-catalyzed synthesis of fully substituted polypyrrolic macrocycles”*, II National Workshop AICIng, Messina, 12-14 September **2007**.
4. L. Lvova, G. Romeo, G. Pomarico, R. Paolesse, C. Di Natale, A. D’Amico: *“Potentiometric electrodes based on electropolymerized 5,10,15-Tris(4-aminophenyl)-20-phenylporphyrinates of Cu(II) and Co(II): enhanced selectivity towards CO₃²⁻ ion”*, PITTCON 2007, Chicago, 25 February-1 March **2007**.
5. G. Pomarico, R. Paolesse, A. Alimelli, E. Martinelli, A. Macagnano, E. Sgreccia, C. Di Natale, A. D’Amico: *“Exploitation of 5,10,15,20-Tetrakis-(2,6-dimethoxyphenyl)porphyrin metal derivatives as coating material of quartz microbalances”*, Fourth International Conference on Porphyrins and Phthalocyanines, Rome, 2-7 July **2006**.

Other abstracts:

1. L. Lvova, D. Monti, G. Pomarico, C. Di Natale, A. D’Amico, R. Paolesse; *“Dual-mode chemical sensors based on metalloporphyrin aggregation”*,

- Matrafüred 2008, International Meeting on Chemical Sensors, Dobogókő, 5-10 October **2008**.
2. F. Dini, E. Martinelli, F. Cainero, G. Pomarico, D. Monti, R. Paolesse, D'Amico, C. Di Natale; "*Studies on the chemical sensitivities of self-assembled porphyrin nanotube*", XIII Annual Conference AISEM, Rome, 19-21 February **2008**.
 3. E. Martinelli, F. Dini, I. Iannaccone, D. Monti, G. Pomarico, R. Generosi, M. Luce, A. D'Amico, R. Paolesse, C. Di Natale: "*Chemical sensitivity of porphyrins nanotubes*": Transducers '07 & Eurosensors XXI, Lione, 10-14 June **2007**.
 4. A. Macagnano, R. D'Agostino, R. Paolesse, C. Di Natale, E. Sgreccia, G. Pomarico, E. Zampetti, S. Panatalei, B. Pistillo, G. Caputo, A. D'Amico: "*Sensing behavior of hyphenated hydrophobic polymer-metalloporphyrin layers*", Eurosensors XX, Göteborg, 17-20 September **2006**.
 5. M. Stefanelli, D. Monti, A. Alimelli, G. Pomarico, A. D'Amico, C. Di Natale, R. Paolesse: "*Development and testing of a new sensitive material based on metalloporphyrin-resorcinarene conjugate*", IMCS-11, Brescia, 16-19 July **2006**.
 6. A. Scarpa, F. Olimpico, S. Graco, D. Monti, G. Pomarico, R. Paolesse: "*Sub-phase influence in surface deposition homogeneity of ZnTPP*", Fourth International Conference on Porphyrins and Phthalocyanines, Rome, 2-7 July **2006**.
 7. M. Stefanelli, D. Monti, G. Pomarico, A. Alimelli, R. Paolesse: "*Resorcinarene-porphyrin conjugate: a new ditopic receptor for chemical sensors*", XI Annual Conference AISEM, Lecce, 8-10 February **2006**.
 8. R. Paolesse, S. Nardis, G. Verrelli, F. Mandoj, G. Pomarico, A. Micozzi, C. Lo Sterzo, L. Prodi: "*Luminescent porphyrin conjugated polymers for*

chemical sensors applications”, XI Annual Conference AISEM, Lecce, 8-10 February **2006**.

Oral communications:

1. G. Pomarico, F. Mandoj, S. Nardis, S. Antonaroli, B. Crociani, R. Paolesse; “*Pd-catalyzed synthesis of fully substituted polypyrrolic macrocycles*”, II National Workshop AICIng, Messina, 12-14 September **2007**.

Schools and meetings:

1. V International Conference on Porphyrins and Phthalocyanines, Moscow, 6-11 July **2008**
2. XIII Annual Conference AISEM, Rome, 19-21 February **2008**
3. VIII National Conference on Supramolecular Chemistry, Trieste, 19-22 September **2007**
4. II National Workshop AICIng, Messina, 12-14 September **2007**
5. I School of Nanomaterials and Biomaterials, Rome, 21 May-1 June **2007**
6. PITTCON 2007, Conference and Expo, Chicago (IL-USA), 25 February -1 March **2007**
7. IV International Conference on Porphyrins and Phthalocyanines, Rome, 2-7 July **2006**
8. XI Annual Conference AISEM, Lecce, 8-10 February **2006**.